

Realized Stochastic Volatility Model with Skew- t Distributions for Improved Volatility and Quantile Forecasting*

Makoto Takahashi^{†1}, Yuta Yamauchi², Toshiaki Watanabe³, and Yasuhiro Omori⁴

¹Faculty of Business Administration, Hosei University

²Graduate School of Economics, Nagoya University

³Graduate School of Social Data Science, Hitotsubashi University

⁴Faculty of Economics, University of Tokyo

Abstract

Accurate forecasting of volatility and return quantiles is essential for evaluating financial tail risks such as value-at-risk and expected shortfall. This study proposes an extension of the traditional stochastic volatility model—termed the realized stochastic volatility model—that incorporates realized volatility as an efficient proxy for latent volatility. To better capture the stylized features of financial return distributions, particularly skewness and heavy tails, we introduce three variants of skewed t -distributions, two of which incorporate skew-normal components to flexibly model asymmetry. The models are estimated using a Bayesian Markov chain Monte Carlo approach and applied to daily returns and realized volatilities from major U.S. and Japanese stock indices. Empirical results demonstrate that incorporating both realized volatility and flexible return distributions substantially improves the accuracy of volatility and tail risk forecasts.

Keywords: Bayesian estimation, Markov chain Monte Carlo, Realized volatility, Skew- t distribution, Stochastic volatility

1 Introduction

Volatility, defined as the conditional standard deviation or variance of asset returns, evolves stochastically over time and plays a central role in financial risk management. Accurate volatility forecasting is essential for evaluating tail risks such as value-at-risk (VaR) and expected shortfall (ES). Traditionally, two major classes of time-series models have been used for modeling time-varying volatility: the generalized autoregressive conditional heteroskedasticity (GARCH) family (Engle 1982, Bollerslev 1986), and the stochastic volatility (SV) model (Taylor 1986). These models successfully capture key features of financial volatility, including volatility clustering and persistence, and

*The authors gratefully acknowledge the Ministry of Education, Culture, Sports, Science and Technology of the Japanese Government through Grant-in-Aid for Scientific Research (Nos. 22K13376, 23H00048, and 24H00142), the Hitotsubashi Institute for Advanced Study, and Hosei University’s Innovation Management Research Center.

[†]Corresponding author. Email: m-takahashi@hosei.ac.jp

have been extended to account for leverage effects—i.e., the negative correlation between current returns and future volatility. A prominent example is the exponential GARCH (EGARCH) model by Nelson (1991).

More recently, realized volatility (RV), calculated as the sum of squared intraday returns, has gained popularity as a nonparametric and more efficient measure of daily volatility. Comprehensive surveys on RV are provided by Andersen & Benzoni (2009) and McAleer & Medeiros (2008). To model the time-series behavior of RV, researchers have proposed long-memory models such as autoregressive fractionally integrated moving average (ARFIMA) models (Beran 1994), as well as the heterogeneous autoregressive (HAR) model (Corsi 2009), which approximates long-memory dynamics using a small number of lags.

Although ARFIMA and HAR models often outperform traditional GARCH and SV models in volatility forecasting, RV estimates are prone to biases caused by market microstructure noise and non-trading hours. Several techniques have been developed to address these issues, including multiscale estimators (Zhang et al. 2005, Zhang 2006), pre-averaging methods (Jacod et al. 2009), and realized kernel (RK) estimators (Barndorff-Nielsen et al. 2008, 2009). For further refinements and applications, see Aït-Sahalia & Mykland (2009), Ubukata & Watanabe (2014), and Liu et al. (2015).

To exploit the advantages of both parametric and nonparametric approaches, hybrid models have been proposed. These include the realized stochastic volatility (RSV) model (Takahashi et al. 2009, Dobrev & Szerszen 2010, Koopman & Scharth 2013), as well as the realized GARCH (RGARCH) and realized EGARCH (REGARCH) models (Hansen et al. 2012, Hansen & Huang 2016). While several studies have compared forecasting performance within each class, comprehensive cross-model evaluations remain limited. Recent studies such as Takahashi et al. (2023, 2024) have attempted to bridge this gap.

Beyond volatility, accurate prediction of financial tail risks requires appropriate modeling of return distributions, which often exhibit skewness and leptokurtosis. While time-varying volatility captures some of this behavior, the conditional distribution of returns may remain non-Gaussian even after accounting for volatility. To address this, skewed Student’s t -distributions have been widely applied in volatility models (Abanto-Valle et al. 2015, Kobayashi 2016). Among them, the generalized hyperbolic (GH) skew- t distribution has shown strong empirical performance in SV (Nakajima & Omori 2012, Leão et al. 2017) and RSV models (Trojan 2013, Nugroho & Morimoto 2014, 2016, Takahashi et al. 2016).

Score-driven (SD) models, introduced by Creal et al. (2013) and Harvey (2013), have also gained popularity as a flexible alternative to SV and GARCH.¹ Catania & Grassi (2022) apply the GH skew- t distribution within an SD-GARCH setting, while Catania & Proietti (2020) develop a joint SD model for returns and realized volatility using a time-varying bivariate t specification. These approaches are conceptually related to ours, but their dynamic updating rules and likelihood evaluations are substantially more complex. We therefore focus on SV/RSV-type models, while acknowledging SD-based specifications as an important complementary direction in the broader volatility-modeling literature.

In this paper, we extend the RSV framework by incorporating three types of skew- t distributions: the Azzalini-type skew- t distribution (Azzalini 1985), the Fernández and Steel (FS) skew- t distribution (Fernández & Steel 1995), and the GH skew- t distribution (Aas & Haff 2006). We adopt a Bayesian estimation strategy using Markov chain Monte Carlo (MCMC) simulation and apply the models to daily returns of the Dow Jones Industrial Average (DJIA) and the Nikkei 225 (N225).

¹An extensive and regularly updated list of SD models proposed in the literature is available at <https://www.gasmodel.com/>.

Our empirical analysis evaluates the performance of RSV models alongside benchmark SV, EGARCH, and REGARCH models. Volatility forecasts are assessed using the quasi-likelihood loss function, while VaR and ES forecasts are evaluated using the joint loss function proposed by Fissler & Ziegel (2016) and specified in Patton et al. (2019). To test forecast performance, we implement the predictive ability test of Giacomini & White (2006) and the model confidence set procedure by Hansen et al. (2011). The results show that incorporating realized volatility substantially improves forecasting performance. In particular, RSV models with skew- t innovations exhibit superior predictive accuracy, confirming and extending findings from prior research.

The remainder of the paper is organized as follows. Section 2 presents the SV and RSV models, including skewed innovations and a brief overview of realized measures. Section 3 outlines the Bayesian estimation method and forecast evaluation metrics. Section 4 reports the empirical results. Section 5 concludes with a summary of findings and implications.

2 Model

2.1 Stochastic Volatility Model

Let y_t denote the daily log return of an asset:

$$y_t = \log p_t - \log p_{t-1},$$

where p_t is the closing price on day t . The conditional return variance is modeled as

$$E[y_t^2 \mid \mathcal{I}_{t-1}] = \sigma_t^2 = \exp(h_t),$$

where \mathcal{I}_{t-1} denotes the information set available at time $t-1$ and h_t denotes the conditional log volatility, treated as a latent process.

The log volatility h_t is assumed to follow a stationary AR(1) process:

$$\begin{aligned} y_t &= \epsilon_t \exp\left(\frac{h_t}{2}\right), \quad t = 1, \dots, n, \\ h_{t+1} &= \mu + \phi(h_t - \mu) + \eta_t, \quad t = 1, \dots, n-1, \quad |\phi| < 1, \\ h_1 &\sim \mathcal{N}\left(\mu, \frac{\sigma_\eta^2}{1 - \phi^2}\right), \\ \epsilon_t &\sim \mathcal{N}(0, 1), \\ \eta_t \mid \epsilon_t &\sim \mathcal{N}(\rho\sigma_\eta\epsilon_t, (1 - \rho^2)\sigma_\eta^2). \end{aligned}$$

Here, ϕ is the persistence parameter, and μ is the unconditional mean of log volatility. Stationarity is ensured by $|\phi| < 1$. The initial state h_1 is drawn from its unconditional distribution.

The bivariate error term $(\epsilon_t, \eta_t)'$ follows a jointly normal distribution with correlation ρ . This structure allows for a leverage effect: a negative return shock ($\epsilon_t < 0$) tends to increase future volatility (h_{t+1}), reflected by $\rho < 0$. This feature captures the empirically observed asymmetry in financial markets, where volatility tends to rise following negative returns.

2.2 Realized Volatility

In the SV model, volatility $\exp(h_t)$ is treated as a latent variable, since the log-volatility h_t is unobserved. With the increasing availability of high-frequency data, RV has emerged as a prominent nonparametric estimator of true volatility.

Let $p(s)$ denote the logarithm of the asset price at time s , and suppose it follows the continuous-time diffusion process:

$$dp(s) = \mu(s)ds + \sigma(s)dW(s),$$

where $\mu(s)$ and $\sigma(s)^2$ are the drift and instantaneous variance, respectively, and $W(s)$ is a standard Brownian motion. The integrated volatility (IV) over a single day is defined as

$$IV_t = \int_{t-1}^t \sigma^2(s)ds.$$

Assume that m intraday returns are observed on day t , denoted by $\{r_{t-1+1/m}, r_{t-1+2/m}, \dots, r_t\}$. Then, the realized volatility is defined as

$$RV_t = \sum_{i=1}^m r_{t-1+i/m}^2.$$

Under ideal conditions (e.g., no microstructure noise or missing observations), RV_t converges to IV_t as $m \rightarrow \infty$.

However, these ideal conditions are often violated in practice. One source of bias arises from non-trading hours, which are not captured in intraday data. Ignoring these periods leads to an underestimation of daily volatility. To address this, Hansen & Lunde (2005) proposed a scaling adjustment:

$$RV_t^{HL} = c_{HL}RV_t, \quad c_{HL} = \frac{\sum_{t=1}^n (y_t - \bar{y})^2}{\sum_{t=1}^n RV_t}, \quad \bar{y} = \frac{1}{n} \sum_{t=1}^n y_t. \quad (1)$$

This adjustment ensures that the average of the scaled RV matches the sample variance of daily returns.

Another significant bias stems from microstructure noise. Observed prices deviate from the efficient price due to bid-ask bounce, price discreteness, and asynchronous trading, introducing autocorrelation and distortions in high-frequency returns. The bias tends to worsen as the sampling interval becomes shorter. Optimal sampling frequency and alternative estimators have been studied extensively (Aït-Sahalia et al. 2005, Bandi & Russell 2006, 2008, Liu et al. 2015).

Among various alternatives, the RK estimator (Barndorff-Nielsen et al. 2008) has been widely adopted due to its robustness. It is defined as:

$$RK_t = \sum_{h=-H}^H k\left(\frac{h}{H+1}\right) \gamma_h,$$

where H is the bandwidth, $k(\cdot)$ is a weight function, and

$$\gamma_h = \sum_{i=|h|+1}^m r_{t-1+i/m} \cdot r_{t-1+(i-|h|)/m}.$$

Barndorff-Nielsen et al. (2009) provide guidelines for choosing the bandwidth H .

To account for these biases in modeling, hybrid frameworks such as the RSV and RGARCH models have been developed. In particular, the RSV model of Takahashi et al. (2009) addresses RV bias by jointly estimating model parameters, as detailed in Section 2.3.

2.3 Realized Stochastic Volatility Model

Takahashi et al. (2009) proposed enhancing the SV model by incorporating additional information from RV. In their framework, the daily log-return y_t and the logarithm of realized volatility $x_t = \log RV_t$ are jointly modeled, with the latent log volatility $h_t = \log IV_t$ serving as a common driver.

The RSV model is specified as:

$$x_t = \xi + h_t + u_t, \quad t = 1, \dots, n, \quad (2)$$

$$y_t = \epsilon_t \exp\left(\frac{h_t}{2}\right), \quad t = 1, \dots, n, \quad (3)$$

$$h_{t+1} = \mu + \phi(h_t - \mu) + \eta_t, \quad |\phi| < 1, \quad (4)$$

$$h_1 \sim \mathcal{N}\left(\mu, \frac{\sigma_\eta^2}{1 - \phi^2}\right), \quad (5)$$

$$u_t \sim \mathcal{N}(0, \sigma_u^2), \quad (6)$$

$$\epsilon_t \sim \mathcal{N}(0, 1), \quad (7)$$

$$\eta_t | \epsilon_t \sim \mathcal{N}(\rho\sigma_\eta\epsilon_t, (1 - \rho^2)\sigma_\eta^2). \quad (8)$$

The error term u_t is assumed to be independent of (ϵ_t, η_t) .

Equation (2) may be generalized as $x_t = \xi + \psi h_t + u_t$, but empirical evidence suggests that estimating $\psi \neq 1$ does not improve forecasting performance. Accordingly, we fix $\psi = 1$, following Takahashi et al. (2009).

The parameter ξ adjusts for systematic bias in $x_t = \log RV_t$. When $\xi = 0$, x_t is an unbiased estimate of h_t . In practice, however, RV_t may be biased downward due to non-trading hours and upward due to microstructure noise. Hansen & Lunde (2006) show that the net bias can be either positive or negative. Therefore, the sign of ξ reflects the relative magnitude of these two opposing effects.

The distribution of ϵ_t captures residual return behavior after controlling for time-varying volatility. While the SV structure already accounts for volatility clustering and excess kurtosis, it is well documented that financial returns often exhibit additional heavy tails and asymmetry. To model these features more effectively, several studies have incorporated non-Gaussian innovations.

For the SV model, Nakajima & Omori (2012) and Leão et al. (2017) employed the GH skew- t distribution from Aas & Haff (2006). Other approaches include the skew- t distribution by Azzalini & Capitanio (2003) (used in Abanto-Valle et al. 2015), the skew exponential power distribution (Kobayashi 2016), and the flexible skew- t model by Fernández & Steel (1995), as adopted in Steel (1998). In the context of RSV models, Trojan (2013), Nugroho & Morimoto (2014, 2016), and Takahashi et al. (2016) applied the GH skew- t distribution.

Building on this literature, we extend the RSV model defined in equations (2)–(7)—hereafter referred to as the RSV-N model—by incorporating skewed and heavy-tailed distributions for ϵ_t . This extension allows for more accurate modeling of return asymmetry and tail risk, which is essential for reliable risk forecast applications.

2.4 RSV Model with Student's t Distribution

We extend the RSV-N model by allowing the return innovation ϵ_t to follow a standardized Student's t distribution. The resulting model, referred to as the RSV-T model, modifies equations (6)–(7) as follows:

$$\begin{aligned}\epsilon_t &= z_t \sqrt{\frac{\lambda_t}{\mu_\lambda}}, \\ z_t &\sim \mathcal{N}(0, 1), \\ \eta_t \mid z_t &\sim \mathcal{N}(\rho\sigma_\eta z_t, (1 - \rho^2)\sigma_\eta^2),\end{aligned}$$

where

$$\lambda_t \stackrel{\text{i.i.d.}}{\sim} \mathcal{IG}\left(\frac{\nu}{2}, \frac{\nu}{2}\right), \quad \mu_\lambda = \mathbb{E}[\lambda_t] = \frac{\nu}{\nu - 2}, \quad \nu > 2.$$

Here, λ_t is an inverse-gamma mixing variable, and ν is the degrees of freedom parameter controlling tail thickness. As $\nu \rightarrow \infty$, the model converges to the Gaussian RSV-N specification.

The use of Student's t distribution allows the model to accommodate excess kurtosis beyond what is captured by the stochastic volatility component h_t . For finite ν , the distribution of ϵ_t exhibits heavier tails, improving the model's ability to reflect extreme return events.

Importantly, the contemporaneous correlation between ϵ_t and η_t becomes a function of both ρ and ν , given by:

$$\text{Corr}[\epsilon_t, \eta_t] = \frac{\mathbb{E}[\sqrt{\lambda_t}]}{\sqrt{\mu_\lambda}} \rho,$$

where

$$\mathbb{E}[\sqrt{\lambda_t}] = \sqrt{\frac{\nu}{2}} \cdot \frac{\Gamma(\frac{\nu-1}{2})}{\Gamma(\frac{\nu}{2})}. \quad (8)$$

Note that the variance of ϵ_t exists only when $\nu > 2$, and its fourth moment exists when $\nu > 4$. In empirical applications, ν is typically estimated from the data.

2.5 RSV Model with GH Skew- t Distribution

Takahashi et al. (2016) extended the RSV-N model in equations (2)–(7) by incorporating the GH skew- t distribution, resulting in the RSV-GH-ST model. This is achieved by replacing ϵ_t and η_t in (6)–(7) with the following mixture representation:

$$\begin{aligned}\epsilon_t &= \frac{\beta(\lambda_t - \mu_\lambda) + \sqrt{\lambda_t} z_t}{\sqrt{\beta^2 \sigma_\lambda^2 + \mu_\lambda}}, \\ z_t &\sim \mathcal{N}(0, 1), \\ \eta_t \mid z_t &\sim \mathcal{N}(\rho\sigma_\eta z_t, (1 - \rho^2)\sigma_\eta^2),\end{aligned} \quad (9)$$

where $\lambda_t \sim \mathcal{IG}(\nu/2, \nu/2)$, $\mu_\lambda = \nu/(\nu - 2)$, and

$$\sigma_\lambda^2 = \text{Var}[\lambda_t] = \frac{2\nu^2}{(\nu - 2)^2(\nu - 4)}, \quad \nu > 4.$$

A distinctive feature of the GH skew- t distribution, originally emphasized by Aas & Haff (2006), is its asymmetric tail behavior: one tail exhibits polynomial (power-law) decay, while the opposite tail decays exponentially, depending

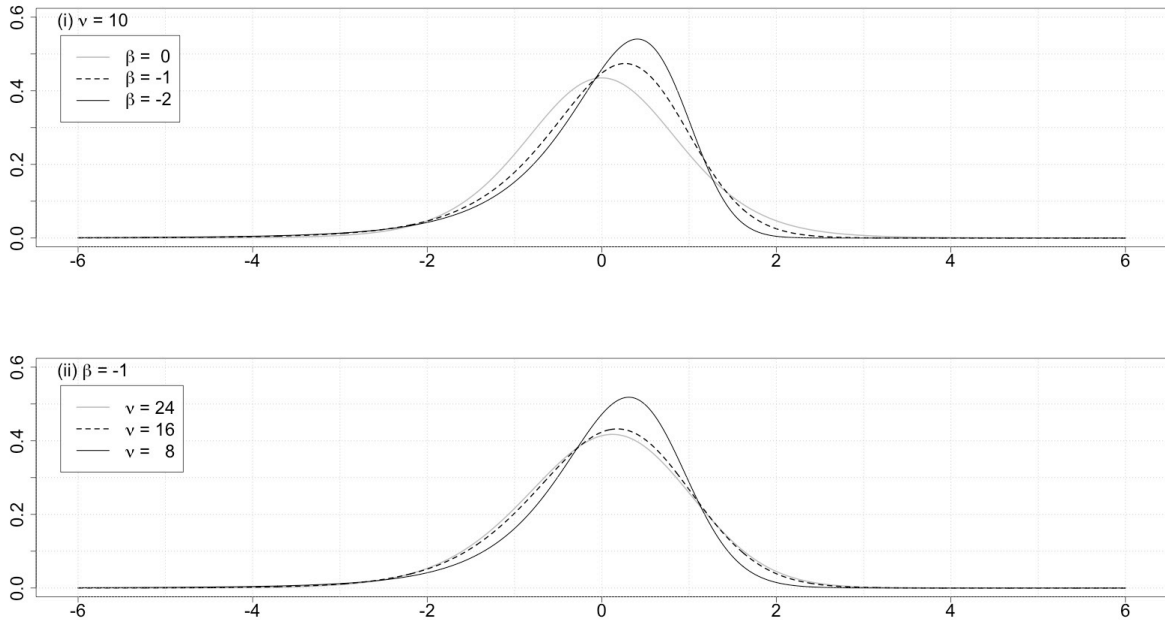


Figure 1: Density of the standardized GH skew- t distribution in equation (9). (i) Varying $\beta = 0, -1, -2$ with fixed $\nu = 10$. (ii) Varying $\nu = 24, 16, 8$ with fixed $\beta = -1$.

on the sign of the skewness parameter β . This feature makes the GH skew- t distribution particularly flexible in capturing return asymmetry and tail risk in financial applications.

The denominator in (9) standardizes ϵ_t so that its conditional variance equals $\exp(h_t)$. In the present formulation, the skewness and tail behavior of ϵ_t are jointly governed by β and ν . The parameter β introduces asymmetry and determines which tail becomes heavier, while ν controls the degree of polynomial tail thickness. When $\beta = 0$, the model reduces to the RSV-T specification in . As $\nu \rightarrow \infty$, or if $\lambda_t = 1$ for all t , the distribution converges to the Gaussian case regardless of β .

The correlation between ϵ_t and η_t depends on ρ , ν , and β , and is given by:

$$\text{Corr}[\epsilon_t, \eta_t] = \frac{E[\sqrt{\lambda_t}]}{\sqrt{\beta^2 \sigma_\lambda^2 + \mu_\lambda}} \rho,$$

where $E[\sqrt{\lambda_t}]$ is as defined in equation (8).

To illustrate the influence of β and ν , Figure 1 plots the simulated densities of ϵ_t under various parameter values. Panel (i) shows that increasing negative values of β yield more pronounced left-skewness and heavier polynomial tails. In contrast, Panel (ii) indicates that as ν increases, the distribution becomes more symmetric and approaches normality, exhibiting thinner tails.

2.6 RSV Model with Azzalini Skew- t Distribution

We extend the RSV-N model defined in equations (2)–(7) by adopting the skew- t distribution proposed by Azzalini (1985).² The resulting model, referred to as RSV-AZ-ST, modifies the return innovation ϵ_t and its correlation with

²See also Azzalini & Capitanio (2003) and Sahu et al. (2003).

η_t as follows:

$$\begin{aligned}\epsilon_t &= \frac{\delta(z_{0t} - c) + \sqrt{1 - \delta^2} z_t}{\sqrt{1 - c^2 \delta^2}} \cdot \sqrt{\frac{\lambda_t}{\mu_\lambda}}, \quad |\delta| < 1, \\ z_t &\sim \mathcal{N}(0, 1), \\ z_{0t} &\stackrel{\text{i.i.d.}}{\sim} \mathcal{TN}_{(0, \infty)}(0, 1), \\ \eta_t | z_t &\sim \mathcal{N}(\rho \sigma_\eta z_t, (1 - \rho^2) \sigma_\eta^2),\end{aligned}\tag{10}$$

where $\lambda_t \sim \mathcal{IG}(\nu/2, \nu/2)$, $\mu_\lambda = \nu/(\nu - 2)$, and $\mathcal{TN}_{(0, \infty)}$ denotes a standard normal distribution truncated above zero. The constants

$$c = \mathbb{E}[z_{0t}] = \sqrt{\frac{2}{\pi}}, \quad \text{Var}[z_{0t}] = 1 - c^2$$

are used to ensure that ϵ_t is standardized, so that its conditional variance remains $\exp(h_t)$.

The contemporaneous correlation between ϵ_t and η_t is now a function of ρ , ν , and δ , and is given by

$$\text{Corr}[\epsilon_t, \eta_t] = \sqrt{\frac{1 - \delta^2}{(1 - c^2 \delta^2) \mu_\lambda}} \cdot \mathbb{E}[\sqrt{\lambda_t}] \cdot \rho,$$

where $\mathbb{E}[\sqrt{\lambda_t}]$ is defined in equation (8). Setting $\delta = 0$ recovers the RSV-T model. Moreover, as $\nu \rightarrow \infty$ or $\lambda_t = 1$, the model simplifies to the RSV-AZ-SN model with a skew-normal distribution.

The shape of the distribution of ϵ_t is governed jointly by δ and ν , which respectively control skewness and tail thickness. From the general moment expression

$$\mathbb{E}[\lambda_t^{m/2}] = \left(\frac{\nu}{2}\right)^{m/2} \cdot \frac{\Gamma\left(\frac{\nu-m}{2}\right)}{\Gamma\left(\frac{\nu}{2}\right)}, \quad \nu > m,$$

we derive the third and fourth moments of ϵ_t as:

$$\begin{aligned}\mathbb{E}[\epsilon_t^3] &= \frac{4 - \pi}{2} \cdot \frac{c^3 \delta^3}{(1 - c^2 \delta^2)^{3/2}} \cdot \left(\frac{\nu - 2}{2}\right)^{3/2} \cdot \frac{\Gamma\left(\frac{\nu-3}{2}\right)}{\Gamma\left(\frac{\nu}{2}\right)}, \\ \mathbb{E}[\epsilon_t^4] &= \left(3 + 2(\pi - 3) \cdot \frac{c^4 \delta^4}{(1 - c^2 \delta^2)^2}\right) \cdot \frac{\nu - 2}{\nu - 4}.\end{aligned}$$

As with the GH skew- t distribution, the skewness and kurtosis of the return distribution are jointly influenced by the parameters. While ν governs tail behavior, δ introduces asymmetry.

Figure 2 illustrates the impact of these parameters on the shape of ϵ_t . Panel (i) shows that increasing negative values of δ lead to stronger left-skewness, with $\delta = 0$ yielding a symmetric t -distribution. Panel (ii) demonstrates that larger values of ν reduce tail thickness and approximate the normal distribution. Notably, even when $\nu \rightarrow \infty$, the distribution remains skewed unless $\delta = 0$, in which case the skew-normal distribution is recovered.

2.7 RSV Model with Fernández–Steel Skew- t Distribution

Following the approach of Fernández & Steel (1995), we define the Fernández–Steel (FS) skew- t density as

$$p_T(w | \gamma, \nu) = \frac{2}{\gamma + \gamma^{-1}} \left\{ f_T\left(\frac{w}{\gamma} | \nu\right) \mathbb{1}\{w \geq 0\} + f_T(\gamma w | \nu) \mathbb{1}\{w < 0\} \right\}, \quad \gamma > 0,$$

where $f_T(\cdot | \nu)$ denotes the probability density function of the standard Student's t distribution:

$$f_T(\tilde{w} | \nu) = c_\nu \left(1 + \frac{\tilde{w}^2}{\nu}\right)^{-\frac{\nu+1}{2}}, \quad c_\nu = \frac{\Gamma\left(\frac{\nu+1}{2}\right)}{\Gamma\left(\frac{\nu}{2}\right) \Gamma\left(\frac{1}{2}\right) \sqrt{\nu}}, \quad \nu > 2.$$

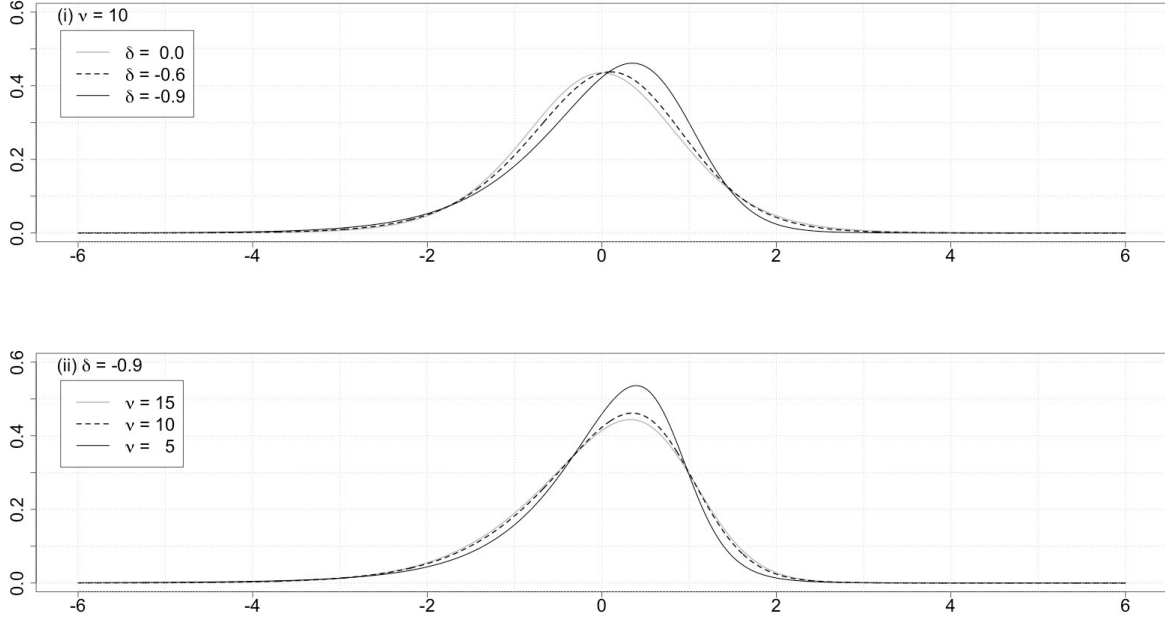


Figure 2: Density of the standardized Azzalini skew- t distribution in equation (10). (i) $\delta = 0, -0.6, -0.9$ with $\nu = 10$ fixed. (ii) $\nu = 15, 10, 5$ with $\delta = -0.9$ fixed.

Here, $\mathbb{1}\{\cdot\}$ denotes the indicator function.

The mean and variance of $w \sim p_T(w \mid \gamma, \nu)$ are:

$$\begin{aligned}\mu_* &= \text{E}[w] = M_1(\gamma - \gamma^{-1}), \\ \sigma_*^2 &= \text{Var}[w] = M_2 \cdot \frac{\gamma^3 + \gamma^{-3}}{\gamma + \gamma^{-1}} - \{M_1(\gamma - \gamma^{-1})\}^2,\end{aligned}$$

where

$$\begin{aligned}M_1 &= 2 \int_0^\infty \tilde{w} f_T(\tilde{w} \mid \nu) d\tilde{w} = \frac{2c_\nu \nu}{\nu - 1}, \\ M_2 &= 2 \int_0^\infty \tilde{w}^2 f_T(\tilde{w} \mid \nu) d\tilde{w} = \frac{\nu}{\nu - 2}.\end{aligned}$$

To obtain a standardized version of the FS skew- t density, we define:

$$w_* = \frac{w - \mu_*}{\sigma_*},$$

so that $\text{E}[w_*] = 0$ and $\text{Var}[w_*] = 1$. The corresponding standardized density becomes:

$$\begin{aligned}q_T(w_* \mid \gamma, \nu) &= \frac{2\sigma_*}{\gamma + \gamma^{-1}} \left\{ f_T \left(\frac{\sigma_* w_* + \mu_*}{\gamma} \mid \nu \right) \mathbb{1} \left\{ w_* \geq -\frac{\mu_*}{\sigma_*} \right\} \right. \\ &\quad \left. + f_T \left(\gamma(\sigma_* w_* + \mu_*) \mid \nu \right) \mathbb{1} \left\{ w_* < -\frac{\mu_*}{\sigma_*} \right\} \right\}.\end{aligned}\tag{11}$$

Replacing f_T with the standard normal density f_N in the above expression yields the standardized FS skew-normal density $q_N(\cdot \mid \gamma)$.

Following Trottier & Ardia (2016), higher-order moments for the FS skew- t distribution and their standardized forms are derived utilizing the absolute moments of the underlying Student's t distribution. For the absolute

moments, we refer to the unified results provided by Kirkby et al. (2025). The k -th absolute moment, denoted by $M_k = 2 \int_0^\infty \tilde{w}^k f_T(\tilde{w} | \nu) d\tilde{w}$, is generally given by:

$$M_k = \nu^{k/2} \frac{\Gamma\left(\frac{k+1}{2}\right) \Gamma\left(\frac{\nu-k}{2}\right)}{\sqrt{\pi} \Gamma\left(\frac{\nu}{2}\right)}, \quad k < \nu.$$

Specifically, for $k = 3$ and $k = 4$, we obtain:

$$M_3 = \frac{\nu^{3/2} \Gamma\left(\frac{\nu-3}{2}\right)}{\sqrt{\pi} \Gamma\left(\frac{\nu}{2}\right)} \quad (\nu > 3),$$

$$M_4 = \frac{3\nu^2}{(\nu-2)(\nu-4)} \quad (\nu > 4).$$

Using the general raw-moment formula provided in Trottier & Ardia (2016):

$$\mu'_r = E[w^r] = M_r \frac{\gamma^{r+1} + (-1)^r \gamma^{-(r+1)}}{\gamma + \gamma^{-1}}, \quad r = 1, 2, 3, 4,$$

the centered third and fourth moments are defined as:

$$\mu_3 = \mu'_3 - 3\mu_*\mu'_2 + 2\mu_*^3, \quad \mu_4 = \mu'_4 - 4\mu_*\mu'_3 + 6\mu_*^2\mu'_2 - 3\mu_*^4.$$

Consequently, the skewness and excess kurtosis of the standardized variable $w_* = (w - \mu_*)/\sigma_*$ are given by:

$$\text{Skew}(w_*) = \frac{\mu_3}{\sigma_*^3},$$

$$\text{Kurt}(w_*) = \frac{\mu_4}{\sigma_*^4} - 3.$$

These expressions implicitly depend on (γ, ν) through the moments M_k and the parameter γ , confirming that γ governs asymmetry while ν determines tail thickness.

We now define the RSV-FS-ST model by assuming:

$$\epsilon_t \sim q_T(\epsilon_t | \gamma, \nu),$$

$$\eta_t | \epsilon_t \sim \mathcal{N}(\rho\sigma_\eta\epsilon_t, (1 - \rho^2)\sigma_\eta^2),$$

where $q_T(\cdot | \gamma, \nu)$ is the standardized FS skew- t density. Replacing q_T with q_N yields the RSV-FS-SN model.

The skewness of the distribution is governed by the parameter γ , where $\gamma = 1$ corresponds to a symmetric t -distribution. If $\gamma < 1$, the distribution becomes left-skewed, while $\gamma > 1$ results in right-skewness. The parameter ν controls tail heaviness.

Figure 3 illustrates how the shape of the distribution varies with γ and ν . Panel (i) shows that decreasing γ induces stronger negative skewness, with $\gamma = 1$ yielding symmetry. Panel (ii) demonstrates that increasing ν reduces tail thickness. Notably, as $\nu \rightarrow \infty$, the distribution converges to a skew-normal form when $\gamma \neq 1$, and to a standard normal when $\gamma = 1$.

2.8 EGARCH Model

GARCH models are widely used to describe time-varying volatility. Among numerous variants, we consider an EGARCH-type model. While the original EGARCH specification of Nelson (1991) involves the term $E[|\epsilon_t|]$, this

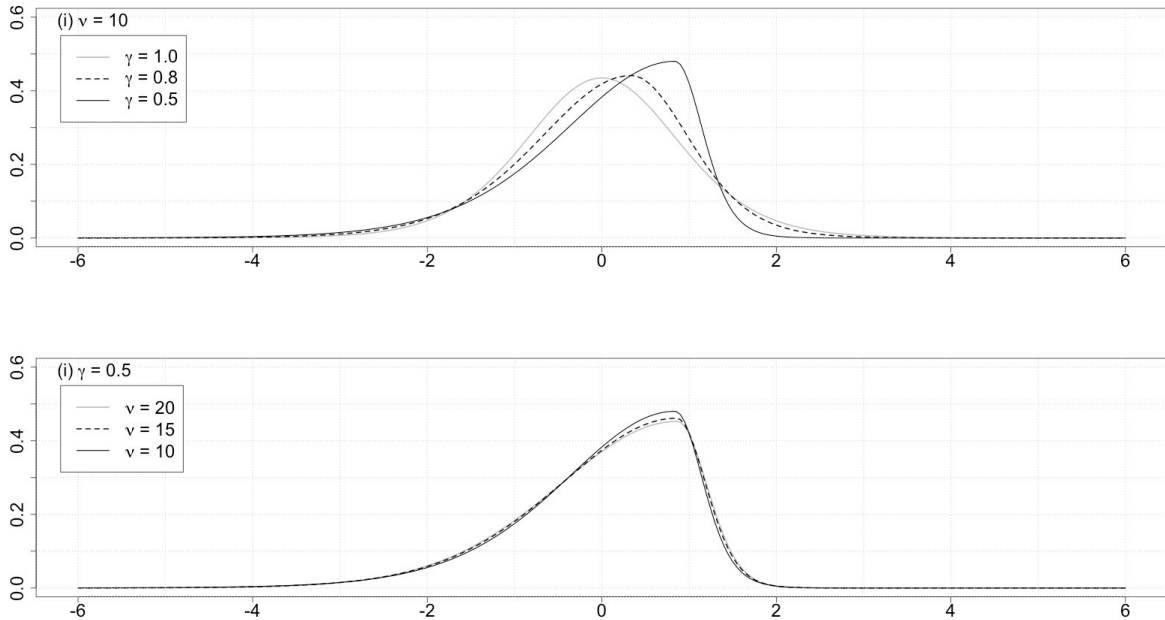


Figure 3: Density of the standardized FS skew- t distribution in equation (11). (i) $\gamma = 1, 0.8, 0.6$ with $\nu = 10$. (ii) $\nu = 20, 15, 10$ with $\gamma = 0.5$.

expectation does not admit a convenient closed-form expression under standardized t innovations. Following Hansen & Huang (2016), we therefore estimate the model using the quadratic term $(\epsilon_t^2 - 1)$ instead, which yields

$$y_t = \epsilon_t \exp\left(\frac{h_t}{2}\right), \quad \epsilon_t \sim \mathcal{N}(0, 1), \quad t = 1, \dots, n,$$

$$h_{t+1} = \omega + \varphi(h_t - \omega) + \tau\epsilon_t + \gamma(\epsilon_t^2 - 1), \quad |\varphi| < 1, \quad t = 1, \dots, n-1,$$

with the initial condition $h_1 = \omega$. The parameter τ captures the asymmetric response of conditional volatility to return shocks, and when $\tau < 0$, negative shocks increase volatility more than positive ones, reflecting the leverage effect. For expositional clarity, we present the model above under the Gaussian assumption for ϵ_t . In Section 4, we relax this assumption and consider a standardized Student- t distribution with degrees-of-freedom parameter ν , allowing for heavy-tailed return behavior.

Remark. Nelson (1991) noted that estimating EGARCH with Student- t innovations can suffer from stability issues (p. 365), and suggested the generalized error distribution (GED) as a more robust alternative. While Nelson (1991) originally proposed a quasi-maximum likelihood (QML) estimation procedure, in this study we estimate the model parameters using a Bayesian approach. We acknowledge the importance of the EGARCH-GED specification; however, given the additional computational complexity of Bayesian estimation and the main goal of this study to compare realized volatility-based stochastic volatility models, we leave the estimation of EGARCH-GED for future work.

2.9 REGARCH Model

Hansen et al. (2012) and Hansen & Huang (2016) extend the conventional GARCH and EGARCH models to the RGARCH and REGARCH frameworks, respectively, by incorporating realized measures into the volatility dynamics. Since the REGARCH model allows a more flexible characterization of the joint dynamics between returns and volatility than the RGARCH model, we adopt the REGARCH specification, which can be written as

$$\begin{aligned} y_t &= \epsilon_t \exp\left(\frac{h_t}{2}\right), \quad \epsilon_t \sim \mathcal{N}(0, 1), \quad t = 1, \dots, n, \\ h_{t+1} &= \omega + \varphi(h_t - \omega) + \tau_1 \epsilon_t + \tau_2(\epsilon_t^2 - 1) + \gamma v_t, \quad |\varphi| < 1, \quad t = 1, \dots, n-1, \\ x_t &= \zeta + h_t + \delta_1 \epsilon_t + \delta_2(\epsilon_t^2 - 1) + v_t, \quad v_t \sim \mathcal{N}(0, \sigma_v^2), \quad t = 1, \dots, n, \end{aligned}$$

with the initial condition $h_1 = \omega$. Similarly to the EGARCH model, in Section 4 we also consider a standardized Student- t distribution for ϵ_t in the REGARCH model, with degrees-of-freedom parameter ν , allowing for heavy-tailed return behavior.

The latent log-volatility process h_t and the realized measure x_t each include a quadratic form of the leverage function, given by $\tau_1 \epsilon_t + \tau_2(\epsilon_t^2 - 1)$ and $\delta_1 \epsilon_t + \delta_2(\epsilon_t^2 - 1)$, respectively. Following Hansen & Huang (2016), one can introduce an additional scaling parameter ψ as

$$x_t = \zeta + \psi h_t + \delta_1 \epsilon_t + \delta_2(\epsilon_t^2 - 1) + v_t,$$

but since the estimate of ψ is typically close to unity, we fix $\psi = 1$ for brevity. The parameter ζ captures the bias in $\log RV_t$; $\zeta = 0$ implies an unbiased realized measure.

3 Bayesian Estimation Methodology

Each RSV model introduced in Section 2 can be formulated as a nonlinear Gaussian state space model with a large number of latent variables. This structure renders the likelihood function intractable in closed form, and consequently makes maximum likelihood estimation computationally difficult. To overcome this, we adopt a Bayesian estimation framework via MCMC simulation, following established approaches in the literature.

We assign prior distributions to the common model parameters $(\mu, \phi, \sigma_\eta^2, \rho, \xi, \sigma_u^2)$ as follows:

$$\begin{aligned} \mu &\sim \mathcal{N}(m_\mu, s_\mu^2), \quad \frac{\phi + 1}{2} \sim \mathcal{B}(a_{\phi 0}, b_{\phi 0}), \\ \frac{\rho + 1}{2} &\sim \mathcal{B}(a_{\rho 0}, b_{\rho 0}), \quad \sigma_\eta^2 \sim \mathcal{IG}\left(\frac{n_\eta}{2}, \frac{S_\eta}{2}\right), \\ \xi &\sim \mathcal{N}(m_\xi, s_\xi^2), \quad \sigma_u^2 \sim \mathcal{IG}\left(\frac{n_u}{2}, \frac{S_u}{2}\right), \end{aligned}$$

where $\mathcal{B}(\cdot, \cdot)$ and $\mathcal{IG}(\cdot, \cdot)$ denote the beta and inverse-gamma distributions, respectively. The hyperparameters $(m_\mu, s_\mu, a_{\phi 0}, b_{\phi 0}, a_{\rho 0}, b_{\rho 0}, n_\eta, S_\eta, m_\xi, s_\xi, n_u, S_u)$ are chosen to reflect prior beliefs or to be weakly informative when such prior knowledge is unavailable.

For notational convenience, let $\mathbf{y} = (y_1, \dots, y_n)'$, $\mathbf{x} = (x_1, \dots, x_n)'$, and $\mathbf{h} = (h_1, \dots, h_n)'$. Denote the parameter vector by $\boldsymbol{\theta}$, and let $\pi(\boldsymbol{\theta})$ be its joint prior density. The joint likelihood of $(\mathbf{y}, \mathbf{x}, \mathbf{h})$ given $\boldsymbol{\theta}$ is denoted by $f(\mathbf{y}, \mathbf{x}, \mathbf{h} \mid \boldsymbol{\theta})$.

In the following, we detail the MCMC sampling algorithms specifically for the RSV-AZ-ST and RSV-FS-ST models.³ We also outline the procedure for computing one-step-ahead forecasts of volatility and returns, from which

³See Takahashi et al. (2009) and Takahashi et al. (2016) for the algorithms used in the RSV-N and RSV-GH-ST models, respectively.

we derive one-step-ahead VaR and ES.

3.1 RSV-AZ-ST Model

Let $\boldsymbol{\theta} = (\mu, \phi, \rho, \sigma_\eta^2, \delta, \xi, \sigma_u^2, \nu)'$ denote the full vector of model parameters, and define the latent variable vectors $\boldsymbol{\lambda} = (\lambda_1, \dots, \lambda_n)'$ and $\mathbf{z}_0 = (z_{01}, \dots, z_{0n})'$. For the prior distributions of the model-specific parameters δ and ν , we assume:

$$\frac{\delta + 1}{2} \sim \mathcal{B}(a_{\delta 0}, b_{\delta 0}), \quad \nu \sim \mathcal{G}(n_{\nu 0}, S_{\nu 0}) \mathbb{1}\{\nu > 4\},$$

where $\mathcal{G}(\cdot, \cdot)$ denotes the gamma distribution.

The MCMC algorithm proceeds as follows:

1. Initialize \mathbf{h} , $\boldsymbol{\theta}$, \mathbf{z}_0 , and $\boldsymbol{\lambda}$.
2. Sample $\mu \mid \boldsymbol{\theta}_{-\mu}, \mathbf{h}, \mathbf{z}_0, \boldsymbol{\lambda}, \mathbf{x}, \mathbf{y}$.
3. Sample $\phi \mid \boldsymbol{\theta}_{-\phi}, \mathbf{h}, \mathbf{z}_0, \boldsymbol{\lambda}, \mathbf{x}, \mathbf{y}$.
4. Jointly sample $(\rho, \sigma_\eta^2) \mid \boldsymbol{\theta}_{-(\rho, \sigma_\eta^2)}, \mathbf{h}, \mathbf{z}_0, \boldsymbol{\lambda}, \mathbf{x}, \mathbf{y}$.
5. Sample $\delta \mid \boldsymbol{\theta}_{-\delta}, \mathbf{h}, \mathbf{z}_0, \boldsymbol{\lambda}, \mathbf{x}, \mathbf{y}$.
6. Sample $\xi \mid \boldsymbol{\theta}_{-\xi}, \mathbf{h}, \mathbf{z}_0, \boldsymbol{\lambda}, \mathbf{x}, \mathbf{y}$.
7. Sample $\sigma_u^2 \mid \boldsymbol{\theta}_{-\sigma_u^2}, \mathbf{h}, \mathbf{z}_0, \boldsymbol{\lambda}, \mathbf{x}, \mathbf{y}$.
8. Sample $\nu \mid \boldsymbol{\theta}_{-\nu}, \mathbf{h}, \mathbf{z}_0, \boldsymbol{\lambda}, \mathbf{x}, \mathbf{y}$.
9. Sample $\mathbf{z}_0 \mid \boldsymbol{\theta}, \mathbf{h}, \boldsymbol{\lambda}, \mathbf{x}, \mathbf{y}$.
10. Sample $\mathbf{h} \mid \boldsymbol{\theta}, \mathbf{z}_0, \boldsymbol{\lambda}, \mathbf{x}, \mathbf{y}$.
11. Sample $\boldsymbol{\lambda} \mid \boldsymbol{\theta}, \mathbf{h}, \mathbf{z}_0, \mathbf{x}, \mathbf{y}$.
12. Repeat steps 2–11 for a sufficiently large number of iterations.

Details of each sampling step, including full conditional distributions and implementation strategies (e.g., Gibbs sampling or Metropolis–Hastings updates), are provided in Appendix A.1.

3.2 RSV-FS-ST Model

Let $\boldsymbol{\theta} = (\mu, \phi, \rho, \sigma_\eta^2, \gamma, \xi, \sigma_u^2, \nu)'$ denote the full set of model parameters. For the model-specific parameters γ and ν , we assign the following prior distributions:

$$\gamma \sim \mathcal{G}(n_{\gamma 0}, S_{\gamma 0}), \quad \nu \sim \mathcal{G}(n_{\nu 0}, S_{\nu 0}) \mathbb{1}\{\nu > 4\}.$$

The MCMC algorithm proceeds as follows:

1. Initialize \mathbf{h} and $\boldsymbol{\theta}$.
2. Sample $\mu \mid \boldsymbol{\theta}_{-\mu}, \mathbf{h}, \mathbf{x}, \mathbf{y}$.

3. Sample $\phi \mid \boldsymbol{\theta}_{-\phi}, \mathbf{h}, \mathbf{x}, \mathbf{y}$.
4. Sample $\rho \mid \boldsymbol{\theta}_{-\rho}, \mathbf{h}, \mathbf{x}, \mathbf{y}$.
5. Sample $\sigma_\eta^2 \mid \boldsymbol{\theta}_{-\sigma_\eta^2}, \mathbf{h}, \mathbf{x}, \mathbf{y}$.
6. Sample $\xi \mid \boldsymbol{\theta}_{-\xi}, \mathbf{h}, \mathbf{x}, \mathbf{y}$.
7. Sample $\sigma_u^2 \mid \boldsymbol{\theta}_{-\sigma_u^2}, \mathbf{h}, \mathbf{x}, \mathbf{y}$.
8. Sample $\gamma \mid \boldsymbol{\theta}_{-\gamma}, \mathbf{h}, \mathbf{x}, \mathbf{y}$.
9. Sample $\nu \mid \boldsymbol{\theta}_{-\nu}, \mathbf{h}, \mathbf{x}, \mathbf{y}$.
10. Sample $\mathbf{h} \mid \boldsymbol{\theta}, \mathbf{x}, \mathbf{y}$.
11. Repeat steps 2–10 for a sufficiently large number of iterations.

The full conditional distributions and implementation details for each step are provided in Appendix A.2.

3.3 One-day-ahead Forecast

To obtain one-day-ahead forecasts of financial returns and volatilities, we utilize the predictive distribution within each state-space model. Let $\boldsymbol{\theta}^{(i)}$ and $\mathbf{h}^{(i)}$ represent the i th sample of parameters and latent log-volatilities in the MCMC simulation, respectively. The one-step-ahead predictive samples are then generated as follows:

1. Generate $h_{n+1}^{(i)} \mid \mathbf{x}, \mathbf{y}, \mathbf{h}^{(i)}, \boldsymbol{\theta}^{(i)} \sim N(\mu_{n+1}^{(i)}, (\sigma_{n+1}^{(i)})^2)$ where

$$\begin{aligned} \mu_{n+1}^{(i)} &= \mu^{(i)} + \phi^{(i)} h_n^{(i)} - \mu^{(i)} + \rho^{(i)} \sigma_\eta^{(i)} y_n \exp\left(-\frac{h_n^{(i)}}{2}\right), \\ (\sigma_{n+1}^{(i)})^2 &= (1 - (\rho^{(i)})^2)(\sigma_\eta^{(i)})^2. \end{aligned}$$

2. Generate $\epsilon_{n+1}^{(i)}$ from the distribution corresponding to the chosen RSV model given $\boldsymbol{\theta}^{(i)}$ and $\mathbf{h}^{(i)}$.
3. Compute $y_{n+1}^{(i)}$ as

$$y_{n+1}^{(i)} = \epsilon_{n+1}^{(i)} \exp\left(-\frac{h_{n+1}^{(i)}}{2}\right).$$

Repetition of the above procedure for M times allows us to obtain the generated samples $\{h_{n+1}^{(i)}\}_{i=1}^M$ and $\{y_{n+1}^{(i)}\}_{i=1}^M$.

One-day-ahead quantile forecasts, such as VaR and ES, can be derived from the distribution of $\{y_{n+1}^{(i)}\}_{i=1}^M$ for each model. The one-day-ahead VaR forecast at time $n + 1$ at level α , denoted by $\text{VaR}_{n+1}(\alpha)$, is defined as

$$\Pr(y_{n+1} < \text{VaR}_{n+1}(\alpha) \mid \mathcal{I}_n) = \alpha,$$

where \mathcal{I}_n denotes the information set available at time n . The corresponding ES forecast, denoted by $\text{ES}_{n+1}(\alpha)$, is given as

$$\text{ES}_{n+1}(\alpha) = E[y_{n+1} \mid y_{n+1} < \text{VaR}_{n+1}(\alpha), \mathcal{I}_n].$$

The one-day-ahead VaR and ES can be obtained as the $(1 - \alpha)$ th quantile and conditional average of $\{y_{n+1}^{(i)}\}_{i=1}^M$, respectively.

We evaluate the obtained forecasts for volatility, VaR, and ES using appropriate loss or scoring functions. To evaluate the volatility forecasts, we compute the Gaussian quasi-likelihood (QLIKE) loss function, defined as:

$$L_{QLIKE}(x, f) = \frac{x}{f} - \log \frac{x}{f} - 1,$$

where x and f represent a volatility proxy and a volatility forecast, respectively. The QLIKE loss function is robust, as defined by Patton (2011), meaning that it provides consistent rankings regardless of whether the ranking is based on true volatility or a conditionally unbiased volatility proxy. Furthermore, Patton & Sheppard (2009) demonstrated its superior power compared to the mean squared error (MSE), another robust loss function, in the predictive accuracy test proposed by Diebold & Mariano (1995).

For evaluating the forecasts of VaR and ES, we employ the joint loss function introduced by Fissler & Ziegel (2016) (FZ loss). Following the approach of Patton et al. (2019), we utilize a specific form of the FZ loss function, referred to as the FZ0 loss function, which is expressed as:

$$L_{FZ0}(y, v, e; \alpha) = -\frac{1}{\alpha e} \mathbb{1}\{y \leq v\}(v - y) + \frac{v}{e} + \log(-e) - 1, \quad (12)$$

where y , v , and e represent a return, VaR, and ES, respectively. Patton et al. (2019) demonstrated that the FZ0 loss function is unique in producing loss differences that are homogeneous of degree zero.

While average losses derived from the aforementioned loss functions offer initial insights into the forecast performance of the models in contention, they do not indicate if the differences in losses are statistically significant. To ascertain this, we utilize the conditional and unconditional predictive ability tests by Giacomini & White (2006), hereinafter referred to as GW tests, on the loss differences. The GW tests are particularly pertinent to this paper's objectives. This is because they accommodate the rolling window methods adopted in Section 4, enabling a unified assessment of both nested and non-nested models, including the RSV models described in Section 2.

For the *unconditional* predictive ability, the GW test statistic conforms to that proposed by Diebold & Mariano (1995) and is, under the null hypothesis, asymptotically standard normally distributed. For the *conditional* predictive ability, the GW test defines the null hypothesis as

$$H_{0,h} : \mathbb{E}[\Delta L_{t+1} | \mathcal{I}_t] = 0, \quad t = n, n+1, \dots, n+n_f-1,$$

where ΔL_t is the loss difference between two models at forecast date t , and \mathcal{I}_t is the information set at time t .

Given a test function \mathfrak{h}_t , a $q \times 1$ vector measurable with respect to \mathcal{I}_t (Stinchcombe & White 1998), the null hypothesis translates to

$$H_{0,h} : \mathbb{E}[\mathfrak{h}_t \Delta L_{t+1}] = 0, \quad t = n, n+1, \dots, n+n_f-1.$$

Defining $Z_{t+1} = \mathfrak{h}_t \Delta L_{t+1}$ and $\bar{Z}_{n_f} = n_f^{-1} \sum_{t=n}^{n+n_f-1} Z_{t+1}$, the alternative hypothesis becomes

$$H_{A,h} : \mathbb{E}[\bar{Z}'_{n_f}] \mathbb{E}[\bar{Z}_{n_f}] \geq d > 0, \quad \text{for sufficiently large } n_f.$$

We employ the Wald-type test statistic

$$T_{n_f} = n \bar{Z}'_{n_f} \hat{\Omega}_{n_f}^{-1} \bar{Z}_{n_f},$$

where $\hat{\Omega}_{n_f} = n_f^{-1} \sum_{t=n}^{n+n_f-1} Z_{t+1} Z'_{t+1}$ consistently estimates the variance of Z_{t+1} . Under the null, T_{n_f} follows a chi-square distribution with q degrees of freedom, χ_q^2 . At the significance level p , the null hypothesis is rejected if $T_{n_f} > \chi_{q,1-p}^2$, where $\chi_{q,1-p}^2$ is the $(1-p)$ quantile of χ_q^2 .

In practice, the selection of \mathfrak{h}_t should discern between the forecast performances of the models. Focusing on one-day-ahead forecasts, we follow the specifications of Takahashi et al. (2023) and define $\mathfrak{h}_t = (1, \Delta L_t)'$ for $t = n, n+1, \dots, n+n_f-1$. If the null is rejected, it implies that the lagged loss differences, ΔL_t , can help predict the subsequent loss differences, ΔL_{t+1} . Using \hat{b} to represent the regression coefficient of ΔL_{t+1} on \mathfrak{h}_t , the predicted loss differences $\{\hat{b}'\mathfrak{h}_t\}_{t=n}^{n+n_f-1}$ serve as indicators for assessing model performances across different time points. In Section 4, we measure relative performance by the frequency with which one model forecasts larger losses than the other, as expressed by

$$I_{n_f,0} = \frac{1}{n_f} \sum_{t=n}^{n+n_f-1} I(\hat{b}'\mathfrak{h}_t > 0). \quad (13)$$

3.4 EGARCH and REGARCH Models

Following Mitsui & Watanabe (2003), we use the Metropolis–Hastings (MH) algorithm to sample the parameters of the EGARCH and REGARCH models from the posterior distribution.⁴ First, we obtain the mode of the posterior density, and then set the proposal density to a multivariate normal distribution centered at the posterior mode, with a covariance matrix proportional to the inverse Hessian of the log posterior density evaluated at the mode, scaled by a factor of 1.2. The scaling factor is introduced to ensure sufficient exploration of the tails of the posterior distribution. Asai (2006) shows that this method is efficient for sampling the parameters of GARCH-type models from the posterior distribution.

The prior distributions for the EGARCH model are specified as follows:

$$\omega \sim \mathcal{N}(0, 100), \quad \frac{\varphi+1}{2} \sim \mathcal{B}(1, 1), \quad -\tau \sim \mathcal{G}(0.1, 0.1), \quad \gamma \sim \mathcal{G}(0.1, 0.1), \quad \nu \sim \mathcal{G}(5, 0.5)\mathbb{I}(\nu > 4),$$

For the additional parameters of the REGARCH model, the prior distributions are given by

$$-\tau_1 \sim \mathcal{G}(0.1, 0.1), \quad \tau_2 \sim \mathcal{G}(0.1, 0.1), \quad \zeta \sim \mathcal{N}(0, 10), \quad -\delta_1 \sim \mathcal{G}(0.1, 0.1), \quad \delta_2 \sim \mathcal{G}(0.1, 0.1), \quad \sigma_v^2 \sim \mathcal{IG}(2.5, 0.5).$$

The parameters τ , τ_1 , τ_2 , γ , δ_1 , and δ_2 are, in principle, unrestricted in sign. However, empirical evidence typically suggests $\tau < 0$ for EGARCH, and $\tau_1 < 0$, $\tau_2 > 0$, $\gamma > 0$, $\delta_1 < 0$, and $\delta_2 > 0$ for REGARCH models. Accordingly, we employ Gamma priors with appropriate sign restrictions to confine these parameters to economically meaningful regions.

Based on the posterior draws, one-day-ahead forecasts of volatility, VaR, and ES are obtained. This approach allows us to jointly sample both parameters and the implied conditional volatilities from the posterior distribution, thereby explicitly incorporating parameter uncertainty into volatility and return forecasts.

Importantly, this feature addresses concerns raised in the literature that ignoring parameter uncertainty in GARCH-type models may lead to unfair comparisons with stochastic volatility models; see, for example, Ardia et al. (2018), who document that accounting for parameter uncertainty improves volatility and risk forecasts in

⁴For other Bayesian approaches to REGARCH-type models and their applications to volatility and tail risk forecasting, see Chen et al. (2023).

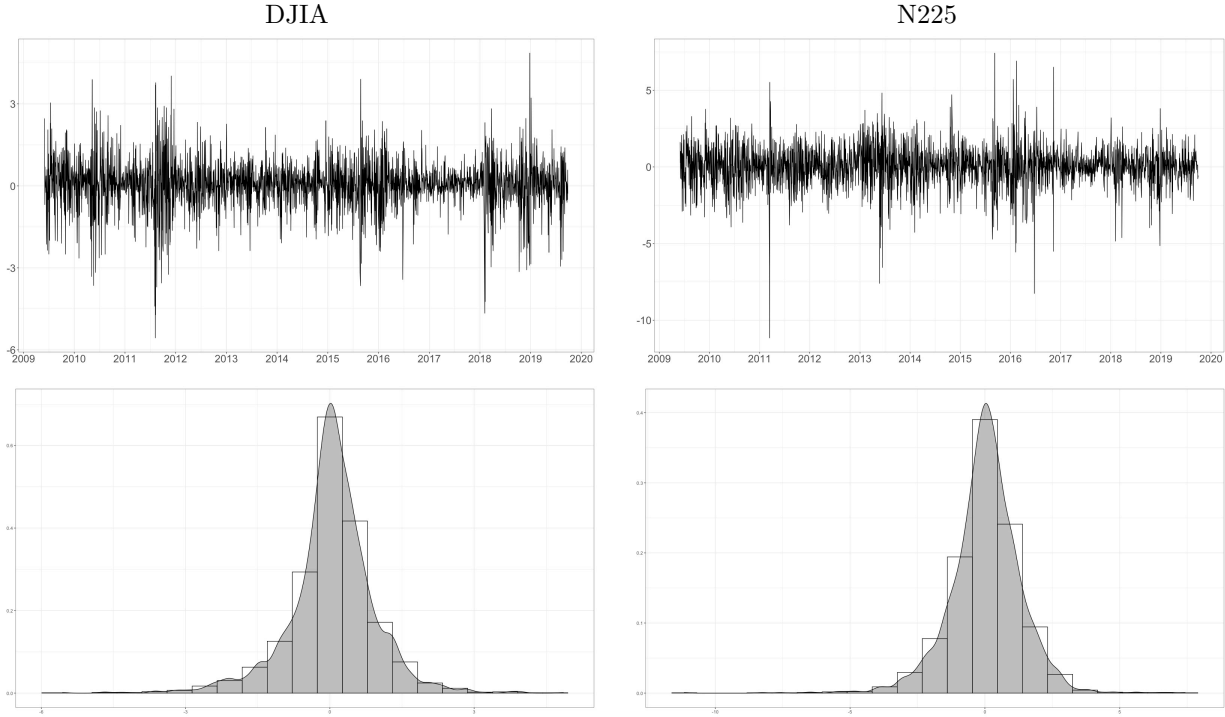


Figure 4: Time series plots (top) and histograms (bottom) of daily returns (in percentage points) for the DJIA and N225.

GARCH frameworks. By adopting a fully Bayesian estimation strategy, our framework ensures that parameter uncertainty is treated consistently across models, providing a fair basis for comparison and yielding coherent predictive distributions for one-step-ahead volatility and return forecasts.

4 Empirical Study

4.1 Data and Descriptive Statistics

We estimate the SV and RSV models described in Section 2 using daily (close-to-close) returns and RVs for two major stock indices: the DJIA and the N225. Following Liu et al. (2015), we adopt the 5-minute RV estimator, computed during trading hours only, among several available alternatives. The DJIA data are obtained from the Oxford-Man Institute’s Realized Library,⁵ while the N225 data are constructed from the Nikkei NEEDS-TICK dataset.⁶

The sample period spans from June 2009 to September 2019 for both indices. Specifically, the DJIA sample covers 2,596 trading days from June 1, 2009, to September 27, 2019, and the N225 sample includes 2,532 trading days from June 1, 2009, to September 30, 2019.

Figure 4 presents time series plots and histograms of daily returns for the DJIA and N225. Both return series exhibit considerable variation around zero and show frequent large negative returns, indicating negatively skewed distributions.

⁵The website <https://realized.oxford-man.ox.ac.uk/> is no longer accessible.

⁶See Ubukata & Watanabe (2014) for details on the construction of the N225 dataset.

Table 1: Descriptive statistics of daily returns for the DJIA and N225.

	Mean	SD	Skew	Kurt	Min	Max	JB	LB
DJIA	0.044 (0.018)	0.895	-0.448 (0.048)	6.675 (0.096)	-5.562	4.857	0.00	0.52
N225	0.033 (0.026)	1.321	-0.544 (0.049)	8.101 (0.097)	-11.153	7.426	0.00	0.55

Notes: Standard errors are shown in parentheses. JB refers to the p -value of the Jarque–Bera test. LB denotes the p -value of the Ljung & Box (1978) statistic, adjusted as in Diebold (1988).

Table 1 reports the descriptive statistics for the daily returns. The mean return is significantly different from zero for the DJIA, but not for the N225. However, since the means are negligible in magnitude, we do not demean the series in the subsequent analysis. The p -values from the Ljung–Box statistic (Ljung & Box 1978), adjusted for heteroskedasticity as in Diebold (1988), do not reject the null of no autocorrelation up to 10 lags in either series. This allows us to estimate the models directly using raw returns.

Both return series are characterized by significantly negative skewness and high kurtosis, suggesting leptokurtic distributions—a stylized fact in financial returns. The Jarque–Bera (JB) statistic confirms that normality is strongly rejected for both series. These empirical features motivate our use of skewed- t distributions for the return innovations, as discussed in Section 2.

Figure 5 shows the time series and histograms of the 5-minute RVs and their logarithmic transformations for both indices. Both series exhibit strong temporal clustering, high persistence, and occasional sharp spikes.⁷ These spikes lead to positively skewed distributions in the log-RVs.

Table 2 summarizes the descriptive statistics of the log-RVs. The Ljung–Box test strongly rejects the null of no autocorrelation, confirming the presence of volatility clustering in both markets. The distributions are positively skewed and leptokurtic, and the JB test rejects the normality of the log-RVs. This finding is inconsistent with the normality assumption for the error term u_t in equation (5), which we retain for tractability.

Remark. The positive skewness of the log-RVs suggests that more flexible innovations could be considered. In particular, specifying u_t as skew- t would allow the model to directly accommodate distributional asymmetry. Incorporating such an extension into the RSV framework would require additional development, so we leave this promising direction for future work.

4.2 Competing Models

We evaluate the forecasting performance of the following RSV models, which differ in the distributional assumption for ϵ_t :

1. **RSV-N:** ϵ_t follows a normal distribution.

⁷For the DJIA, the largest RV spike occurred on August 24, 2015, amid heightened market turbulence (see *The New York Times*: <https://www.nytimes.com/2015/08/25/business/dealbook/daily-stock-market-activity.html>). For the N225, the most notable spike on March 15, 2011, reflects the aftermath of the Great East Japan Earthquake on March 11, 2011.

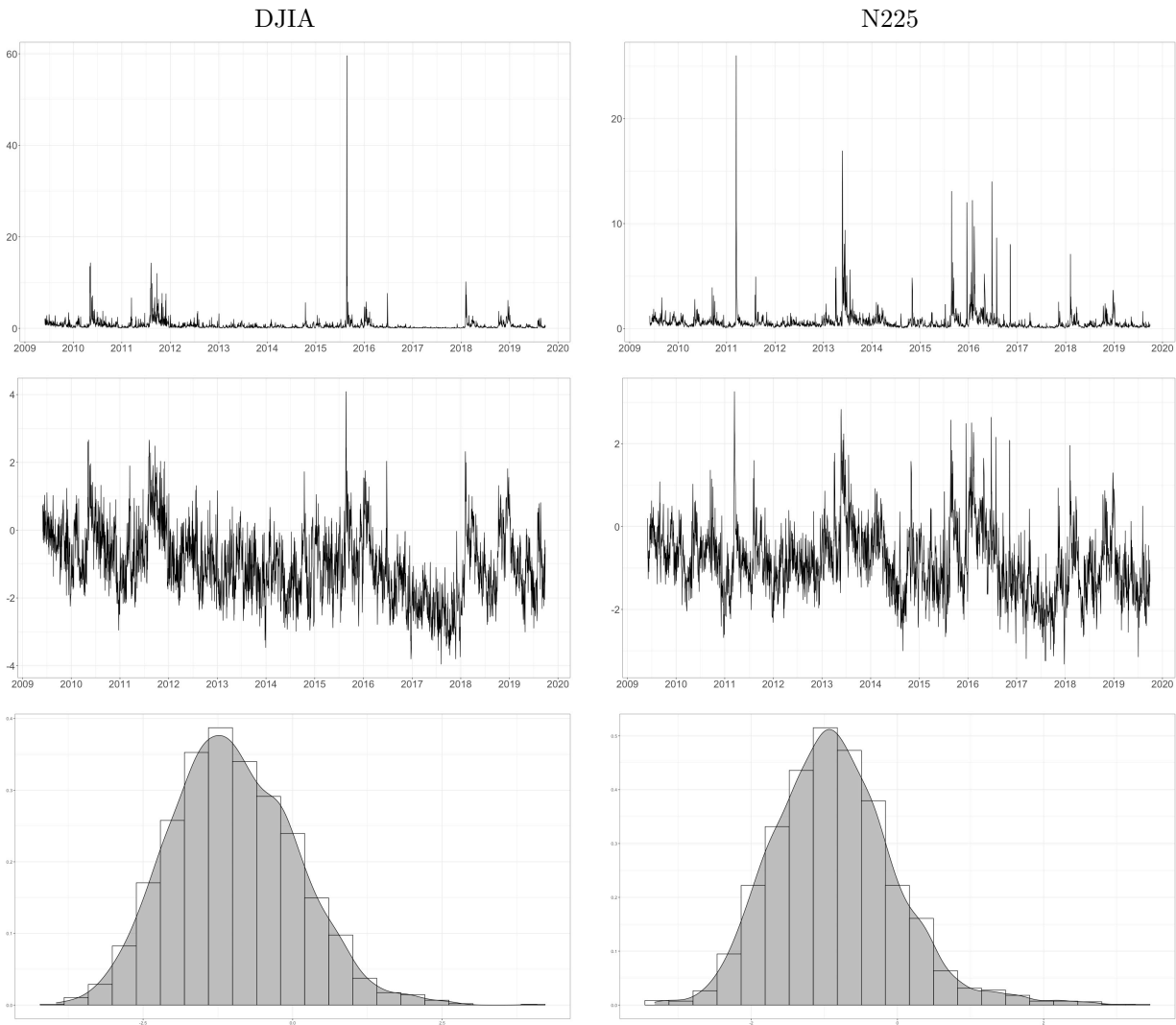


Figure 5: Time series plots of 5-minute RVs (top), their logarithms (middle), and corresponding histograms (bottom) for the DJIA and N225.

Table 2: Descriptive statistics of the logarithms of 5-minute RVs for the DJIA and N225.

	Mean	SD	Skew	Kurt	Min	Max	JB	LB
DJIA	−0.987 (0.021)	1.048	0.317 (0.048)	3.177 (0.096)	−3.953	4.087	0.00	0.00
N225	−0.858 (0.017)	0.844	0.589 (0.049)	4.219 (0.097)	−3.321	3.258	0.00	0.00

Notes: Standard errors are shown in parentheses. See Table 1 for additional details.

2. **RSV-T**: ϵ_t follows a Student’s t distribution.
3. **RSV-GH-ST**: ϵ_t follows the GH skew- t distribution.
4. **RSV-AZ-SN**: ϵ_t follows the Azzalini skew normal distribution.
5. **RSV-AZ-ST**: ϵ_t follows the Azzalini skew- t distribution.
6. **RSV-FS-SN**: ϵ_t follows the Fernández–Steel skew normal distribution.
7. **RSV-FS-ST**: ϵ_t follows the Fernández–Steel skew- t distribution.

The prior distributions for the common parameters are specified as follows:

$$\begin{aligned} \mu &\sim \mathcal{N}(0, 100), & \frac{\phi + 1}{2} &\sim \mathcal{B}(1, 1), & \frac{\rho + 1}{2} &\sim \mathcal{B}(1, 1), & \sigma_\eta^2 &\sim \mathcal{IG}(0.05, 0.05), \\ \xi &\sim \mathcal{N}(0, 10), & \sigma_u^2 &\sim \mathcal{IG}(2.5, 0.1). \end{aligned}$$

These priors are chosen to be weakly informative and follow standard specifications commonly adopted in the stochastic volatility literature, allowing the data to dominate posterior inference.

For the additional distributional parameters, we set:

$$\nu \sim \mathcal{G}(5, 0.5) \mathbb{1}\{\nu > 4\}, \quad \beta \sim \mathcal{N}(0, 1), \quad \frac{\delta + 1}{2} \sim \mathcal{B}(1, 1), \quad \gamma \sim G(1, 1).$$

The truncation $\nu > 4$ ensures the existence of the fourth moment, which is required for volatility forecasting and risk evaluation.

In addition, to isolate the contribution of RV, we estimate standard SV models with the same innovation distributions as in the RSV specifications. These include SV-N, SV-T, SV-GH-ST, SV-AZ-SN, SV-AZ-ST, SV-FS-SN, and SV-FS-ST, mirroring the distributional assumptions used in the RSV models. This setup allows us to directly assess the added value of incorporating RV in terms of predictive performance.

To further benchmark the RSV models, we also consider the EGARCH and REGARCH models described in Sections 2.8 and 2.9, respectively. These models are estimated within a Bayesian framework using the MH algorithm under standard normal and Student’s t innovations. One-day-ahead forecasts of volatility, VaR, and ES are then obtained based on the posterior draws. For other Bayesian approaches to RGARCH-type models and their applications to volatility and tail risk forecasting, see Chen et al. (2023).

4.3 Out-of-sample Forecasting

Following the approach of Takahashi et al. (2016), we implement a rolling window estimation procedure to evaluate the out-of-sample performance of each model. The window size is kept fixed throughout the forecasting period. For the DJIA, we use a window of 1,993 observations, generating forecasts from May 1, 2017, to September 27, 2019. For the N225, the window consists of 1,942 observations, with forecast dates ranging from May 1, 2017, to September 30, 2019. After each estimation step, we produce one-day-ahead forecasts of volatility, VaR, and ES.

At each forecast point, we draw 15,000 predictive samples from the posterior predictive distribution. For the SV and RSV models, we compute both the posterior means and medians of the volatility forecasts.⁸ Additionally, we calculate predictive quantiles of the return distribution to obtain VaR and ES estimates. This procedure yields 603 forecasts for the DJIA and 590 for the N225, covering the period from early May 2017 to late September 2019.

4.3.1 Volatility Forecasts

To evaluate the accuracy of volatility forecasts, we compute the average loss using the QLIKE loss function, as described in Section 3.3. The QLIKE loss is known for its robustness, yielding model rankings that align closely with those based on latent volatility, provided the proxy is conditionally unbiased. Simulation evidence from Patton & Sheppard (2009) and empirical findings by Hansen & Lunde (2005) and Patton (2011) suggest that QLIKE has greater statistical power than MSE to discriminate between models.

To mitigate market microstructure noise, we employ multiple volatility proxies: realized kernel (RK) with a flat-top Tukey-Hanning₂ kernel (Barndorff-Nielsen et al. 2008), bipower variation (BV) (Barndorff-Nielsen & Shephard 2004), and median realized volatility (Med) (Andersen et al. 2012), in addition to the standard 5-minute realized volatility (RV5).

To correct for biases due to non-trading hours, we adopt the adjustment method proposed by Hansen & Lunde (2005), as given in equation (1), using the following correction factor:

$$c_{HL} = \frac{\sum_{s=t-n+1}^t (y_s - \bar{y})^2}{\sum_{s=t-n+1}^t x_s}, \quad \bar{y} = \frac{1}{n} \sum_{s=t-n+1}^t y_s,$$

where n is the window size and x_s denotes the volatility proxy at time s .

Figures 6 and 7 display the log-scale volatility forecasts alongside the adjusted RV5 series for the DJIA and N225. For the DJIA, SV model forecasts—especially those from the SV-GH-ST specification—exhibit pronounced volatility spikes. Across both indices, forecast patterns are more homogeneous within model families (e.g., SV, RSV, EGARCH, REGARCH) than across different distributional assumptions, indicating that model structure plays a more dominant role than distributional form. Figures with alternative realized volatility proxies are omitted for brevity, as the volatility forecasts are identical.

Table 3 reports QLIKE scores across all models and volatility proxies. An asterisk (*) denotes inclusion in the 90% model confidence set (MCS) of Hansen et al. (2011).⁹ Overall, RSV and REGARCH models attain lower QLIKE scores than SV and EGARCH counterparts. For the DJIA, REGARCH-T achieves the lowest scores under RV5 and BV, while SV-FS-ST achieves the lowest scores under RK and Med. For the N225, RSV models dominate

⁸We report the median rather than the mean for volatility forecasts of SV models, as the posterior predictive distribution of the one-step-ahead volatility forecast occasionally exhibits heavy tails, which can disproportionately inflate the posterior mean.

⁹The rolling window scheme satisfies the stationarity assumption required by the MCS bootstrap. We use 1,000 bootstrap replications with a block size of 10. See Hansen et al. (2011), Section 4.3.

Table 3: QLIKE scores of volatility forecasts for the DJIA and N225.

	DJIA				N225				Average	
	RV5	RK	BV	Med	RV5	RK	BV	Med	Score	Rank
SV-N	0.349	0.532	0.587	0.641	0.176	0.177	0.169	0.169	0.350	14.8
SV-T	0.329	0.502	0.563	0.620	0.189	0.192	0.178	0.172	0.343	15.2
SV-AZ-SN	0.362	0.557	0.617	0.680	0.183	0.183	0.174	0.174	0.366	16.2
SV-AZ-ST	0.337	0.519	0.580	0.646	0.189	0.191	0.179	0.174	0.352	16.0
SV-FS-SN	0.273*	0.392*	0.446*	0.502*	0.165	0.170	0.159	0.146	0.282	7.5
SV-FS-ST	0.267*	0.378*	0.432*	0.487*	0.172	0.178	0.165	0.148	0.278	7.9
SV-GH-ST	0.346	0.522	0.582	0.657	0.188	0.189	0.181	0.174	0.355	16.5
RSV-N	0.245*	0.454	0.489*	0.571	0.043*	0.047	0.047*	0.043*	0.242	7.1
RSV-T	0.231*	0.433*	0.469*	0.548*	0.043*	0.048	0.047*	0.041*	0.233	5.9
RSV-AZ-SN	0.240*	0.449	0.485*	0.566	0.043*	0.048	0.047*	0.043*	0.240	6.2
RSV-AZ-ST	0.227*	0.425*	0.462*	0.540*	0.043*	0.049	0.048*	0.041*	0.229	5.0
RSV-FS-SN	0.252*	0.471	0.505	0.589	0.042*	0.046*	0.047*	0.045	0.250	7.5
RSV-FS-ST	0.242*	0.452	0.487*	0.569	0.042*	0.047	0.047*	0.043*	0.241	6.4
RSV-GH-ST	0.223*	0.416*	0.453*	0.531*	0.044	0.049	0.048	0.041*	0.226	4.9
EGARCH-N	0.321	0.431*	0.499*	0.563*	0.166	0.174	0.161	0.141	0.307	10.6
EGARCH-T	0.303*	0.401*	0.465*	0.516*	0.184	0.193	0.178	0.155	0.299	11.0
REGARCH-N	0.240*	0.417*	0.464*	0.543*	0.057	0.063	0.060	0.045*	0.236	7.2
REGARCH-T	0.221*	0.382*	0.428*	0.504*	0.057	0.063	0.060	0.044*	0.220	5.0

Notes: An asterisk (*) indicates that the model belongs to the 90% MCS. The average columns report the mean QLIKE scores and ranks across the two indices.

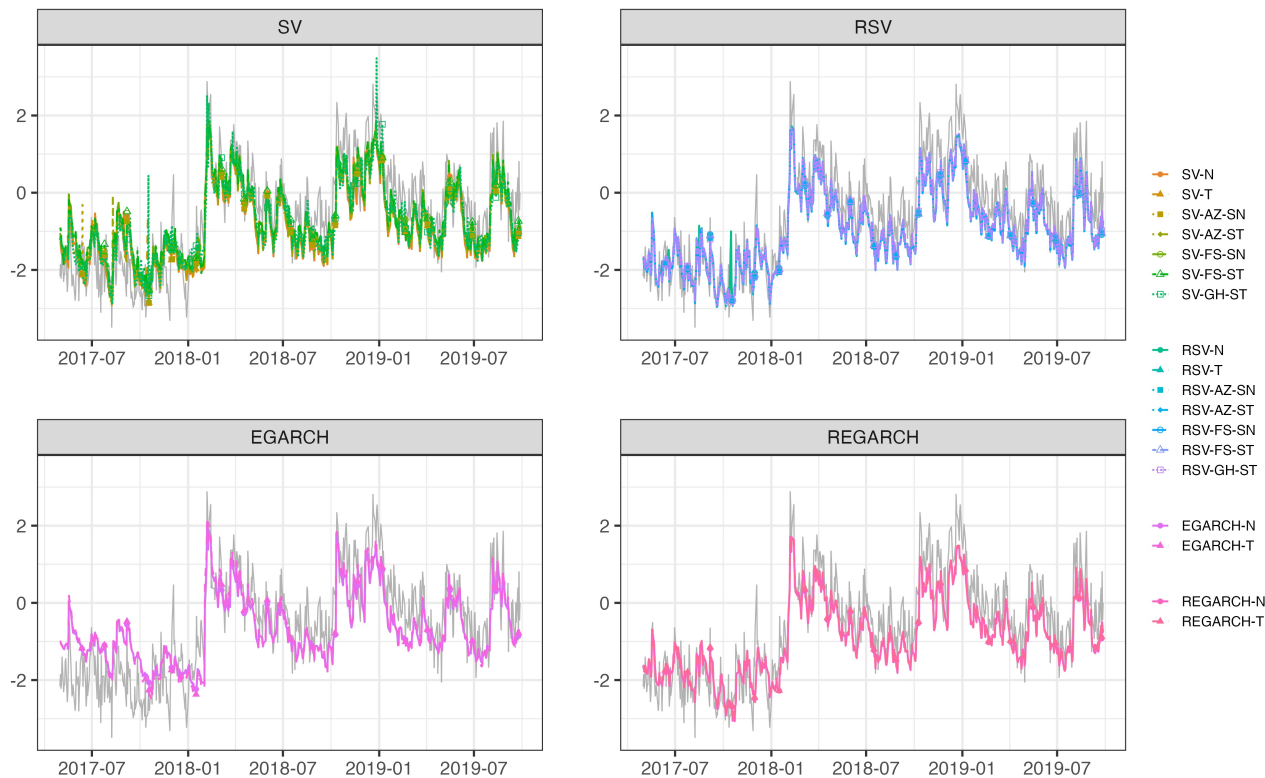


Figure 6: Log-scale volatility forecasts together with the adjusted RV5 for the DJIA.

REGARCH models. On average, the RSV-GH-ST model delivers the best performance across indices, followed by the RSV-AZ-ST and REGARCH-T models, with very small margins.

To assess time-varying performance, Figures 8 and 9 depict cumulative loss differences (CLDs) relative to SV-N, based on RV5 as the volatility proxy.¹⁰ Positive values indicate superior performance. The RSV and REGARCH models consistently outperform the SV and EGARCH models across the entire forecast horizon for both the DJIA and N225, underscoring the value of incorporating realized volatility in prediction. In particular, the performance advantage of RSV and REGARCH is stable over time, with clear and persistent separations from the SV and EGARCH benchmarks in both markets.

Figures 10 and 11 visualize the GW test results, based on RV5 as the volatility proxy, using heatmaps.¹¹ The lower triangular part presents unconditional GW test statistics, whereas the upper triangular part reports win proportions as defined in Equation (13). Lower values (green) favor the row model, while larger values (orange) indicate better performance by the column model. Double and single asterisks (** and *) denote significance at the 1% and 5% levels, respectively, based on unconditional and conditional GW test p-values for the lower and upper triangular parts.

For the DJIA, SV-FS-SN and SV-FS-ST outperform other SV variants and EGARCH models, while RSV and REGARCH models generally dominate SV and EGARCH. RSV-AZ-ST is significantly superior to even FS-type SV models, although RSV and REGARCH differ less markedly. Conditional GW tests further confirm the superiority

¹⁰Results based on alternative realized volatility proxies are reported in the Supplementary Material.

¹¹Results based on alternative realized volatility proxies are reported in the Supplementary Material.

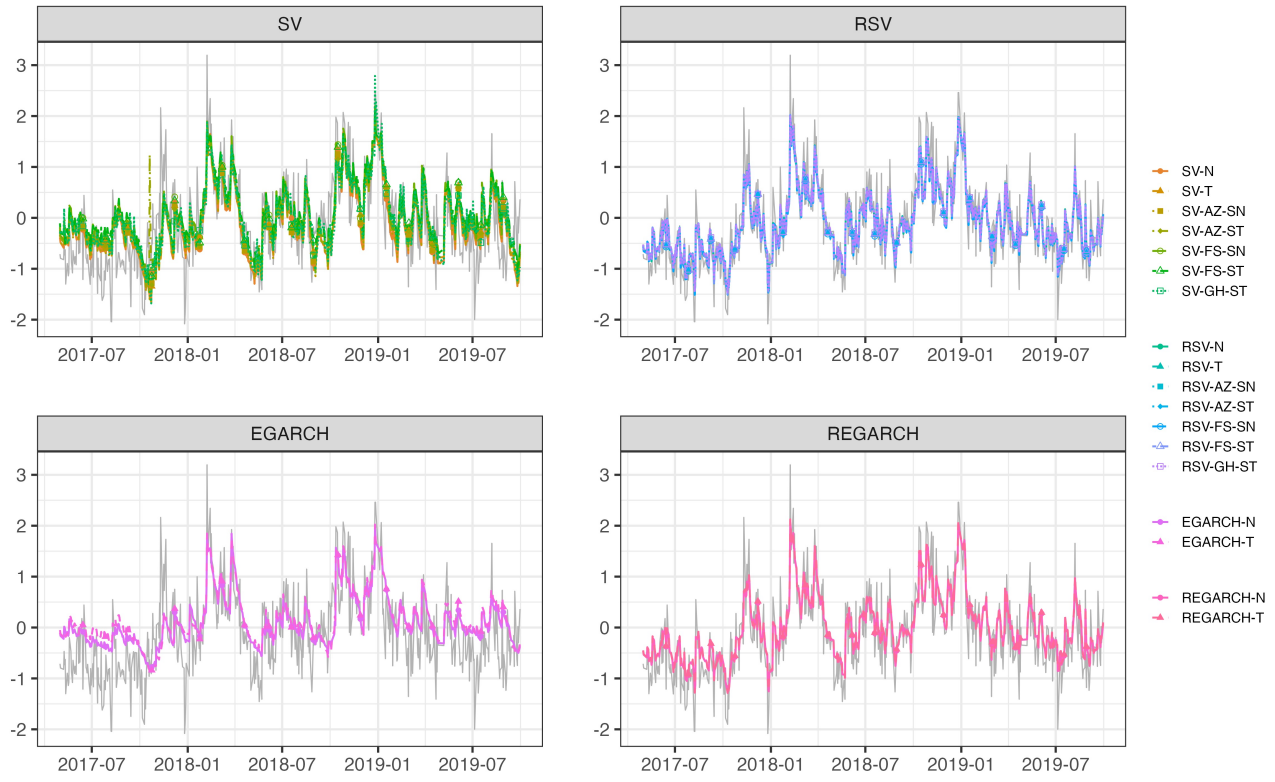


Figure 7: Log-scale volatility forecasts together with the adjusted RV5 for the N225.

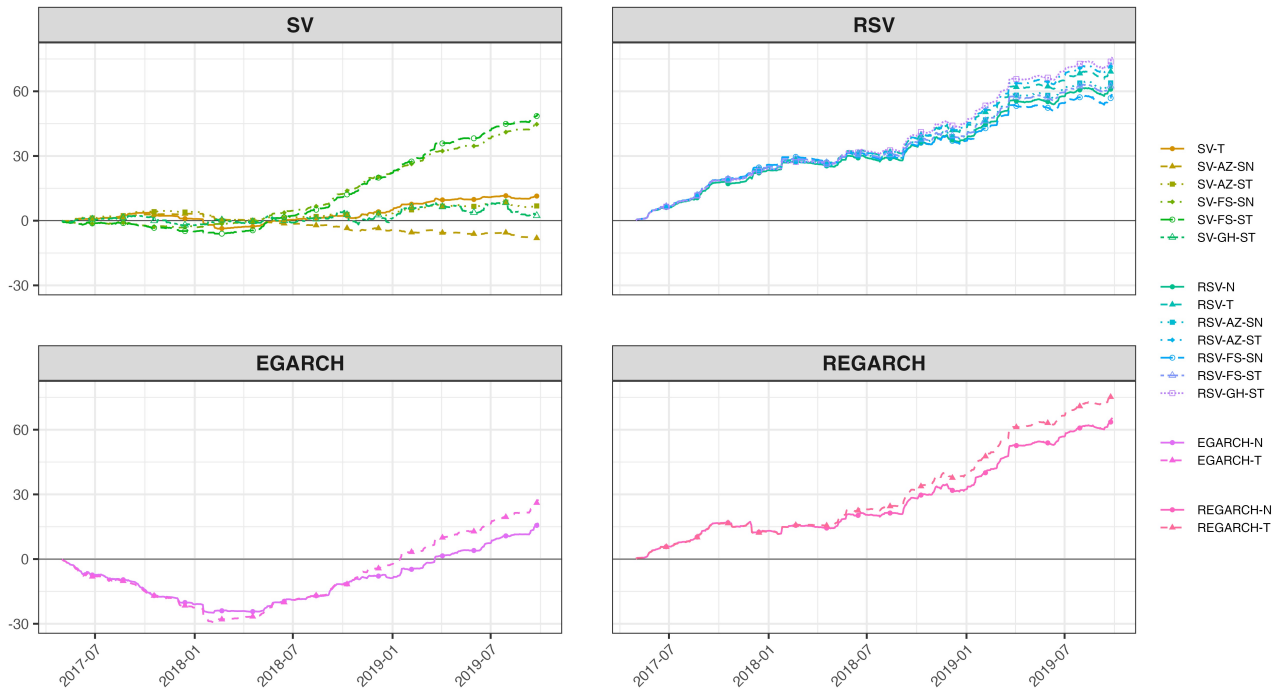


Figure 8: Cumulative QLIKE loss differences relative to the SV-N model, based on RV5 as the volatility proxy, for the DJIA.

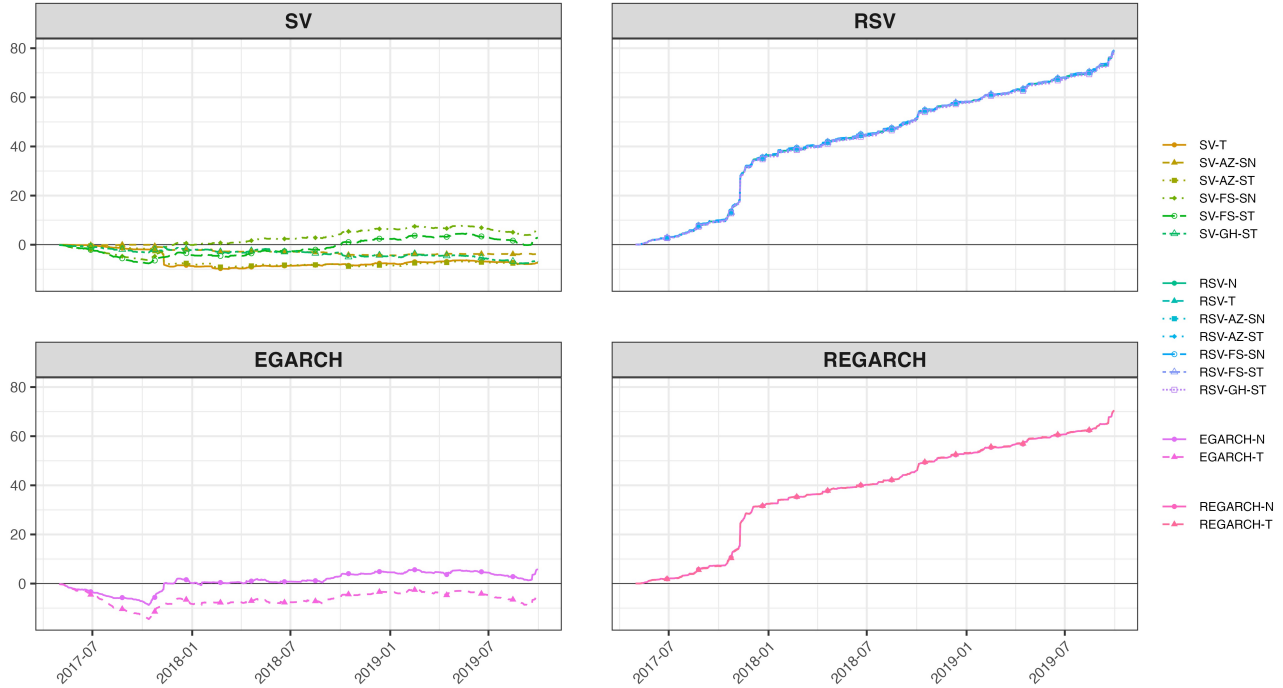


Figure 9: Cumulative QLIKE loss differences relative to the SV-N model, based on RV5 as the volatility proxy, for the N225.

of RSV models, particularly over SV and EGARCH.

For the N225, both unconditional and conditional GW tests support the outperformance of RSV and REGARCH over SV and EGARCH, with RSV models often exceeding REGARCH. FS-type distributions enhance forecast accuracy within the SV and RSV frameworks. Among RSV specifications, RSV-GH-ST lags significantly.

In summary, incorporating RV substantially improves forecast accuracy, with RSV and REGARCH models consistently outperforming SV and EGARCH counterparts. These results corroborate prior findings (Takahashi et al. 2023, 2024). The added flexibility of FS-type distributions further improves forecast accuracy, especially in SV models. The next section examines whether these improvements carry over to tail risk measures, including VaR and ES.

4.3.2 VaR and ES forecasts

Figure 12 illustrates the 1% VaR and ES forecasts for the DJIA and N225 indices, as generated by the RSV-AZ-ST and REGARCH-T models. VaR violations—instances where realized returns fall below the forecasted VaR—are observed across both models, occurring during periods of market stress such as early 2018 and late 2019, as well as during more tranquil phases. For clarity, the forecasts from other models, which follow similar patterns with minor differences in scale, are omitted.

Table 4 presents the empirical violation rates ($\hat{\alpha}$), the average FZ0 loss values (as defined in Equation (12)), and the corresponding p -values from the dynamic quantile (DQ) test of Engle & Manganelli (2004) and the MCS procedure for the DJIA. At the 1% level, all models tend to underestimate tail risk, as indicated by violation rates exceeding the nominal level. In contrast, for $\alpha = 5\%$, the violation rates are generally well aligned with the target.



Figure 10: Pairwise comparison of GW tests on QLIKE of volatility forecasts, based on RV5 as the volatility proxy, for the DJIA. The lower triangular part reports unconditional GW test statistics, while the upper triangular part shows win proportions as defined in Equation (13). Lower values (green) indicate superior performance of the row model, whereas higher values (orange) favor the column model. Double and single asterisks (** and *) denote statistical significance at the 1% and 5% levels, respectively, based on unconditional GW test p-values for the lower triangular part and conditional GW test p-values for the upper triangular part.

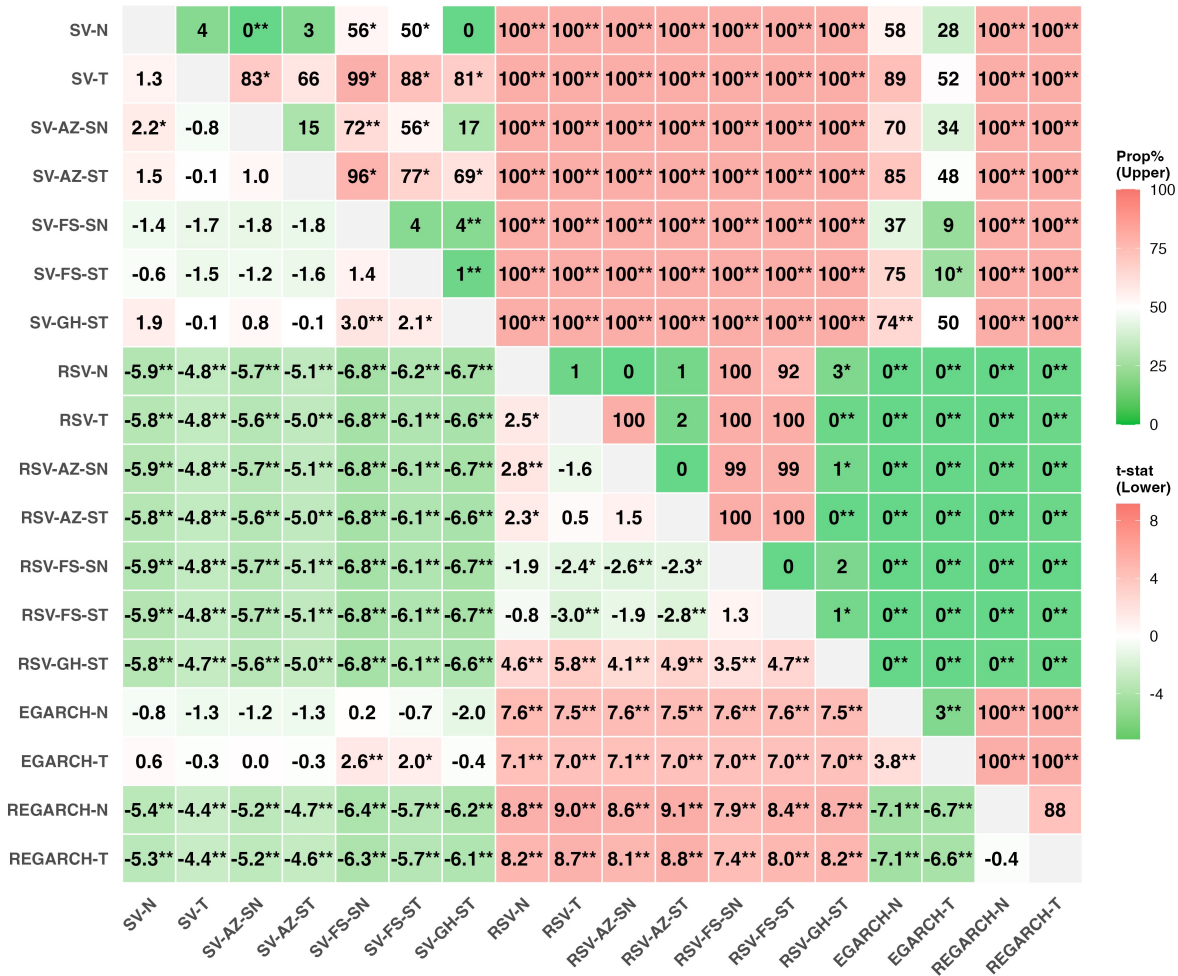


Figure 11: Pairwise comparison of GW tests on QLIKE of volatility forecasts, based on RV5 as the volatility proxy, for the N225. See Figure 10 for additional details.

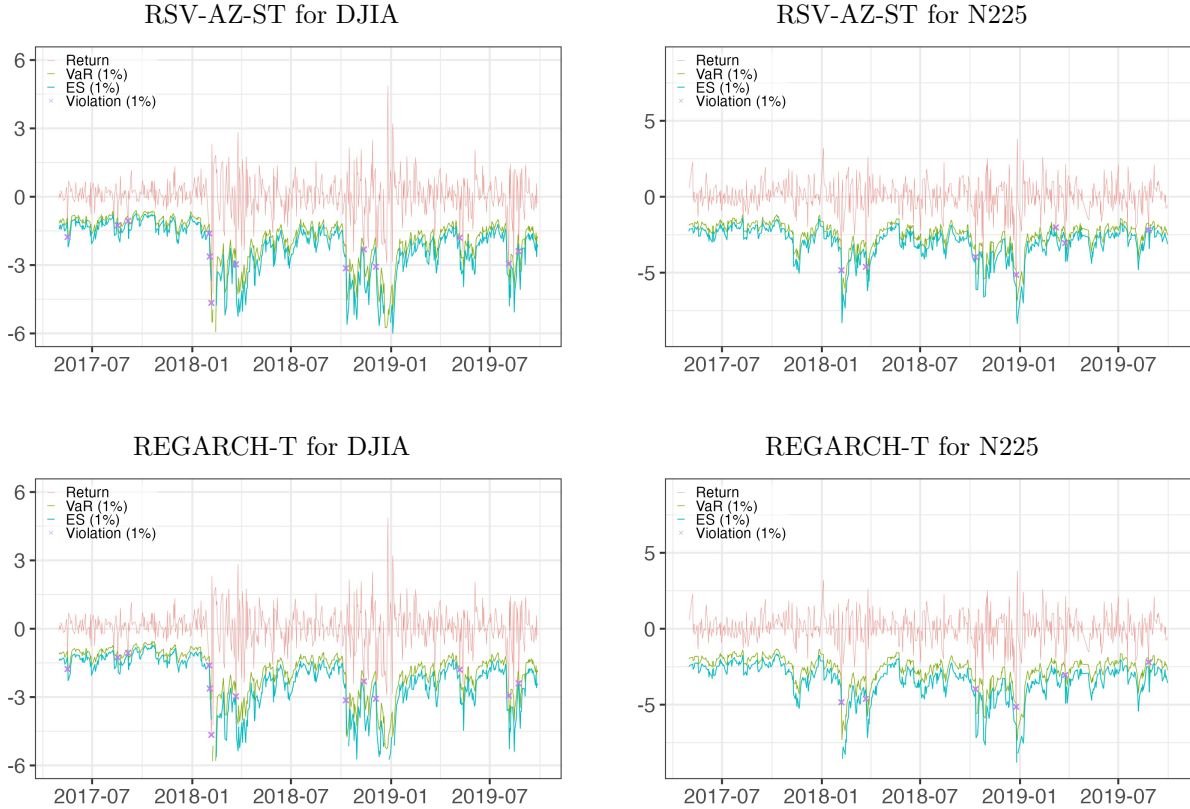


Figure 12: 1% VaR and ES forecasts of RSV-FS-ST and REGARCH-T models for the DJIA and N225.

Regarding predictive accuracy based on the FZ0 loss, the SV-AZ-SN and RSV-AZ-ST models achieve the lowest losses at $\alpha = 1\%$ and 5% , respectively. Most models—except SV-GH-ST at $\alpha = 5\%$ —are included in the 75% MCS, indicating comparable performance in tail risk forecasting.

The DQ test, which regresses VaR violations on a constant, the forecasted VaR, and a one-period lagged violation indicator, suggests that the SV-FS-ST and SV-GH-ST models fail the independence test at the 1% level. This implies potential misspecification in their dynamic structures.

Table 5 summarizes the results for the N225. Across both target levels, most models yield violation rates consistent with the nominal levels. The RSV-AZ-ST model again performs best in terms of FZ0 loss, and both RSV and REGARCH models are included in the 75% MCS. Notably, the SV-GH-ST and EGARCH-N models fall outside the MCS at the 5% level, while the EGARCH-T model remains outside the MCS even at the 1% level, indicating weaker predictive accuracy. Unlike the DJIA case, none of the models are rejected by the DQ test for the N225.

Figures 13 and 14 show the CLDs relative to the SV-N benchmark for the DJIA. At the 1% level, REGARCH models perform poorly during the early 2018 volatility spike. From mid-2018 onwards, however, REGARCH and RSV models consistently outperform SV and EGARCH models at the 5% level, highlighting the benefits of incorporating realized volatility into tail risk forecasting. Consistent results are obtained for the N225, reinforcing the benefit of incorporating RV, and are therefore reported in the Supplementary Material.

GW test results



Figure 13: Cumulative loss differences (FZ0) relative to the SV-N model ($\alpha = 1\%$) for the DJIA.

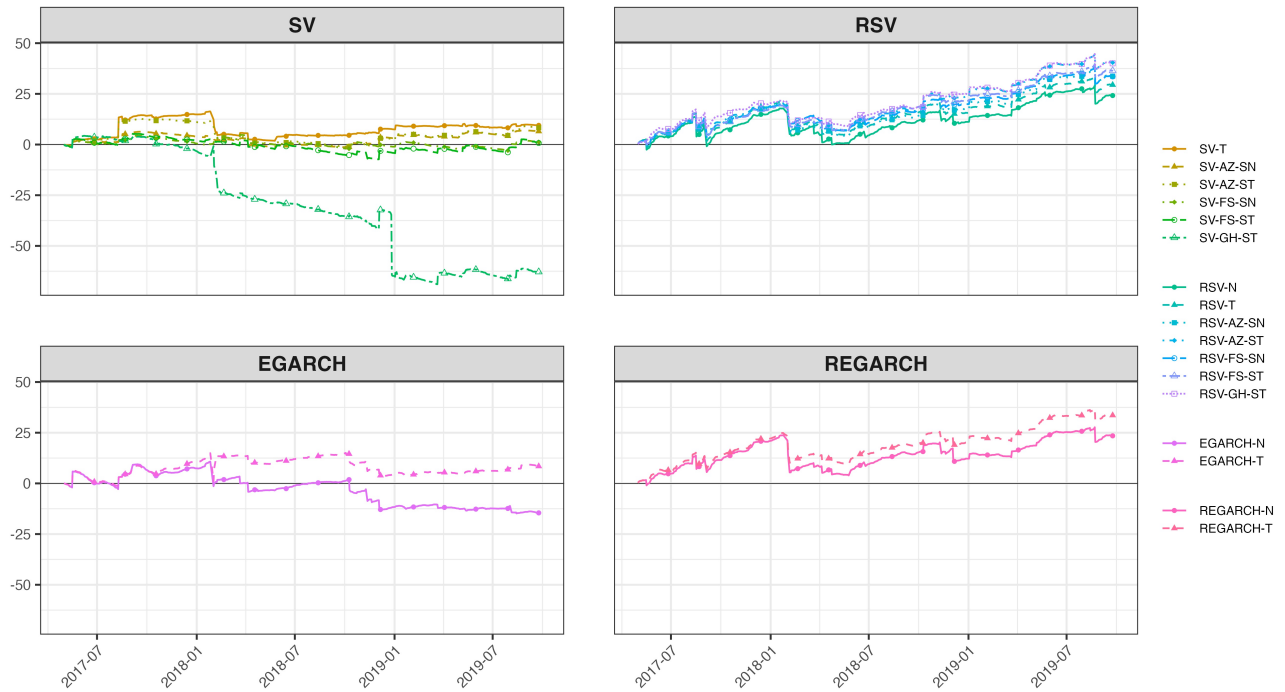


Figure 14: Cumulative loss differences (FZ0) relative to the SV-N model ($\alpha = 5\%$) for the DJIA.

Table 4: Violation rates and FZ0 losses of VaR and ES forecasts for the DJIA.

	$\alpha = 1\%$				$\alpha = 5\%$			
	$\hat{\alpha}$	p_{DQ}	FZ0	p_{MCS}	$\hat{\alpha}$	p_{DQ}	FZ0	p_{MCS}
SV-N	2.32	0.17	1.0714	1.00	4.64	0.97	0.5965	0.70
SV-T	1.99	0.12	1.0483	1.00	4.31	0.89	0.5809	1.00
SV-AZ-SN	1.82	0.08	0.9698	1.00	4.31	0.89	0.5858	0.97
SV-AZ-ST	1.82	0.08	1.0180	1.00	4.31	0.65	0.5830	0.99
SV-FS-SN	1.49	0.93	0.9786	1.00	4.15	0.84	0.5947	0.86
SV-FS-ST	1.49	0.02	0.9899	1.00	4.15	0.84	0.5954	0.79
SV-GH-ST	1.33	0.01	1.1224	1.00	4.31	0.92	0.7012	0.11
RSV-N	2.82	0.23	1.2345	0.34	5.80	0.67	0.5567	1.00
RSV-T	2.65	0.23	1.1709	0.72	5.80	0.57	0.5480	1.00
RSV-AZ-SN	2.32	0.19	1.1275	0.98	5.47	0.67	0.5411	1.00
RSV-AZ-ST	2.16	0.16	1.0780	1.00	5.14	0.68	0.5299	1.00
RSV-FS-SN	2.32	0.19	1.0490	1.00	5.64	0.64	0.5411	1.00
RSV-FS-ST	2.49	0.21	1.0958	1.00	5.31	0.63	0.5365	1.00
RSV-GH-ST	1.99	0.12	1.0186	1.00	4.98	0.58	0.5307	1.00
EGARCH-N	2.49	0.21	1.2822	0.35	4.64	0.85	0.6206	0.27
EGARCH-T	1.49	0.92	1.0605	1.00	4.98	0.91	0.5826	1.00
REGARCH-N	3.15	0.24	1.3048	0.31	5.31	0.78	0.5580	1.00
REGARCH-T	2.16	0.16	1.0476	1.00	5.47	0.81	0.5413	1.00

Notes: $\hat{\alpha}$ represents the empirical violation rate (%). p_{DQ} indicates the p -value of the dynamic quantile test of Engle & Manganelli (2004). FZ0 denotes the average FZ0 loss. p_{MCS} indicates the MCS p -value.

Figures 15 and 16 visualize the GW test results based on the FZ0 loss function for the DJIA using heatmaps. The interpretation of the lower and upper triangular elements follows that of volatility forecasts in Section 4.3.1. The main findings are summarized below.

At the 1% level, the *unconditional* GW test reveals that SV-AZ-SN significantly outperforms SV-N, while SV-GH-ST is significantly outperformed by SV-AZ-SN. Among RSV models, RSV-N exhibits inferior predictive accuracy relative to all other RSV specifications. For EGARCH models, EGARCH-T significantly outperforms EGARCH-N, while REGARCH models are significantly outperformed by several RSV specifications.

The *conditional* GW test at the 1% level indicates that SV-T performs significantly worse than SV-AZ-SN, but better than EGARCH-N. RSV-N is significantly outperformed by RSV-T, RSV-AZ-SN, RSV-FS-SN, and RSV-FS-ST. Moreover, RSV models with skew(-t) distributions significantly outperform REGARCH-N and REGARCH-T.

At the 5% level, the *unconditional* test shows that SV-GH-ST is significantly outperformed by SV-T, SV-AZ-SN, SV-AZ-ST, and all RSV and REGARCH models. In addition, RSV-GH-ST outperforms SV-N, and RSV-AZ-ST significantly outperforms RSV-AZ-SN. Among EGARCH and REGARCH models, the T specifications consistently outperform their N counterparts.

Table 5: Violation rates and FZ0 losses of VaR and ES forecasts for the N225.

	$\alpha = 1\%$				$\alpha = 5\%$			
	$\hat{\alpha}$	p_{DQ}	FZ0	p_{MCS}	$\hat{\alpha}$	p_{DQ}	FZ0	p_{MCS}
SV-N	1.02	1.00	1.2034	0.94	3.90	0.85	0.8163	0.45
SV-T	0.85	0.99	1.2158	0.57	3.39	0.64	0.7973	1.00
SV-AZ-SN	0.85	0.99	1.2047	0.93	3.56	0.71	0.8178	0.52
SV-AZ-ST	0.85	0.99	1.2053	0.96	3.56	0.75	0.8156	0.60
SV-FS-SN	0.85	0.98	1.1979	1.00	3.39	0.65	0.8105	0.87
SV-FS-ST	0.85	0.97	1.1870	1.00	3.39	0.64	0.8093	0.94
SV-GH-ST	0.68	0.96	1.2720	0.30	4.24	0.87	0.8846	0.00
RSV-N	1.53	0.83	1.1468	1.00	5.08	0.99	0.7854	1.00
RSV-T	1.36	0.87	1.1357	1.00	4.92	0.98	0.7833	1.00
RSV-AZ-SN	1.36	0.84	1.1544	1.00	4.75	0.97	0.7857	1.00
RSV-AZ-ST	1.19	0.82	1.1260	1.00	4.75	0.97	0.7822	1.00
RSV-FS-SN	1.19	0.83	1.1533	1.00	5.25	0.99	0.7887	1.00
RSV-FS-ST	1.19	0.83	1.1301	1.00	5.25	1.00	0.7865	1.00
RSV-GH-ST	1.19	0.83	1.1283	1.00	4.75	0.98	0.7871	1.00
EGARCH-N	1.02	0.95	1.2944	0.49	3.56	0.72	0.8480	0.00
EGARCH-T	1.02	0.90	1.2448	0.17	3.56	0.67	0.8319	0.15
REGARCH-N	1.69	0.70	1.1744	1.00	4.41	0.94	0.7988	1.00
REGARCH-T	1.02	0.78	1.1343	1.00	4.75	0.98	0.7922	1.00

Notes: See Table 4 for additional details.

For the *conditional* GW test at the 5% level, SV-GH-ST is significantly outperformed by RSV-AZ-SN, RSV-AZ-ST, RSV-FS-SN, RSV-FS-ST, and RSV-GH-ST. RSV-T performs significantly worse than RSV-GH-ST. EGARCH-N is significantly outperformed by EGARCH-T, and REGARCH-N by REGARCH-T.

In summary, the results highlight the superior performance of RSV models—especially RSV-AZ-ST, RSV-FS-ST, and RSV-GH-ST—compared to SV, EGARCH, and REGARCH models, particularly under stringent risk levels. The inclusion of RV consistently improves the accuracy of tail risk forecasts. Moreover, as the FZ0 loss function jointly evaluates VaR and ES by emphasizing tail behavior, these results underscore the importance of capturing skewness and heavy tails in return distributions. The results for the N225 are broadly consistent with those for the DJIA at the 5% level and are therefore reported in the Supplementary Material.

Distributional characteristics of daily return forecasts under RSV models

To explore differences among RSV models, we examine the distributional properties of their one-day-ahead return forecasts. Table 6 reports the mean and standard deviation of skewness, kurtosis, and several lower percentiles (0.1%, 1%, 5%, and 10%) based on the posterior predictive distributions. Figures 17 and 18 present the histograms of these statistics across the forecast horizon for the DJIA and N225, respectively.

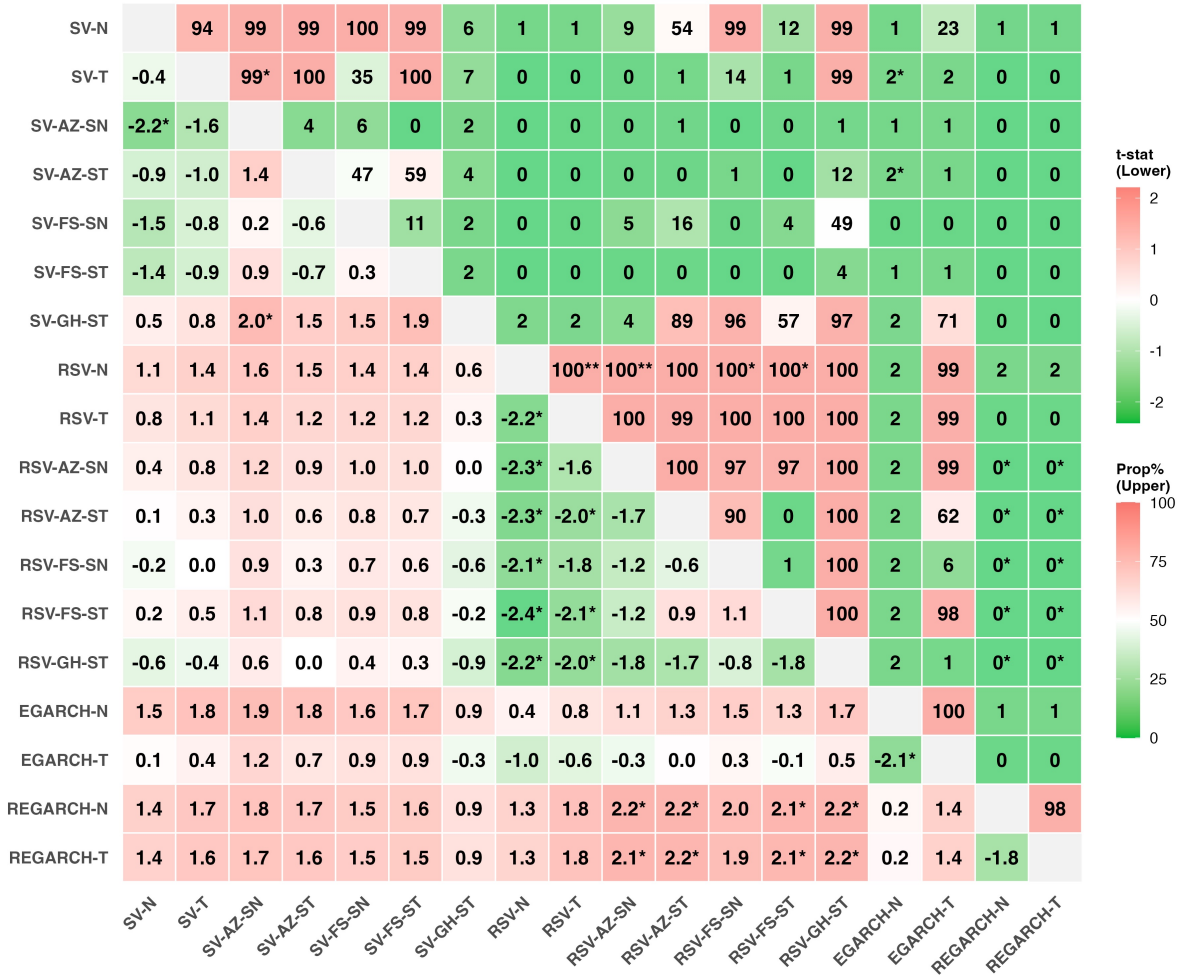


Figure 15: Pairwise comparison of GW tests on FZ0 loss of VaR and ES forecasts ($\alpha = 1\%$) for the DJIA. See Figure 10 for additional details.

For both indices, the RSV-FS-SN and RSV-GH-ST models tend to generate more negatively skewed and heavy-tailed predictive distributions, as reflected in their higher kurtosis and lower percentile values. Among all models, RSV-GH-ST exhibits the most negative skewness, while RSV-FS-SN displays the highest kurtosis.

For the N225 index, the histograms of the 0.1st and 1st percentiles indicate that RSV-FS-SN consistently produces more conservative forecasts in the extreme left tail. Interestingly, its 10th percentile is relatively higher than those of other models. These distributional characteristics may help explain the variation in VaR and ES forecast performance observed across RSV models.

Remark. Additional results for the COVID-19 period are reported in the Supplementary Material. While RSV models with skew- t specifications improve forecast accuracy for volatility in the main sample, their relative performance for VaR and ES forecasts deteriorates during the COVID-19 period. This finding suggests that the benefits of modeling conditional asymmetry in the return distribution may be less pronounced under extreme market stress, where tail risk dynamics are dominated by abrupt and persistent shocks. A more detailed investigation of this issue is left for future research.

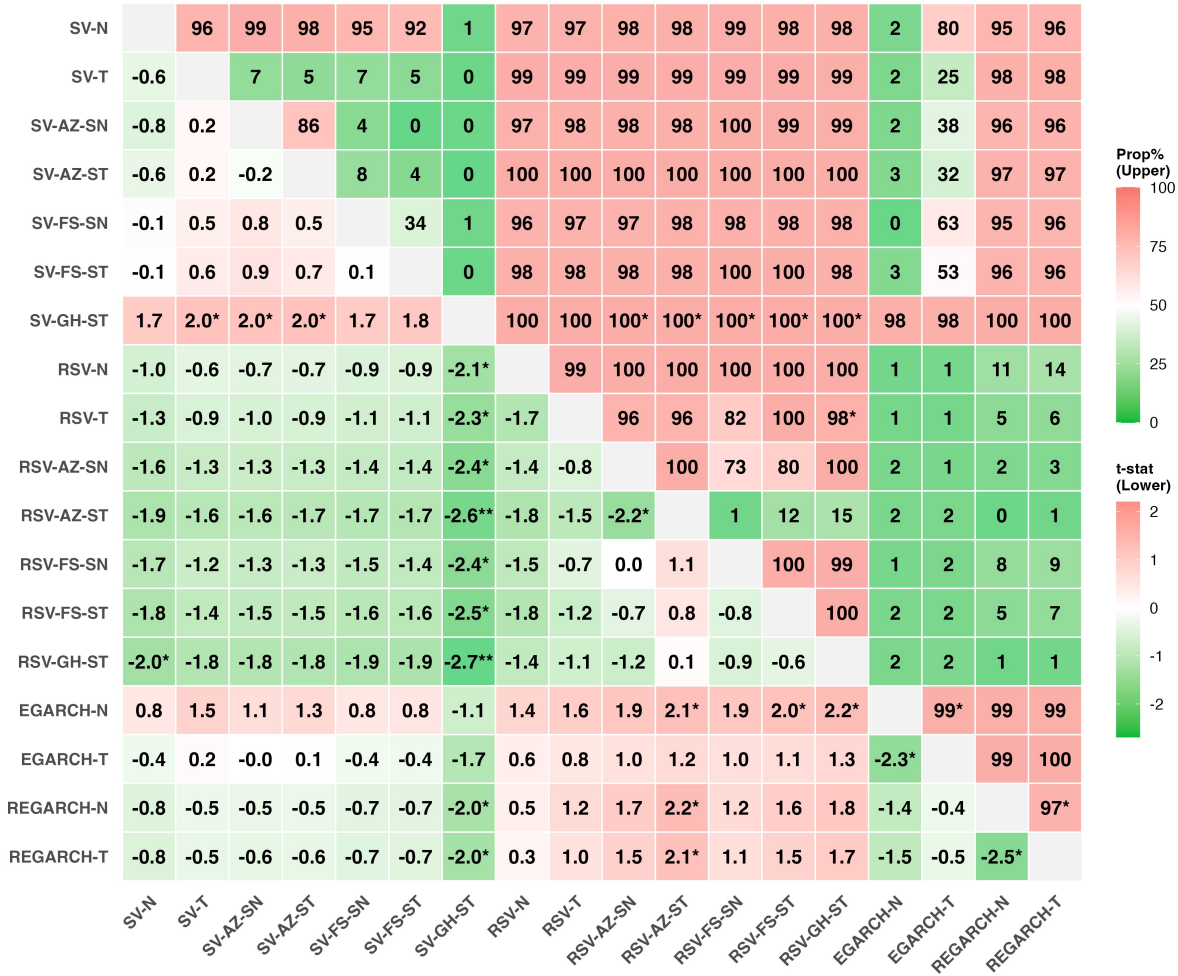


Figure 16: Pairwise comparison of GW tests on FZ0 loss of VaR and ES forecasts ($\alpha = 5\%$) for the DJIA. See Figure 10 for additional details.

Table 6: Mean characteristics of one-day-ahead return forecasts under RSV models

DJIA						
	Skewness	Kurtosis	0.1%	1%	5%	10%
RSV-N	0.000 (0.03)	3.588 (0.36)	-3.473 (0.18)	-2.436 (0.05)	-1.633 (0.02)	-1.245 (0.02)
RSV-T	0.002 (0.04)	4.050 (0.20)	-3.716 (0.15)	-2.496 (0.03)	-1.624 (0.01)	-1.222 (0.01)
RSV-AZ-SN	-0.241 (0.05)	3.691 (0.10)	-3.783 (0.13)	-2.599 (0.04)	-1.695 (0.02)	-1.265 (0.01)
RSV-AZ-ST	-0.255 (0.06)	4.166 (0.17)	-4.019 (0.16)	-2.656 (0.04)	-1.684 (0.02)	-1.242 (0.01)
RSV-FS-SN	-0.244 (0.07)	4.764 (0.35)	-4.225 (0.19)	-2.690 (0.05)	-1.659 (0.02)	-1.219 (0.01)
RSV-FS-ST	-0.216 (0.05)	4.004 (0.22)	-3.894 (0.17)	-2.613 (0.04)	-1.679 (0.02)	-1.249 (0.01)
RSV-GH-ST	-0.388 (0.07)	4.390 (0.32)	-4.250 (0.20)	-2.716 (0.05)	-1.694 (0.02)	-1.241 (0.01)
N225						
	Skewness	Kurtosis	0.1%	1%	5%	10%
RSV-N	-0.001 (0.03)	3.487 (0.08)	-3.420 (0.10)	-2.425 (0.03)	-1.636 (0.01)	-1.249 (0.01)
RSV-T	0.001 (0.04)	3.892 (0.14)	-3.639 (0.12)	-2.475 (0.03)	-1.627 (0.01)	-1.229 (0.01)
RSV-AZ-SN	-0.017 (0.03)	3.498 (0.08)	-3.451 (0.10)	-2.435 (0.03)	-1.639 (0.01)	-1.251 (0.01)
RSV-AZ-ST	-0.019 (0.03)	3.896 (0.13)	-3.665 (0.12)	-2.490 (0.04)	-1.632 (0.01)	-1.231 (0.01)
RSV-FS-SN	-0.064 (0.07)	4.661 (0.28)	-4.041 (0.20)	-2.577 (0.05)	-1.624 (0.02)	-1.204 (0.01)
RSV-FS-ST	-0.066 (0.05)	3.850 (0.17)	-3.670 (0.16)	-2.510 (0.04)	-1.645 (0.02)	-1.238 (0.01)
RSV-GH-ST	-0.081 (0.04)	3.903 (0.15)	-3.749 (0.14)	-2.524 (0.04)	-1.644 (0.01)	-1.235 (0.01)

Notes: The table reports the means of skewness, kurtosis, and lower percentiles (0.1%, 1%, 5%, and 10%) computed from the posterior predictive distributions of one-day-ahead return forecasts. Standard deviations are shown in parentheses. These statistics are calculated across 603 and 590 forecast days for the DJIA and N225, respectively.

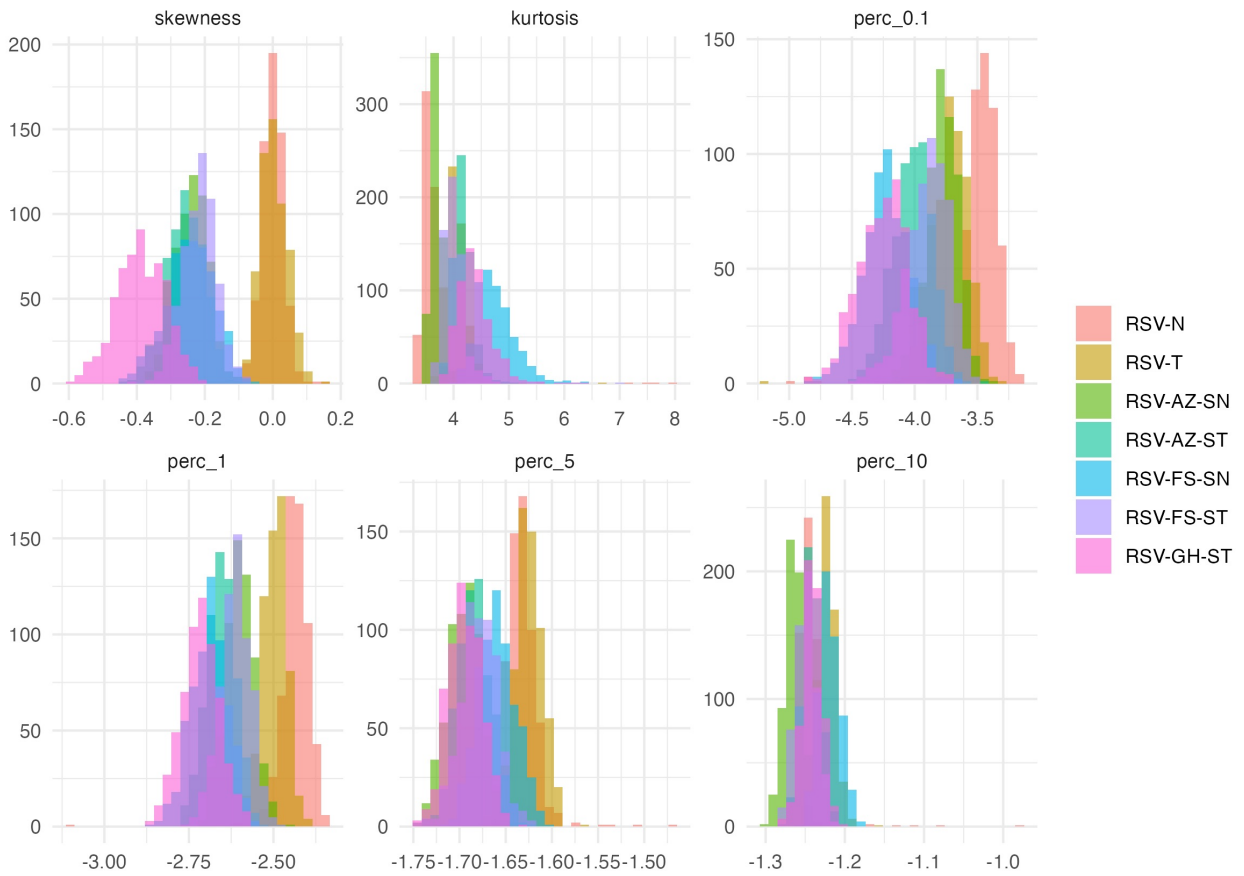


Figure 17: Histograms of skewness, kurtosis, and lower percentiles (0.1%, 1%, 5%, and 10%) computed from the posterior predictive distributions of one-day-ahead return forecasts for the DJIA.

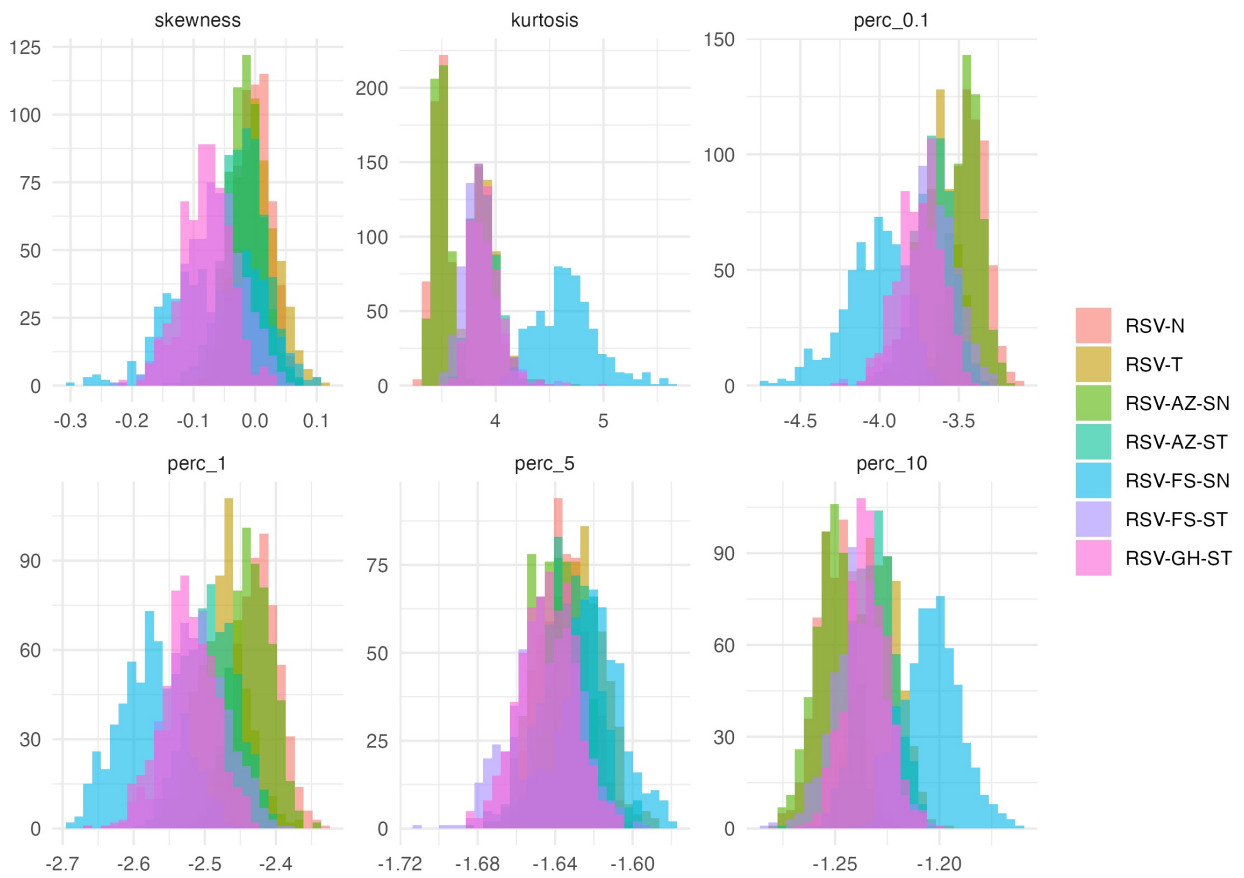


Figure 18: Histograms of skewness, kurtosis, and lower percentiles (0.1%, 1%, 5%, and 10%) computed from the posterior predictive distributions of one-day-ahead return forecasts for the N225.

4.4 Summary

Table 7 presents the rankings of average losses for volatility, VaR, and ES forecasts. The average ranking in the final column highlights the overall superiority of the RSV models, with RSV-AZ-ST and RSV-GH-ST achieving the best performance.

Our findings demonstrate that RV is a valuable predictor for forecasting not only volatility but also tail risk measures such as VaR and ES. Overall, RSV models tend to deliver superior performance, particularly for the N225, while REGARCH-T remains highly competitive for the DJIA. Incorporating a skewed t -distribution within the RSV framework further enhances forecast accuracy, especially for tail risk measures.

Table 7: Ranking of average losses for volatility, VaR, and ES forecasts

	DJIA				N225				Average				
	QLIKE				FZ0		QLIKE				FZ0		
	RV5	RK	BV	Med	1%	5%	RV5	RK		BV	Med	1%	5%
SV-N	17	17	17	15	10	16	13	12	13	14	12	14	14.17
SV-T	14	14	14	14	7	10	18	17	16	15	15	9	13.58
SV-AZ-SN	18	18	18	18	1	13	14	14	14	16	13	15	14.33
SV-AZ-ST	15	15	15	16	4	12	17	16	17	17	14	13	14.25
SV-FS-SN	11	3	3	2	2	14	10	10	10	11	11	12	8.25
SV-FS-ST	10	1	2	1	3	15	12	13	12	12	10	11	8.50
SV-GH-ST	16	16	16	17	13	18	16	15	18	18	17	18	16.50
RSV-N	8	12	11	12	16	8	3	3	3	5	6	3	7.50
RSV-T	4	9	8	8	15	7	5	5	5	3	5	2	6.33
RSV-AZ-SN	5	10	9	10	14	4	4	4	4	4	8	4	6.67
RSV-AZ-ST	3	7	5	6	11	1	6	6	6	1	1	1	4.50
RSV-FS-SN	9	13	13	13	8	5	1	1	1	9	7	7	7.25
RSV-FS-ST	7	11	10	11	12	3	2	2	2	6	3	5	6.17
RSV-GH-ST	2	5	4	5	5	2	7	7	7	2	2	6	4.50
EGARCH-N	13	8	12	9	17	17	11	11	11	10	18	17	12.83
EGARCH-T	12	4	7	4	9	11	15	18	15	13	16	16	11.67
REGARCH-N	6	6	6	7	18	9	9	8	8	8	9	10	8.67
REGARCH-T	1	2	1	3	6	6	8	9	9	7	4	8	5.33

Notes: QLIKE denotes the Gaussian Quasi Likelihood loss for volatility forecasts using four volatility proxies: RV5, RK, BV, and Med. FZ0 refers to the FZ0 loss functions for VaR and ES forecasts at significance levels $\alpha = 1\%$ and 5% . The last column indicates the average rank across all categories.

5 Conclusion

This study has evaluated the predictive performance of multiple models for forecasting volatility, VaR, and ES using data from two major financial indices: the DJIA and N225. Our comprehensive assessment, summarized in Table 7, demonstrates that the RSV models consistently outperform alternative approaches across all forecast objectives.

Among the models analyzed, the RSV-AZ-ST specification achieves the best overall performance. This highlights not only the value of incorporating RV but also the benefit of accounting for skewness and heavy tails in return distributions. Specifically, the use of skewed t -distributions within the RSV framework substantially improves forecast accuracy for both volatility and tail risk measures.

A key contribution of this study is the joint validation of these modeling enhancements: integrating RV and adopting flexible return distributions. These improvements offer methodological guidance for constructing robust models for financial risk forecasting.

In sum, our findings suggest that RSV models—particularly those incorporating skewed t -distributions—constitute a robust and effective approach for forecasting volatility, VaR, and ES. These results emphasize the critical role of model specification and distributional assumptions in improving the reliability of financial risk forecasts.

An interesting avenue for future research is to extend the proposed framework to allow for alternative or multiple realized measures within the measurement equation. In the present study, the RSV specification relies on log-RV5 as a single realized proxy, while forecast evaluation is conducted using several realized measures, including RK, BV, and Med. Allowing the model to incorporate alternative realized measures, or a multi-measure RSV specification, could help assess the robustness of the reported gains with respect to the choice of realized volatility proxy and may also mitigate the distributional mismatch suggested by the non-normality of log-RV documented in the empirical analysis.

A related line of research is provided by score-driven volatility models with flexible innovation distributions, such as the GH skew- t -based SD-GARCH specification of Catania & Grassi (2022), as well as joint SD models for returns and realized volatility proposed by Catania & Proietti (2020). While these approaches require more elaborate dynamic updating rules and likelihood evaluations, they provide informative points of comparison and could offer further insights into the role of realized measures and distributional flexibility in volatility modeling.

References

- Aas, K. & Haff, I. H. (2006), ‘The generalized hyperbolic skew Student’s t -distribution’, *Journal of Financial Econometrics* **4**(2), 275–309.
- Abanto-Valle, C. A., Lachos, V. H. & Dey, D. K. (2015), ‘Bayesian estimation of a skew-Student- t stochastic volatility model’, *Methodology and Computing in Applied Probability* **17**(3), 721–738.
- Aït-sahalia, Y. & Mykland, P. A. (2009), Estimating volatility in the presence of market microstructure noise: A review of the theory and practical considerations, in T. G. Andersen, R. A. Davis, J.-P. Kreiß & T. Mikosch, eds, ‘Handbook of Financial Time Series’, Springer-Verlag, Berlin, pp. 577–598.
- Aït-Sahalia, Y., Mykland, P. A. & Zhang, L. (2005), ‘How often to sample a continuous-time process in the presence of market microstructure noise’, *Review of Financial Studies* **18**(2), 351–416.

- Andersen, T. G. & Benzoni, L. (2009), Realized volatility, *in* T. G. Andersen, R. A. Davis, J.-P. Kreiß & T. Mikosch, eds, ‘Handbook of Financial Time Series’, Springer-Verlag, Berlin, pp. 555–575.
- Andersen, T. G., Dobrev, D. & Schaumburg, E. (2012), ‘Jump-robust volatility estimation using nearest neighbor truncation’, *Journal of Econometrics* **169**(1), 75–93.
- Ardia, D., Bluteau, K., Boudt, K. & Catania, L. (2018), ‘Forecasting risk with markov-switching garch models: a large-scale performance study’, *International Journal of Forecasting* **34**(4), 733–747.
- Asai, M. (2006), ‘Comparison of MCMC methods for estimating GARCH models’, *Journal of the Japan Statistical Society* **36**, 199–212.
- Azzalini, A. (1985), ‘A class of distributions which includes the normal ones’, *Scandinavian Journal of Statistics* **12**(2), 171–178.
- Azzalini, A. & Capitanio, A. (2003), ‘Distributions generated by perturbation of symmetry with emphasis on a multivariate skew t-distribution’, *Journal of the Royal Statistical Society B* **65**(2), 367–389.
- Bandi, F. M. & Russell, J. R. (2006), ‘Separating microstructure noise from volatility’, *Journal of Financial Economics* **79**(3), 367–389.
- Bandi, F. M. & Russell, J. R. (2008), ‘Microstructure noise, realized volatility, and optimal sampling’, *Review of Economic Studies* **75**(2), 655–692.
- Barndorff-Nielsen, O. E., Hansen, P. R., Lunde, A. & Shephard, N. (2008), ‘Designing realized kernels to measure the ex post variation of equity prices in the presence of noise’, *Econometrica* **76**(6), 1481–1536.
- Barndorff-Nielsen, O. E., Hansen, P. R., Lunde, A. & Shephard, N. (2009), ‘Realized kernels in practice: Trades and quotes’, *Econometrics Journal* **12**(3), C1–C32.
- Barndorff-Nielsen, O. E. & Shephard, N. (2004), ‘Power and bipower variation with stochastic volatility and jumps’, *Journal of Financial Econometrics* **2**(1), 1–37.
- Beran, J. (1994), *Statistics for Long-Memory Processes*, 1st edn, Chapman & Hall.
- Bollerslev, T. (1986), ‘Generalized autoregressive conditional heteroskedasticity’, *Journal of Econometrics* **31**(3), 307–327.
- Catania, L. & Grassi, S. (2022), ‘Forecasting cryptocurrency volatility’, *International Journal of Forecasting* **38**(3), 878–894.
- Catania, L. & Proietti, T. (2020), ‘Forecasting volatility with time-varying leverage and volatility of volatility effects’, *International Journal of Forecasting* **36**(4), 1301–1317.
- Chen, C. W., Watanabe, T. & Lin, E. M. (2023), ‘Bayesian estimation of realized GARCH-type models with application to financial tail risk management’, *Econometrics and Statistics* **28**, 30–46.
- Corsi, F. (2009), ‘A simple approximate long memory model of realized volatility’, *Journal of Financial Econometrics* **7**(2), 174–196.

- Creal, D., Koopman, S. J. & Lucas, A. (2013), ‘Generalized autoregressive score models with applications’, *Journal of Applied Econometrics* **28**(5), 777–795.
- Diebold, F. X. (1988), *Empirical Modeling of Exchange Rate Dynamics*, Springer-Verlag, Berlin.
- Diebold, F. X. & Mariano, R. S. (1995), ‘Comparing predictive accuracy’, *Journal of Business & Economic Statistics* **13**(3), 134–144.
- Dobrev, D. P. & Szerszen, P. J. (2010), The information content of high-frequency data for estimating equity return models and forecasting risk. FRB Working Paper 2010-45.
- Engle, R. F. (1982), ‘Autoregressive conditional heteroscedasticity with estimates of the variance of United Kingdom inflation’, *Econometrica* **50**(4), 987–1008.
- Engle, R. F. & Manganelli, S. (2004), ‘CAViaR: Conditional autoregressive value at risk by regression quantiles’, *Journal of Business & Economic Statistics* **22**(4), 367–381.
- Fernández, C. & Steel, M. F. (1995), ‘On Bayesian modeling of fat tails and skewness’, *Journal of the American Statistical Association* **93**(441), 359–371.
- Fissler, T. & Ziegel, J. F. (2016), ‘Higher order elicibility and Osband’s principle’, *The Annals of Statistics* **44**(4), 1680–1707.
- Giacomini, F. & White, H. (2006), ‘Tests of conditional predictive ability’, *Econometrica* **74**(6), 1545–1578.
- Hansen, P., Lunde, A. & Nason, J. (2011), ‘The model confidence set’, *Econometrica* **79**(2), 453–497.
- Hansen, P. R. & Huang, Z. (2016), ‘Exponential GARCH modeling with realized measures of volatility’, *Journal of Business & Economic Statistics* **34**(2), 269–287.
- Hansen, P. R., Huang, Z. & Shek, H. (2012), ‘Realized GARCH: A joint model of returns and realized measures of volatility’, *Journal of Applied Econometrics* **27**(6), 877–906.
- Hansen, P. R. & Lunde, A. (2005), ‘A forecast comparison of volatility models: Does anything beat a GARCH(1,1)?’, *Journal of Applied Econometrics* **20**(7), 873–889.
- Hansen, P. R. & Lunde, A. (2006), ‘Realized variance and market microstructure noise’, *Journal of Business & Economic Statistics* **24**(2), 127–161.
- Harvey, A. C. (2013), *Dynamic Models for Volatility and Heavy Tails: With Applications to Financial and Economic Time Series*, Econometric Series Monographs, Cambridge University Press.
- Jacod, J., Li, Y., Mykland, P. A., Podolskij, M. & Vetter, M. (2009), ‘Microstructure noise in the continuous case: The pre-averaging approach’, *Stochastic Processes and their Applications* **119**(7), 2249–2276.
- Kirkby, J. L., Nguyen, D. H. & Nguyen, D. (2025), ‘Moments of Student’s t-distribution: a unified approach’, *Modern Stochastics: Theory and Applications* **12**(4), 393–405.
- Kobayashi, G. (2016), ‘Skew exponential power stochastic volatility model for analysis of skewness, non-normal tails, quantiles and expectiles’, *Computational Statistics* **31**(1), 49–88.

- Koopman, S. J. & Scharth, M. (2013), ‘The analysis of stochastic volatility in the presence of daily realized measures’, *Journal of Financial Econometrics* **11**(1), 76–115.
- Leão, W. L., Abanto-Valle, C. A. & Chen, M.-H. (2017), ‘Bayesian analysis of stochastic volatility-in-mean model with leverage and asymmetrically heavy-tailed error using generalized hyperbolic skew Student’s t-distribution’, *Statistics and Its Interface* **10**(4), 529–541.
- Liu, L. Y., Patton, A. J. & Sheppard, K. (2015), ‘Does anything beat 5-minute RV? A comparison of realized measures across multiple asset classes’, *Journal of Econometrics* **187**(1), 293–311.
- Ljung, G. M. & Box, G. E. P. (1978), ‘On a measure of lack of fit in time series analysis’, *Biometrika* **65**(2), 297–303.
- McAleer, M. & Medeiros, M. C. (2008), ‘Realized volatility: A review’, *Econometric Reviews* **27**(1–3), 10–45.
- Mitsui, H. & Watanabe, T. (2003), ‘Bayesian analysis of GARCH option pricing models’, *Journal of the Japan Statistical Society (Japanese Issue)* **33**, 307–324.
- Nakajima, J. & Omori, Y. (2012), ‘Stochastic volatility model with leverage and asymmetrically heavy-tailed error using GH skew Student’s t-distribution’, *Computational Statistics & Data Analysis* **56**(11), 3690–3704.
- Nelson, D. B. (1991), ‘Conditional heteroskedasticity in asset returns: A new approach’, *Econometrica* **59**(2), 347–370.
- Nugroho, D. B. & Morimoto, T. (2014), ‘Realized non-linear stochastic volatility models with asymmetric effects and generalized Student’s t-distributions’, *Journal of Japan Statistical Society* **44**(1), 83–118.
- Nugroho, D. B. & Morimoto, T. (2016), ‘Box-Cox realized asymmetric stochastic volatility models with generalized Student’s t-error distributions’, *Journal of Applied Statistics* **43**(10), 1906–1927.
- Omori, Y., Chib, S., Shephard, N. & Nakajima, J. (2007), ‘Stochastic volatility with leverage: Fast and efficient likelihood inference’, *Journal of Econometrics* **140**(2), 425–449.
- Omori, Y. & Watanabe, T. (2008), ‘Block sampler and posterior mode estimation for asymmetric stochastic volatility models’, *Computational Statistics & Data Analysis* **52**(6), 2892–2910.
- Omori, Y. & Watanabe, T. (2015), Stochastic volatility and realized stochastic volatility models, in S. K. Upadhyay, U. Singh, D. K. Dey & L. Appaia, eds, ‘Current Trends in Bayesian Methodology with Applications’, 1st edn, Chapman and Hall/CRC, New York.
- Patton, A. J. (2011), ‘Volatility forecast comparison using imperfect volatility proxies’, *Journal of Econometrics* **160**(1), 246–256.
- Patton, A. J. & Sheppard, K. (2009), Evaluating volatility and correlation forecasts, in T. Mikosch, J.-P. Kreiß, R. A. Davis & T. G. Andersen, eds, ‘Handbook of Financial Time Series’, Springer, pp. 801–838.
- Patton, A. J., Ziegel, J. F. & Chen, R. (2019), ‘Dynamic semiparametric models for expected shortfall (and value-at-risk)’, *Journal of Econometrics* **211**(2), 388–413.
- Sahu, S. K., Dey, D. K. & Branco, M. D. (2003), ‘A new class of multivariate skew distributions with applications to bayesian regression models’, *Canadian Journal of Statistics* **31**(2), 129–150.

- Steel, M. F. J. (1998), ‘Bayesian analysis of stochastic volatility models with flexible tails’, *Econometric Reviews* **17**(2), 109–143.
- Stinchcombe, M. B. & White, H. (1998), ‘Consistent specification testing with nuisance parameters present only under the Alternative’, *Econometric Theory* **14**(3), 295–325.
- Takahashi, M., Omori, Y. & Watanabe, T. (2009), ‘Estimating stochastic volatility models using daily returns and realized volatility simultaneously’, *Computational Statistics & Data Analysis* **53**(6), 2404–2426.
- Takahashi, M., Omori, Y. & Watanabe, T. (2023), *Stochastic Volatility and Realized Stochastic Volatility Models*, SpringerBriefs in Statistics, JSS Research Series in Statistics, Springer Singapore.
- Takahashi, M., Watanabe, T. & Omori, Y. (2016), ‘Volatility and quantile forecasts by realized stochastic volatility models with generalized hyperbolic distribution’, *International Journal of Forecasting* **32**(2), 437–457.
- Takahashi, M., Watanabe, T. & Omori, Y. (2024), ‘Forecasting Daily Volatility of Stock Price Index Using Daily Returns and Realized Volatility’, *Econometrics and Statistics* **32**, 34–56.
- Taylor, S. J. (1986), *Modelling Financial Time Series*, Wiley, New York.
- Trojan, S. (2013), Regime switching stochastic volatility with skew, fat tails and leverage using returns and realized volatility contemporaneously. Discussion Paper Series No. 2013- 41, Department of Economics, School of Economics and Political Science, University of St. Gallen.
- Trottier, D.-A. & Ardia, D. (2016), ‘Moments of standardized fernandez–steel skewed distributions: Applications to the estimation of garch-type models’, *Finance Research Letters* **18**, 311–316.
- Ubukata, M. & Watanabe, T. (2014), ‘Pricing Nikkei 225 options using realized volatility’, *The Japanese Economic Review* **65**(4), 431–467.
- Zhang, L. (2006), ‘Efficient estimation of stochastic volatility using noisy observations: A multi-scale approach’, *Bernoulli* **12**(6), 1019–1043.
- Zhang, L., Mykland, P. A. & Ait-Sahalia (2005), ‘A tale of two time scales: Determining integrated volatility with noisy high-frequency data’, *Journal of the American Statistical Association* **100**(472), 1394–1411.

Appendix

A MCMC Sampling Scheme

A.1 RSV-AZ-ST Model

The joint probability density of (y_t, h_{t+1}) conditional on z_{0t}, h_t , and parameters $\boldsymbol{\theta}$ is given by

$$\begin{aligned}
 f(y_t, h_{t+1} | z_{0t}, h_t, \boldsymbol{\theta}) &= \frac{1}{2\pi k(\delta) \sqrt{(1-\rho^2)\sigma_\eta^2}} \sqrt{\frac{\mu_\lambda}{\lambda_t}} \exp\left(-\frac{1}{2}h_t\right) \\
 &\times \exp\left\{ -\frac{\mu_\lambda \exp(-h_t)}{2\lambda_t k(\delta)^2 (1-\rho^2)} \left[y_t - \sqrt{\frac{\lambda_t}{\mu_\lambda}} \frac{\exp(h_t/2)\delta(z_{0t}-c)}{\sqrt{1-c^2\delta^2}} \right. \right. \\
 &\quad \left. \left. - \sqrt{\frac{\lambda_t}{\mu_\lambda}} \rho \exp(h_t/2) \frac{k(\delta)}{\sigma_\eta} (h_{t+1} - \mu - \phi(h_t - \mu)) \right]^2 \right\} \\
 &\times \exp\left\{ -\frac{1}{2\sigma_\eta^2} (h_{t+1} - \mu - \phi(h_t - \mu))^2 \right\},
 \end{aligned}$$

where

$$k(\delta) = \sqrt{\frac{1-\delta^2}{1-c^2\delta^2}}.$$

The full conditional posterior density is then given by

$$\begin{aligned}
 \pi(\mathbf{h}, \boldsymbol{\theta}, \mathbf{z}_0, \boldsymbol{\lambda} | \mathbf{x}, \mathbf{y}) &\propto k(\delta)^{-T} (1-\rho^2)^{-\frac{T-1}{2}} \sigma_\eta^{-T} (1-\phi^2)^{\frac{1}{2}} \\
 &\times \exp\left\{ -\frac{1}{2} \sum_{t=1}^T h_t - \frac{\mu_\lambda \exp(-h_T)}{2\lambda_T k(\delta)^2} \left[y_T - \sqrt{\frac{\lambda_T}{\mu_\lambda}} \frac{\exp(h_T/2)\delta(z_{0T}-c)}{\sqrt{1-c^2\delta^2}} \right]^2 \right\} \\
 &\times \exp\left\{ -\sum_{t=1}^{T-1} \frac{\mu_\lambda \exp(-h_t)}{2\lambda_t k(\delta)^2 (1-\rho^2)} \left[y_t - \sqrt{\frac{\lambda_t}{\mu_\lambda}} \frac{\exp(h_t/2)\delta(z_{0t}-c)}{\sqrt{1-c^2\delta^2}} \right. \right. \\
 &\quad \left. \left. - \sqrt{\frac{\lambda_t}{\mu_\lambda}} \rho \exp(h_t/2) \frac{k(\delta)}{\sigma_\eta} (h_{t+1} - \mu - \phi(h_t - \mu)) \right]^2 \right\} \\
 &\times \exp\left\{ -\frac{1}{2\sigma_\eta^2} \sum_{t=1}^{T-1} (h_{t+1} - \mu - \phi(h_t - \mu))^2 - \frac{(1-\phi^2)}{2\sigma_\eta^2} (h_1 - \mu)^2 \right\} \\
 &\times \exp\left\{ -\frac{1}{2} \sum_{t=1}^T z_{0t}^2 I(z_{0t} > 0) \right\} \times \prod_{t=1}^T \frac{\mu_\lambda^{1/2} (\nu/2)^{\nu/2}}{\Gamma(\nu/2)} \lambda_t^{-(\nu+1)/2-1} \exp\left(-\frac{\nu}{2\lambda_t}\right) \\
 &\times \sigma_u^{-T} \times \exp\left\{ -\frac{1}{2\sigma_u^2} \sum_{t=1}^T (x_t - \xi - h_t)^2 \right\} \times \pi(\boldsymbol{\theta}),
 \end{aligned}$$

where $\pi(\boldsymbol{\theta})$ denotes the prior distribution of the model parameters.

A.1.1 Generation of μ

The conditional posterior distribution of μ follows a normal distribution:

$$\mu | \cdot \sim \mathcal{N}(\mu_1, \sigma_{\mu_1}^2),$$

where

$$\begin{aligned}\sigma_{\mu_1}^{-2} &= \sigma_{\mu_0}^{-2} + \sigma_{\eta}^{-2} [1 - \phi^2 + (T-1)(1-\phi)^2(1-\rho^2)^{-1}], \\ \mu_1 &= \sigma_{\mu_1}^2 \left\{ \sigma_{\mu_0}^{-2} \mu_0 + \sigma_{\eta}^{-2} \left[(1-\phi^2)h_1 + \frac{1-\phi}{1-\rho^2} \sum_{t=1}^{T-1} (h_{t+1} - \phi h_t \right. \right. \\ &\quad \left. \left. - \sqrt{\frac{\mu_{\lambda}}{\lambda_t}} \cdot \frac{\rho \sigma_{\eta} \exp(-h_t/2)}{k(\delta)} \cdot \left(y_t - \sqrt{\frac{\lambda_t}{\mu_{\lambda}}} \cdot \frac{\exp(h_t/2) \delta(z_{0t} - c)}{\sqrt{1-c^2 \delta^2}} \right) \right] \right\}.\end{aligned}$$

A.1.2 Generation of ϕ

The conditional posterior density of ϕ is given by

$$\begin{aligned}\pi(\phi | \cdot) &\propto (1+\phi)^{a_{\phi_0}-1} (1-\phi)^{b_{\phi_0}-1} (1-\phi^2)^{1/2} \\ &\quad \times \exp \left\{ - \sum_{t=1}^{T-1} \frac{\mu_{\lambda} \exp(-h_t)}{2\lambda_t k(\delta)^2 (1-\rho^2)} \left[y_t - \sqrt{\frac{\lambda_t}{\mu_{\lambda}}} \cdot \frac{\exp(h_t/2) \delta(z_{0t} - c)}{\sqrt{1-c^2 \delta^2}} \right. \right. \\ &\quad \left. \left. - \sqrt{\frac{\lambda_t}{\mu_{\lambda}}} \cdot \rho \cdot \exp(h_t/2) \cdot \frac{k(\delta)}{\sigma_{\eta}} (h_{t+1} - \mu - \phi(h_t - \mu)) \right]^2 \right\} \\ &\quad \times \exp \left\{ - \frac{1}{2\sigma_{\eta}^2} \sum_{t=1}^{T-1} (h_{t+1} - \mu - \phi(h_t - \mu))^2 - \frac{1-\phi^2}{2\sigma_{\eta}^2} (h_1 - \mu)^2 \right\} \\ &\propto g(\phi) \cdot \exp \left\{ - \frac{1}{2\sigma_{\phi}^2} (\phi - \mu_{\phi})^2 \right\},\end{aligned}$$

where

$$\begin{aligned}g(\phi) &= (1+\phi)^{a_{\phi_0}-1/2} (1-\phi)^{b_{\phi_0}-1/2}, \\ \sigma_{\phi}^2 &= \frac{\sigma_{\eta}^2 (1-\rho^2)}{\rho^2 (h_1 - \mu)^2 + \sum_{t=2}^{T-1} (h_t - \mu)^2}, \\ \mu_{\phi} &= \frac{\sigma_{\phi}^2}{\sigma_{\eta}^2 (1-\rho^2)} \sum_{t=1}^{T-1} \left[(h_{t+1} - \mu) - \sqrt{\frac{\mu_{\lambda}}{\lambda_t}} \cdot \frac{\rho \sigma_{\eta} \exp(-h_t/2)}{k(\delta)} \left(y_t - \sqrt{\frac{\lambda_t}{\mu_{\lambda}}} \cdot \frac{\exp(h_t/2) \delta(z_{0t} - c)}{\sqrt{1-c^2 \delta^2}} \right) \right] (h_t - \mu).\end{aligned}$$

We then propose a candidate $\phi^{\dagger} \sim \mathcal{N}(\mu_{\phi}, \sigma_{\phi}^2)$ and accept it with probability $\min \left\{ 1, \frac{g(\phi^{\dagger})}{g(\phi)} \right\}$.

Generation of σ_{η}^2 and ρ

Instead of sampling σ_{η}^2 and ρ separately, we sample them jointly. Let $\vartheta = (\sigma_{\eta}, \rho)'$. The conditional posterior density of ϑ is given by

$$\begin{aligned}\pi(\vartheta | \cdot) &\propto (\sigma_{\eta}^2)^{-(n_0+T)/2-1} \exp \left(- \frac{S_0}{2\sigma_{\eta}^2} \right) (1+\rho)^{a_{\rho_0}-1} (1-\rho)^{b_{\rho_0}-1} (1-\rho^2)^{-(T-1)/2} \\ &\quad \times \exp \left\{ - \sum_{t=1}^{T-1} \frac{\mu_{\lambda} \exp(-h_t)}{2\lambda_t k(\delta)^2 (1-\rho^2)} \left[y_t - \sqrt{\frac{\lambda_t}{\mu_{\lambda}}} \cdot \frac{\exp(h_t/2) \delta(z_{0t} - c)}{\sqrt{1-c^2 \delta^2}} \right. \right. \\ &\quad \left. \left. - \sqrt{\frac{\lambda_t}{\mu_{\lambda}}} \cdot \rho \cdot \exp(h_t/2) \cdot \frac{k(\delta)}{\sigma_{\eta}} (h_{t+1} - \mu - \phi(h_t - \mu)) \right]^2 \right\} \\ &\quad \times \exp \left\{ - \frac{1}{2\sigma_{\eta}^2} \sum_{t=1}^{T-1} (h_{t+1} - \mu - \phi(h_t - \mu))^2 - \frac{1-\phi^2}{2\sigma_{\eta}^2} (h_1 - \mu)^2 \right\}.\end{aligned}$$

To handle the parameter constraints $\sigma_\eta > 0$ and $|\rho| < 1$, we perform a transformation:

$$\omega_1 = \log \sigma_\eta, \quad \omega_2 = \log(1 + \rho) - \log(1 - \rho).$$

This transformation allows unconstrained sampling of $\omega = (\omega_1, \omega_2)$. Let $\hat{\vartheta}$ be the mode of the conditional posterior, and $\hat{\omega}$ its corresponding transformed value. We approximate the conditional posterior of ω by a normal distribution $\mathcal{N}(\omega_*, \Sigma_{\eta*})$, where

$$\begin{aligned} \omega_* &= \hat{\omega} + \Sigma_{\eta*} \cdot \left. \frac{\partial \log \pi(\omega | \cdot)}{\partial \omega} \right|_{\omega=\hat{\omega}}, \\ \Sigma_{\eta*}^{-1} &= - \left. \frac{\partial^2 \log \pi(\omega | \cdot)}{\partial \omega \partial \omega'} \right|_{\omega=\hat{\omega}}. \end{aligned}$$

We then propose a candidate $\omega^\dagger \sim \mathcal{N}(\omega_*, \Sigma_{\eta*})$, and accept it with probability

$$\min \left\{ 1, \frac{\pi(\vartheta^\dagger | \cdot) f_N(\omega | \omega_*, \Sigma_{\eta*}) |J(\vartheta)|}{\pi(\vartheta | \cdot) f_N(\omega^\dagger | \omega_*, \Sigma_{\eta*}) |J(\vartheta^\dagger)|} \right\},$$

where $f_N(\cdot | \mu, \Sigma)$ denotes the density of a multivariate normal distribution, $J(\cdot)$ is the Jacobian of the inverse transformation, and ϑ^\dagger is the back-transformed candidate.

A.1.3 Generation of δ

The conditional posterior density of δ is given by

$$\begin{aligned} \pi(\delta | \cdot) &\propto (1 + \delta)^{a_{s0}-1} (1 - \delta)^{b_{s0}-1} \cdot k(\delta)^{-T} \\ &\times \exp \left\{ - \frac{\mu_\lambda \exp(-h_T)}{2\lambda_T k(\delta)^2} \left[y_T - \sqrt{\frac{\lambda_T}{\mu_\lambda}} \cdot \frac{\exp(h_T/2)\delta(z_{0T} - c)}{\sqrt{1 - c^2\delta^2}} \right]^2 \right\} \\ &\times \exp \left\{ - \sum_{t=1}^{T-1} \frac{\mu_\lambda \exp(-h_t)}{2\lambda_t k(\delta)^2 (1 - \rho^2)} \left[y_t - \sqrt{\frac{\lambda_t}{\mu_\lambda}} \cdot \frac{\exp(h_t/2)\delta(z_{0t} - c)}{\sqrt{1 - c^2\delta^2}} \right. \right. \\ &\quad \left. \left. - \sqrt{\frac{\lambda_t}{\mu_\lambda}} \cdot \rho \cdot \exp(h_t/2) \cdot \frac{k(\delta)}{\sigma_\eta} (h_{t+1} - \mu - \phi(h_t - \mu)) \right]^2 \right\}. \end{aligned}$$

We approximate the conditional posterior of δ by a normal distribution $\mathcal{N}(\hat{\delta}, \sigma_\delta^2)$, where $\hat{\delta}$ is the mode of the conditional density and

$$\sigma_\delta^{-2} = - \left. \frac{\partial^2 \log \pi(\delta | \cdot)}{\partial \delta^2} \right|_{\delta=\hat{\delta}}.$$

We then propose a candidate value $\delta^\dagger \sim \mathcal{TN}_{(-1,1)}(\hat{\delta}, \sigma_\delta^2)$ and accept it with probability

$$\min \left\{ 1, \frac{\pi(\delta^\dagger | \cdot) f_N(\delta | \hat{\delta}, \sigma_\delta^2)}{\pi(\delta | \cdot) f_N(\delta^\dagger | \hat{\delta}, \sigma_\delta^2)} \right\},$$

where $\mathcal{TN}_{(a,b)}(\mu, \sigma^2)$ denotes a normal distribution truncated over the interval (a, b) , and $f_N(\cdot | \mu, \sigma^2)$ is the density function of a normal distribution with mean μ and variance σ^2 .

A.1.4 Generation of ξ

The conditional posterior distribution of ξ is normal:

$$\xi | \cdot \sim \mathcal{N}(\mu_\xi, \sigma_\xi^2),$$

where

$$\begin{aligned}\sigma_\xi^{-2} &= \sigma_{\xi 0}^{-2} + T\sigma_u^{-2}, \\ \mu_\xi &= \sigma_\xi^2 \left[\sigma_{\xi 0}^{-2} \mu_{\xi 0} + \sigma_u^{-2} \sum_{t=1}^T (x_t - h_t) \right].\end{aligned}$$

A.1.5 Generation of σ_u^2

The conditional posterior distribution of σ_u^2 follows an inverse gamma distribution:

$$\sigma_u^2 | \cdot \sim \mathcal{IG} \left(\frac{n_{u1}}{2}, \frac{S_{u1}}{2} \right),$$

where

$$\begin{aligned}n_{u1} &= n_{u0} + T, \\ S_{u1} &= S_{u0} + \sum_{t=1}^T (x_t - \xi - h_t)^2.\end{aligned}$$

A.1.6 Generation of ν

The conditional posterior density of ν is given by

$$\begin{aligned}\pi(\nu | \cdot) &\propto \exp \left\{ \frac{T}{2} \log \mu_\lambda + \frac{\nu T}{2} \log \left(\frac{\nu}{2} \right) - T \log \Gamma \left(\frac{\nu}{2} \right) - \frac{\nu}{2} \sum_{t=1}^T (\lambda_t^{-1} + \log \lambda_t) + (n_{\nu 0} - 1) \log \nu - S_{\nu 0} \nu \right\} \\ &\times \exp \left\{ - \sum_{t=1}^{T-1} \frac{\mu_\lambda \exp(-h_t)}{2\lambda_t k(\delta)^2 (1-\rho^2)} \left[y_t - \sqrt{\frac{\lambda_t}{\mu_\lambda}} \cdot \frac{\exp(h_t/2) \delta (z_{0t} - c)}{\sqrt{1-c^2 \delta^2}} \right. \right. \\ &\quad \left. \left. - \sqrt{\frac{\lambda_t}{\mu_\lambda}} \cdot \rho \cdot \exp(h_t/2) \cdot \frac{k(\delta)}{\sigma_\eta} (h_{t+1} - \mu - \phi(h_t - \mu)) \right]^2 \right\} \\ &\times \exp \left\{ - \frac{\mu_\lambda \exp(-h_T)}{2\lambda_T k(\delta)^2} \left[y_T - \sqrt{\frac{\lambda_T}{\mu_\lambda}} \cdot \frac{\exp(h_T/2) \delta (z_{0T} - c)}{\sqrt{1-c^2 \delta^2}} \right]^2 \right\}.\end{aligned}$$

We approximate the conditional posterior of ν by a normal distribution centered at its mode and apply a Metropolis-Hastings (MH) step, as done for the generation of δ .

A.1.7 Generation of z_0

The conditional posterior distribution of z_{0t} follows a truncated normal distribution:

$$z_{0t} | \cdot \sim \mathcal{TN}_{(0, \infty)}(\mu_{z_t}, \sigma_{z_t}^2),$$

where

$$\sigma_{z_t}^{-2} = \begin{cases} 1 + \frac{\delta^2}{(1-\delta^2)(1-\rho^2)}, & t = 1, \dots, T-1, \\ \frac{1}{1-\delta^2}, & t = T, \end{cases}$$

and

$$\mu_{zt} = \begin{cases} \sigma_{zt}^2 \cdot \sqrt{\frac{\mu_\lambda}{\lambda_t}} \cdot \frac{\exp(-h_t/2)\delta}{k(\delta)^2(1-\rho^2)\sqrt{1-c^2\delta^2}} \cdot \left[y_t + \sqrt{\frac{\lambda_t}{\mu_\lambda}} \cdot \frac{\exp(h_t/2)c\delta}{\sqrt{1-c^2\delta^2}} \right. \\ \left. - \sqrt{\frac{\lambda_t}{\mu_\lambda}} \cdot \rho \cdot \exp(h_t/2) \cdot \frac{k(\delta)}{\sigma} (h_{t+1} - \mu - \phi(h_t - \mu)) \right], & t = 1, \dots, T-1, \\ \sigma_{zT}^2 \cdot \sqrt{\frac{\mu_\lambda}{\lambda_T}} \cdot \frac{\exp(-h_T/2)\delta}{k(\delta)^2\sqrt{1-c^2\delta^2}} \cdot \left[y_T + \sqrt{\frac{\lambda_T}{\mu_\lambda}} \cdot \frac{\exp(h_T/2)c\delta}{\sqrt{1-c^2\delta^2}} \right], & t = T. \end{cases}$$

A.1.8 Generation of h

We first rewrite the RSV-AZ-ST model (2), (3), (4), and (10) as

$$\begin{aligned} x_t &= \mu_x + \alpha_t + u_t, & t = 1, \dots, n, \\ y_t &= (\delta \bar{z}_{0t} + \sqrt{1-\delta^2} z_t) \sqrt{\lambda_t} \exp(\alpha_t/2) \gamma, & t = 1, \dots, n, \\ \alpha_{t+1} &= \phi \alpha_t + \eta_t, & t = 0, \dots, n-1, \end{aligned}$$

where

$$\mu_x = \xi + \mu, \quad \alpha_t = h_t - \mu, \quad \bar{z}_{0t} = z_{0t} - c, \quad \gamma = \frac{\exp(\mu/2)}{\sqrt{(1-c^2\delta^2)\mu_\lambda}}.$$

The log-likelihood of (y_t, x_t) given α_t, α_{t+1} , and other parameters (excluding constants) is

$$l_t = -\frac{\alpha_t}{2} - \frac{(y_t - \mu_t)^2}{2\sigma_t^2} - \frac{(x_t - \mu_x - \alpha_t)^2}{2\sigma_u^2},$$

where

$$\begin{aligned} \mu_t &= \begin{cases} \left[\delta \bar{z}_{0t} + \sqrt{1-\delta^2} \frac{\rho}{\sigma_\eta} (\alpha_{t+1} - \phi \alpha_t) \right] \sqrt{\lambda_t} \exp(\alpha_t/2) \gamma, & t = 1, \dots, n-1, \\ \delta \bar{z}_{0t} \sqrt{\lambda_t} \exp(\alpha_t/2) \gamma, & t = n, \end{cases} \\ \sigma_t^2 &= \begin{cases} (1-\rho^2)(1-\delta^2)\lambda_t \exp(\alpha_t)\gamma^2, & t = 1, \dots, n-1, \\ (1-\delta^2)\lambda_t \exp(\alpha_t)\gamma^2, & t = n. \end{cases} \end{aligned}$$

Using this log-likelihood, the latent states $(\alpha_1, \dots, \alpha_n)$ can be efficiently sampled via a multi-move sampler based on Omori et al. (2007), Omori & Watanabe (2008, 2015). For further details, see also Takahashi et al. (2016, 2023).

A.1.9 Generation of λ

The conditional probability density function of λ_t is

$$\begin{aligned} \pi(\lambda_t | \cdot) &\propto \lambda_t^{-(\frac{\nu+1}{2}+1)} \\ &\times \exp \left\{ -\frac{\nu}{2\lambda_t} - \frac{\mu_\lambda \exp(-h_t)}{2\lambda_t k(\delta)^2 (1-\rho^2)} \left[y_t - \sqrt{\frac{\lambda_t}{\mu_\lambda}} \cdot \frac{\exp(h_t/2)\delta(z_{0t}-c)}{\sqrt{1-c^2\delta^2}} \right. \right. \\ &\quad \left. \left. - \sqrt{\frac{\lambda_t}{\mu_\lambda}} \cdot \rho \cdot \exp(h_t/2) \cdot \frac{k(\delta)}{\sigma_\eta} (h_{t+1} - \mu - \phi(h_t - \mu)) \cdot I(t < T) \right]^2 \right\}. \end{aligned}$$

We rewrite this density as a product of an inverse gamma kernel and a correction term:

$$\pi(\lambda_t | \cdot) \propto \lambda_t^{-\left(\frac{a}{2}+1\right)} \exp\left(-\frac{b_t}{2\lambda_t}\right) \times g(\lambda_t),$$

where

$$a = \nu + 1,$$

$$b_t = \begin{cases} \nu + \frac{\mu_\lambda \exp(-h_t) y_t^2}{k(\delta)^2 (1 - \rho^2)}, & t = 1, \dots, n-1, \\ \nu + \frac{\mu_\lambda \exp(-h_t) y_t^2}{k(\delta)^2}, & t = n, \end{cases}$$

$$g(\lambda_t) = \begin{cases} \exp\left\{ \sqrt{\frac{\mu_\lambda}{\lambda_t}} \cdot \frac{\exp(-h_t/2) y_t}{k(\delta)^2 (1 - \rho^2)} \left[\frac{\delta(z_{0t} - c)}{\sqrt{1 - c^2 \delta^2}} + \rho \cdot \frac{k(\delta)}{\sigma_\eta} (h_{t+1} - \mu - \phi(h_t - \mu)) \right] \right\}, & t = 1, \dots, n-1, \\ \exp\left\{ \sqrt{\frac{\mu_\lambda}{\lambda_t}} \cdot \frac{\exp(-h_t/2) y_t}{k(\delta)^2} \cdot \frac{\delta(z_{0t} - c)}{\sqrt{1 - c^2 \delta^2}} \right\}, & t = n. \end{cases}$$

We propose a candidate draw from the inverse gamma distribution,

$$\lambda_t^\dagger \sim \mathcal{IG}\left(\frac{a}{2}, \frac{b_t}{2}\right),$$

and accept it with probability

$$\min\left\{1, \frac{g(\lambda_t^\dagger)}{g(\lambda_t)}\right\}.$$

A.2 RSV-FS-ST Model

The joint probability density of (y_t, h_{t+1}) is given by

$$f(y_t, h_{t+1} | \boldsymbol{\theta}, \lambda_t) = q_T(y_t \exp(-h_t/2) | \gamma, \nu) \exp\left(-\frac{1}{2} h_t\right) \\ \times \frac{1}{\sqrt{2\pi(1 - \rho^2)\sigma_\eta^2}} \exp\left\{-\frac{1}{2(1 - \rho^2)\sigma_\eta^2} [h_{t+1} - \mu - \phi(h_t - \mu) - \rho\sigma_\eta \exp(-h_t/2) y_t]^2\right\},$$

where q_T is defined in (11). Then, the joint posterior density is expressed as

$$\pi(\mathbf{h}, \boldsymbol{\theta} | \mathbf{x}, \mathbf{y}) \propto (1 - \rho^2)^{-\frac{T-1}{2}} \sigma_\eta^{-T} (1 - \phi^2)^{-\frac{1}{2}} \prod_{t=1}^T q_T(y_t \exp(-h_t/2) | \gamma, \nu) \exp\left(-\frac{1}{2} \sum_{t=1}^T h_t\right) \\ \times \exp\left\{-\frac{1}{2(1 - \rho^2)\sigma_\eta^2} \sum_{t=1}^{T-1} [h_{t+1} - \mu - \phi(h_t - \mu) - \rho\sigma_\eta \exp(-h_t/2) y_t]^2\right\} \\ \times \exp\left\{-\frac{(1 - \phi^2)}{2\sigma_\eta^2} (h_1 - \mu)^2\right\} \sigma_u^{-T} \exp\left\{-\frac{1}{2\sigma_u^2} \sum_{t=1}^T (x_t - \xi - h_t)^2\right\} \pi(\boldsymbol{\theta}).$$

A.2.1 Generation of μ

The conditional posterior distribution of μ follows a normal distribution:

$$\mu | \cdot \sim \mathcal{N}(\mu_1, \sigma_{\mu 1}^2),$$

where

$$\begin{aligned}\sigma_{\mu_1}^{-2} &= \sigma_{\mu_0}^{-2} + \sigma_{\eta}^{-2} [1 - \phi^2 + (T-1)(1-\phi)^2(1-\rho^2)^{-1}], \\ \mu_1 &= \sigma_{\mu_1}^2 \left\{ \sigma_{\mu_0}^{-2} \mu_0 + \sigma_{\eta}^{-2} \left[(1-\phi^2)h_1 + \frac{1-\phi}{1-\rho^2} \sum_{t=1}^{T-1} (h_{t+1} - \phi h_t - \rho \sigma_{\eta} \exp(-h_t/2)y_t) \right] \right\}.\end{aligned}$$

A.2.2 Generation of ϕ

The conditional posterior density of ϕ is given by

$$\begin{aligned}\pi(\phi | \cdot) &\propto (1-\phi)^{a_{\phi 0}-1} (1+\phi)^{b_{\phi 0}-1} (1-\phi^2)^{1/2} \\ &\times \exp \left\{ -\frac{1}{2(1-\rho^2)\sigma_{\eta}^2} \sum_{t=1}^{T-1} [h_{t+1} - \mu - \phi(h_t - \mu) - \rho \sigma_{\eta} \exp(-h_t/2)y_t]^2 \right\} \\ &\times \exp \left\{ -\frac{1-\phi^2}{2\sigma_{\eta}^2} (h_1 - \mu)^2 \right\} \\ &\propto k(\phi) \times \exp \left\{ -\frac{1}{2\sigma_{\phi}^2} (\phi - \mu_{\phi})^2 \right\},\end{aligned}$$

where

$$\begin{aligned}k(\phi) &= (1-\phi)^{a_{\phi 0}-1/2} (1+\phi)^{b_{\phi 0}-1/2}, \\ \sigma_{\phi}^2 &= \frac{\sigma_{\eta}^2(1-\rho^2)}{\rho^2(h_1 - \mu)^2 + \sum_{t=2}^{T-1} (h_t - \mu)^2}, \\ \mu_{\phi} &= \frac{\sigma_{\phi}^2}{\sigma_{\eta}^2(1-\rho^2)} \sum_{t=1}^{T-1} [h_{t+1} - \mu - \rho \sigma_{\eta} \exp(-h_t/2)y_t] (h_t - \mu).\end{aligned}$$

We then employ the MH algorithm, proposing a candidate $\phi^{\dagger} \sim \mathcal{N}(\mu_{\phi}, \sigma_{\phi}^2)$, and accept the candidate with probability $\min\{1, k(\phi^{\dagger})/k(\phi)\}$.

A.2.3 Generation of ρ

The conditional posterior density of ρ is given by

$$\begin{aligned}\pi(\rho | \cdot) &\propto (1+\rho)^{a_{\rho 0}-1} (1-\rho)^{b_{\rho 0}-1} (1-\rho^2)^{-\frac{T-1}{2}} \\ &\times \exp \left\{ -\frac{1}{2(1-\rho^2)\sigma_{\eta}^2} \sum_{t=1}^{T-1} [h_{t+1} - \mu - \phi(h_t - \mu) - \rho \sigma_{\eta} \exp(-h_t/2)y_t]^2 \right\}.\end{aligned}$$

We approximate the conditional posterior distribution by $\mathcal{N}(\hat{\rho}, \sigma_{\hat{\rho}}^2)$, where $\hat{\rho}$ is the mode of the conditional density and

$$\sigma_{\hat{\rho}}^{-2} = - \left. \frac{\partial^2 \log \pi(\rho | \cdot)}{\partial \rho^2} \right|_{\rho=\hat{\rho}}.$$

We then propose a candidate $\rho^{\dagger} \sim \mathcal{TN}_{(-1,1)}(\hat{\rho}, \sigma_{\hat{\rho}}^2)$, and accept the candidate with probability

$$\min \left\{ 1, \frac{\pi(\rho^{\dagger} | \cdot) f_N(\rho | \hat{\rho}, \sigma_{\hat{\rho}}^2)}{\pi(\rho | \cdot) f_N(\rho^{\dagger} | \hat{\rho}, \sigma_{\hat{\rho}}^2)} \right\}.$$

A.2.4 Generation of σ_η^2

The conditional posterior density of σ_η^2 is given by

$$\begin{aligned} \pi(\sigma_\eta^2 | \cdot) &\propto (\sigma_\eta^2)^{-\frac{n_0+T}{2}-1} \exp\left\{-\frac{S_0}{2\sigma_\eta^2}\right\} \times \exp\left\{-\frac{1-\phi^2}{2\sigma_\eta^2}(h_1-\mu)^2\right\} \\ &\times \exp\left\{-\frac{1}{2(1-\rho^2)\sigma_\eta^2} \sum_{t=1}^{T-1} [h_{t+1}-\mu-\phi(h_t-\mu)-\rho\sigma_\eta \exp(-h_t/2)y_t]^2\right\} \\ &\propto k(\sigma_\eta^2) \times (\sigma_\eta^2)^{-\frac{n_1}{2}-1} \exp\left\{-\frac{S_1}{2\sigma_\eta^2}\right\}, \end{aligned}$$

where

$$\begin{aligned} n_1 &= n_0 + T, \\ S_1 &= S_0 + (1-\phi^2)(h_1-\mu)^2 + \frac{1}{1-\rho^2} \sum_{t=1}^{T-1} [h_{t+1}-\mu-\phi(h_t-\mu)]^2, \\ k(\sigma_\eta^2) &= \exp\left\{\frac{\rho}{(1-\rho^2)\sigma_\eta} \sum_{t=1}^{T-1} y_t \exp(-h_t/2) [h_{t+1}-\mu-\phi(h_t-\mu)]\right\}. \end{aligned}$$

We then propose a candidate $\sigma_\eta^{2\dagger} \sim \mathcal{IG}(n_1/2, S_1/2)$, and accept the candidate with probability $\min\{1, k(\sigma_\eta^{2\dagger})/k(\sigma_\eta^2)\}$.

A.2.5 Generation of ξ

The conditional posterior distribution of ξ follows a normal distribution:

$$\xi | \cdot \sim \mathcal{N}(\mu_\xi, \sigma_\xi^2),$$

where

$$\begin{aligned} \sigma_\xi^{-2} &= \sigma_{\xi 0}^{-2} + T\sigma_u^{-2}, \\ \mu_\xi &= \sigma_\xi^2 \left[\sigma_{\xi 0}^{-2} \mu_{\xi 0} + \sigma_u^{-2} \sum_{t=1}^T (x_t - h_t) \right]. \end{aligned}$$

A.2.6 Generation of σ_u^2

The conditional posterior distribution of σ_u^2 follows an inverse-gamma distribution:

$$\sigma_u^2 | \cdot \sim \mathcal{IG}\left(\frac{n_{u1}}{2}, \frac{S_{u1}}{2}\right),$$

where

$$\begin{aligned} n_{u1} &= n_{u0} + T, \\ S_{u1} &= S_{u0} + \sum_{t=1}^T (x_t - \xi - h_t)^2. \end{aligned}$$

A.2.7 Generation of γ

The conditional posterior density of γ is given by

$$\pi(\gamma | \cdot) \propto \exp\left\{(n_{\gamma 0} - 1) \log \gamma - S_{\gamma 0} \gamma + \sum_{t=1}^T \log q_T(y_t \exp(-h_t/2) | \gamma, \nu)\right\}.$$

We consider the transformation $\tilde{\gamma} = \log \gamma$, and employ a random walk MH algorithm for $\tilde{\gamma}$, where we include a Jacobian adjustment term $\tilde{\gamma}$ in the log conditional posterior density.

A.2.8 Generation of ν

The conditional posterior density of ν is given by

$$\pi(\nu | \cdot) \propto \exp \left\{ (n_{\nu 0} - 1) \log \nu - S_{\nu 0} \nu + \sum_{t=1}^T \log q_T(y_t \exp(-h_t/2) | \gamma, \nu) \right\}.$$

We consider the transformation $\tilde{\nu} = \log(\nu - 2)$, and employ a random walk MH algorithm for $\tilde{\nu}$, where we include a Jacobian adjustment term $\tilde{\nu}$ in the log conditional posterior density.

A.2.9 Generation of h

First, we define

$$g(h_t | \gamma, \nu) = -\frac{\nu + 1}{2} \log \left\{ 1 + \frac{(\sigma_* y_t \exp(-h_t/2) + \mu_*)^2}{\nu} \left[\gamma^{-2} I \left(y_t \exp(-h_t/2) \geq -\frac{\mu_*}{\sigma_*} \right) + \gamma^2 I \left(y_t \exp(-h_t/2) < -\frac{\mu_*}{\sigma_*} \right) \right] \right\}.$$

(1) For $t = 1$, the conditional posterior density of h_1 is given by

$$\begin{aligned} \pi(h_1 | \cdot) \propto & \exp \left\{ g(h_1 | \gamma, \nu) - \frac{1}{2(1 - \rho^2)\sigma_\eta^2} [h_2 - \mu - \phi(h_1 - \mu) - \rho\sigma_\eta \exp(-h_1/2)y_1]^2 \right\} \\ & \times \exp \left\{ -\frac{1}{2}h_1 - \frac{1 - \phi^2}{2\sigma_\eta^2}(h_1 - \mu)^2 - \frac{1}{2\sigma_u^2}(x_1 - \xi - h_1)^2 \right\}. \end{aligned}$$

Define

$$\begin{aligned} \sigma_{h_1}^{-2} &= \sigma_\eta^{-2} \left(1 - \phi^2 + \frac{\phi^2}{1 - \rho^2} \right) + \sigma_u^{-2}, \\ \mu_{h_1} &= \sigma_{h_1}^2 \left\{ -\frac{1}{2} + \frac{\phi[h_2 - (1 - \phi)\mu]}{\sigma_\eta^2(1 - \rho^2)} + \frac{(1 - \phi^2)\mu}{\sigma_\eta^2} + \frac{x_1 - \xi}{\sigma_u^2} \right\}, \\ k(h_1) &= \exp \left\{ g(h_1 | \gamma, \nu) + \frac{\rho y_1 \exp(-h_1/2)}{(1 - \rho^2)\sigma_\eta} [h_2 - \mu - \phi(h_1 - \mu)] - \frac{\rho^2 y_1^2 \exp(-h_1)}{2(1 - \rho^2)} \right\}. \end{aligned}$$

We then propose a candidate $h_1^\dagger \sim \mathcal{N}(\mu_{h_1}, \sigma_{h_1}^2)$, and accept it with probability $\min\{1, k(h_1^\dagger)/k(h_1)\}$.

(2) For $t = 2, \dots, T - 1$, the conditional posterior density of h_t is given by

$$\begin{aligned} \pi(h_t | \cdot) \propto & \exp \left\{ g(h_t | \gamma, \nu) - \frac{1}{2(1 - \rho^2)\sigma_\eta^2} [h_{t+1} - \mu - \phi(h_t - \mu) - \rho\sigma_\eta \exp(-h_t/2)y_t]^2 \right\} \\ & \times \exp \left\{ -\frac{1}{2(1 - \rho^2)\sigma_\eta^2} [h_t - \mu - \phi(h_{t-1} - \mu) - \rho\sigma_\eta \exp(-h_{t-1}/2)y_{t-1}]^2 \right\} \\ & \times \exp \left\{ -\frac{1}{2}h_t - \frac{1}{2\sigma_u^2}(x_t - \xi - h_t)^2 \right\}. \end{aligned}$$

Define

$$\begin{aligned} \sigma_{h_t}^{-2} &= \sigma_\eta^{-2} \left(\frac{1 + \phi^2}{1 - \rho^2} \right) + \sigma_u^{-2}, \\ \mu_{h_t} &= \sigma_{h_t}^2 \left\{ -\frac{1}{2} + \frac{\phi[h_{t+1} - (1 - \phi)\mu]}{\sigma_\eta^2(1 - \rho^2)} + \frac{(1 - \phi)\mu + \phi h_{t-1}}{\sigma_\eta^2(1 - \rho^2)} + \frac{\rho y_{t-1} \exp(-h_{t-1}/2)}{(1 - \rho^2)\sigma_\eta} + \frac{x_t - \xi}{\sigma_u^2} \right\}, \\ k(h_t) &= \exp \left\{ g(h_t | \gamma, \nu) - \frac{\rho^2 y_t^2 \exp(-h_t)}{2(1 - \rho^2)} + \frac{\rho y_t \exp(-h_t/2)}{(1 - \rho^2)\sigma_\eta} [h_{t+1} - \mu - \phi(h_t - \mu)] \right\}. \end{aligned}$$

We then propose a candidate $h_t^\dagger \sim \mathcal{N}(\mu_{h_t}, \sigma_{h_t}^2)$, and accept it with probability $\min\{1, k(h_t^\dagger)/k(h_t)\}$.

(3) For $t = T$, the conditional posterior density of h_T is given by

$$\begin{aligned} \pi(h_T | \cdot) \propto & \exp \left\{ g(h_T | \gamma, \nu) - \frac{1}{2(1-\rho^2)\sigma_\eta^2} [h_T - \mu - \phi(h_{T-1} - \mu) - \rho\sigma_\eta \exp(-h_{T-1}/2)y_{T-1}]^2 \right\} \\ & \times \exp \left\{ -\frac{1}{2}h_T - \frac{1}{2\sigma_u^2}(x_T - \xi - h_T)^2 \right\}. \end{aligned}$$

Define

$$\begin{aligned} \sigma_{h_T}^{-2} &= \sigma_\eta^{-2} \left(\frac{1}{1-\rho^2} \right) + \sigma_u^{-2}, \\ \mu_{h_T} &= \sigma_{h_T}^2 \left[-\frac{1}{2} + \frac{(1-\phi)\mu + \phi h_{T-1}}{\sigma_\eta^2(1-\rho^2)} + \frac{\rho y_{T-1} \exp(-h_{T-1}/2)}{(1-\rho^2)\sigma_\eta} + \frac{x_T - \xi}{\sigma_u^2} \right], \\ k(h_T) &= \exp \{g(h_T | \gamma, \nu)\}. \end{aligned}$$

We then propose a candidate $h_T^\dagger \sim N(\mu_{h_T}, \sigma_{h_T}^2)$, and accept it with probability $\min\{1, k(h_T^\dagger)/k(h_T)\}$.

Realized Stochastic Volatility Model with Skew-t Distributions for Improved Volatility and Quantile Forecasting

Supplementary Material

1 Simulation Study

This section reports a simulation study designed to assess the performance of the Bayesian MCMC estimation procedure for the proposed RSV models. The simulation focuses on parameter recovery and convergence properties under controlled settings.

The sample size in the simulation study is set to $T = 2,000$. For each model, data are generated from the corresponding data-generating process, and the parameters are estimated using the same MCMC specification as in the empirical analysis. The estimation is based on 50,000 MCMC draws after discarding the first 10,000 as burn-in.

Tables 1 and 2 report the true parameter values, posterior means, posterior standard deviations, and 95% credible intervals. The table also reports the p -values of the Geweke (1992)'s convergence diagnostic test and the inefficiency factors to assess MCMC convergence and sampling efficiency.

Overall, the results indicate that the proposed estimation procedure accurately recovers the true parameters across all models, with credible intervals covering the true values and no evidence of convergence problems. These findings support the reliability of the Bayesian MCMC approach employed in the empirical analysis.

Table 1: Simulation results for the RSV-N, -T-, and GH-ST models.

Model	Parameter	True	Mean	SD	95%L	95%U	CD	IF
RSV-N	μ	0.00	0.0391	0.0855	-0.1298	0.2073	0.184	9.76
	ϕ	0.95	0.9452	0.0084	0.9282	0.9609	0.164	10.14
	σ_η	0.20	0.1934	0.0096	0.1754	0.2131	0.088	29.36
	ρ	-0.30	-0.2729	0.0375	-0.3458	-0.1983	0.537	6.31
	ξ	-0.80	-0.8480	0.0364	-0.9198	-0.7781	0.255	47.38
	σ_u	0.30	0.3058	0.0078	0.2908	0.3213	0.144	12.72
RSV-T	μ	0.00	0.0796	0.0995	-0.1176	0.2763	0.726	21.65
	ϕ	0.95	0.9529	0.0077	0.9376	0.9676	0.984	7.73
	σ_η	0.20	0.1918	0.0087	0.1754	0.2095	0.730	23.13
	ρ	-0.30	-0.3524	0.0374	-0.4254	-0.2791	0.870	8.17
	ν	10.00	9.0892	1.7902	6.2375	13.3261	0.404	113.82
	ξ	-0.80	-0.8844	0.0465	-0.9800	-0.7985	0.765	98.70
	σ_u	0.30	0.2949	0.0075	0.2804	0.3098	0.912	8.91
RSV-GH-ST	μ	0.00	0.0484	0.0918	-0.1310	0.2290	0.294	58.56
	ϕ	0.95	0.9460	0.0084	0.9289	0.9619	0.204	8.08
	σ_η	0.20	0.1925	0.0095	0.1744	0.2118	0.327	22.75
	ρ	-0.30	-0.2675	0.0426	-0.3500	-0.1833	0.888	12.28
	β	-0.70	-0.7808	0.2373	-1.3339	-0.4186	0.063	356.67
	ν	10.00	10.6874	2.6314	6.8163	16.8797	0.060	447.17
	ξ	-0.80	-0.8647	0.0537	-0.9773	-0.7642	0.457	197.59
	σ_u	0.30	0.3066	0.0079	0.2913	0.3223	0.619	10.69

Notes: The true parameter values correspond to the data-generating process used in the simulation study with sample size $T = 2,000$. The estimation is based on 50,000 MCMC draws after discarding the first 10,000 as burn-in. 95%L and 95%U denote the lower and upper limits of the 95% credible interval. CD denotes the p -value of the convergence diagnostic of Geweke (1992), and IF denotes the inefficiency factor.

Table 2: Simulation results for the RSV-AZ-SN, AZ-ST-, FS-SN, and FS-ST models.

Model	Parameter	True	Mean	SD	95%L	95%U	CD	IF
RSV-AZ-SN	μ	-0.50	-0.3960	0.0744	-0.5425	-0.2498	0.865	21.37
	ϕ	0.90	0.9003	0.0108	0.8787	0.9213	0.889	9.63
	σ_η	0.30	0.3096	0.0102	0.2899	0.3299	0.943	23.90
	ρ	-0.40	-0.3829	0.0431	-0.4680	-0.2995	0.447	27.49
	δ	-0.90	-0.8814	0.0206	-0.9157	-0.8350	0.716	46.90
	ξ	-0.50	-0.5284	0.0374	-0.6015	-0.4573	0.740	123.31
	σ_u	0.20	0.1958	0.0108	0.1743	0.2167	0.868	30.28
RSV-AZ-ST	μ	-0.50	-0.3462	0.0800	-0.5038	-0.1888	0.877	43.18
	ϕ	0.90	0.9063	0.0105	0.8851	0.9264	0.691	4.69
	σ_η	0.30	0.2967	0.0100	0.2775	0.3167	0.617	14.32
	ρ	-0.40	-0.4031	0.0501	-0.5027	-0.3076	0.218	48.62
	δ	-0.90	-0.9006	0.0195	-0.9341	-0.8570	0.309	103.90
	ν	10.00	9.6449	1.9002	6.7854	14.1460	0.018	265.25
	ξ	-0.50	-0.5888	0.0447	-0.6781	-0.5000	0.977	175.57
σ_u	0.20	0.2133	0.0100	0.1933	0.2327	0.238	18.48	
RSV-FS-SN	μ	-0.50	-0.5628	0.0693	-0.6991	-0.4258	0.035	23.20
	ϕ	0.90	0.9015	0.0102	0.8813	0.9211	0.371	1.94
	σ_η	0.30	0.3029	0.0092	0.2852	0.3212	0.207	7.83
	ρ	-0.40	-0.4024	0.0248	-0.4506	-0.3534	0.014	6.92
	γ	0.50	0.4942	0.0226	0.4513	0.5393	0.030	36.54
	ξ	-0.50	-0.5316	0.0279	-0.5855	-0.4774	0.025	149.58
	σ_u	0.20	0.1932	0.0089	0.1754	0.2103	0.142	12.59
RSV-FS-ST	μ	-0.50	-0.5665	0.0729	-0.7100	-0.4240	0.540	81.70
	ϕ	0.90	0.9023	0.0096	0.8830	0.9209	0.445	4.79
	σ_η	0.30	0.3025	0.0088	0.2857	0.3202	0.779	22.58
	ρ	-0.40	-0.4098	0.0247	-0.4579	-0.3612	0.508	27.46
	γ	0.50	0.5059	0.0224	0.4629	0.5506	0.638	33.37
	ξ	-0.50	-0.4946	0.0362	-0.5663	-0.4235	0.545	333.69
	σ_u	0.20	0.1890	0.0086	0.1717	0.2054	0.713	23.84
	ν	10.00	11.8080	2.8157	7.7866	18.7360	0.547	86.69

Notes: The true parameter values correspond to the data-generating process used in the simulation study with sample size $T = 2,000$. The estimation is based on 50,000 MCMC draws after discarding the first 10,000 as burn-in. 95%L and 95%U denote the lower and upper limits of the 95% credible interval. CD denotes the p -value of the convergence diagnostic of Geweke (1992), and IF denotes the inefficiency factor.

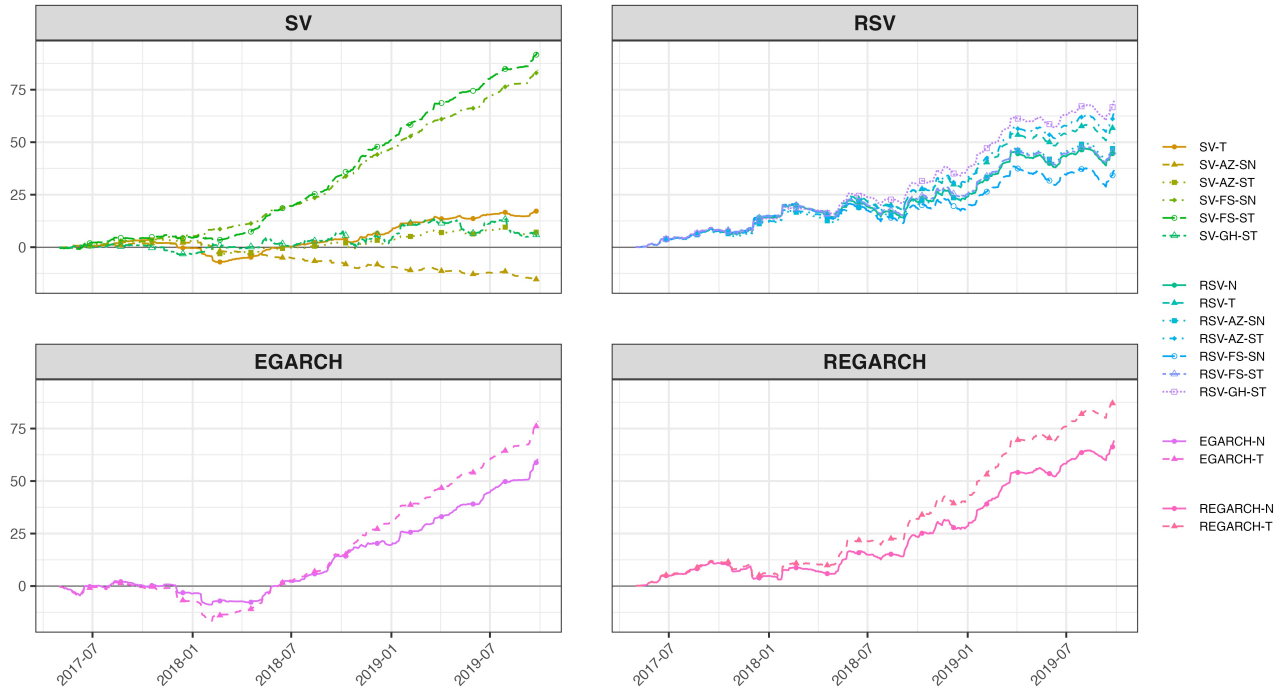


Figure 1: Cumulative QLIKE loss differences relative to the SV-N model, based on RK as the volatility proxy, for the DJIA.

2 Volatility Forecasts

This section reports additional volatility forecasting results based on alternative realized volatility proxies, including the realized kernel (RK), bipower variation (BV), and median realized volatility (Med). These results are provided as robustness checks for the findings reported in the main text, which focuses on forecasts evaluated against RV5.

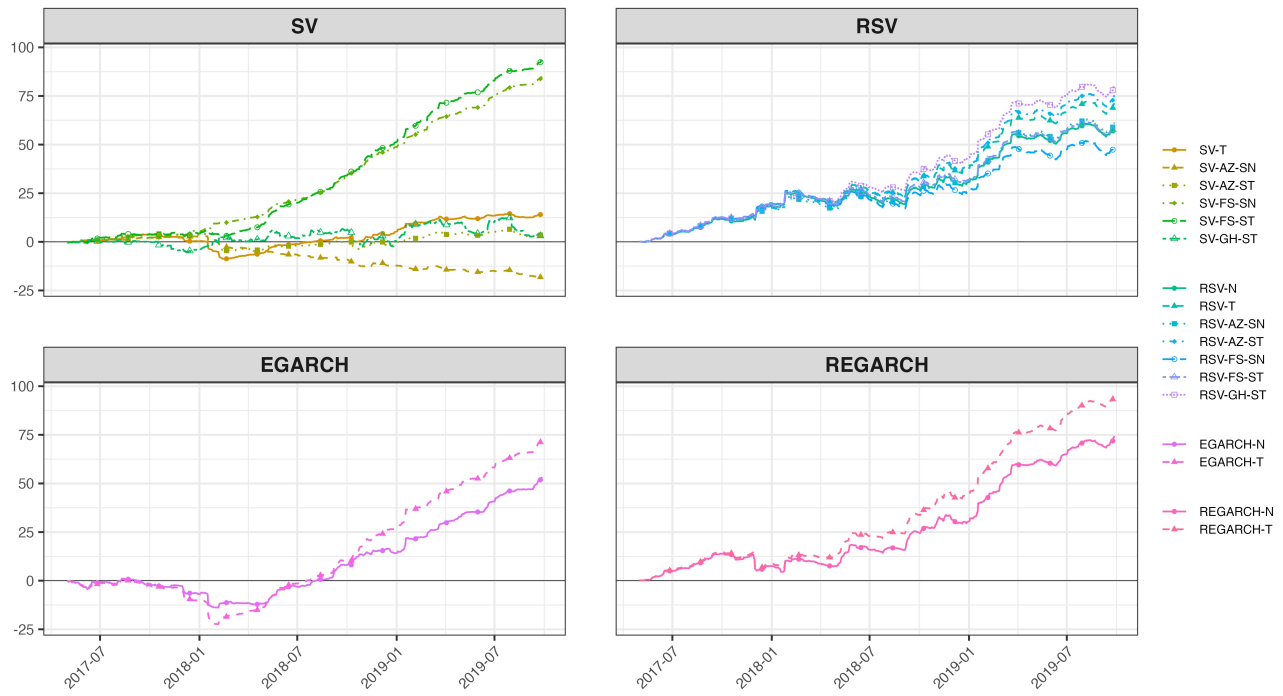


Figure 2: Cumulative QLIKE loss differences relative to the SV-N model, based on BV as the volatility proxy, for the DJIA.

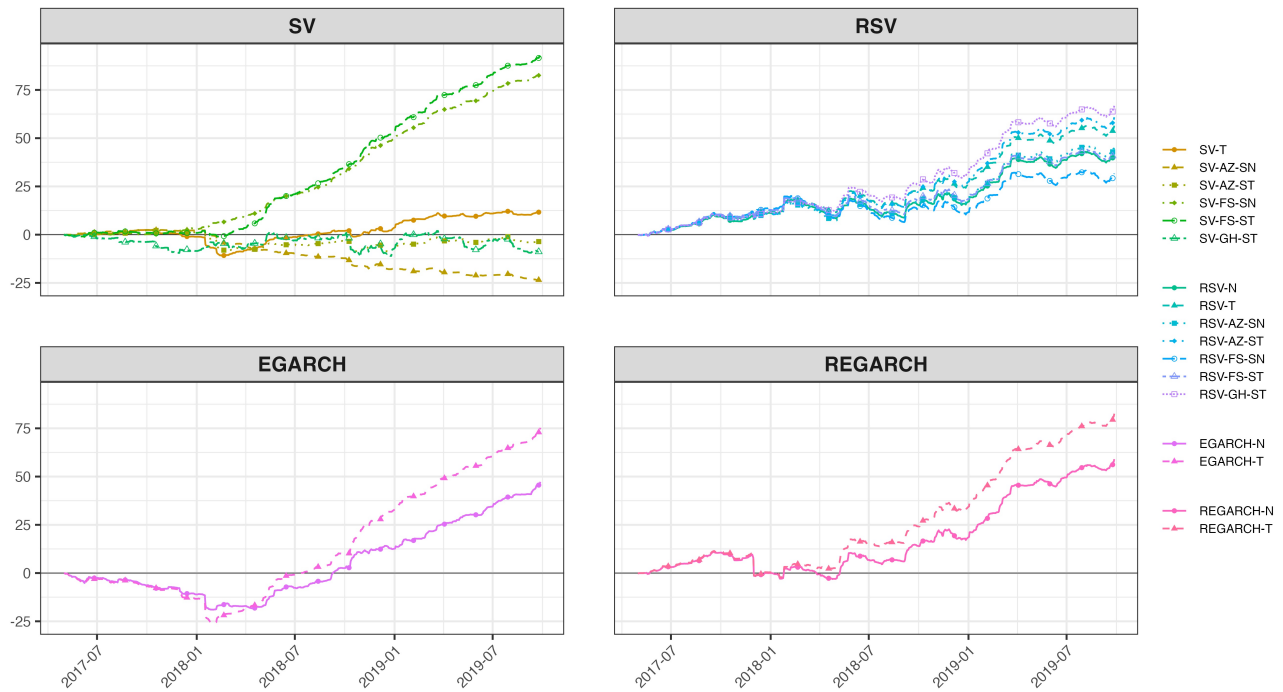


Figure 3: Cumulative QLIKE loss differences relative to the SV-N model, based on Med as the volatility proxy, for the DJIA.

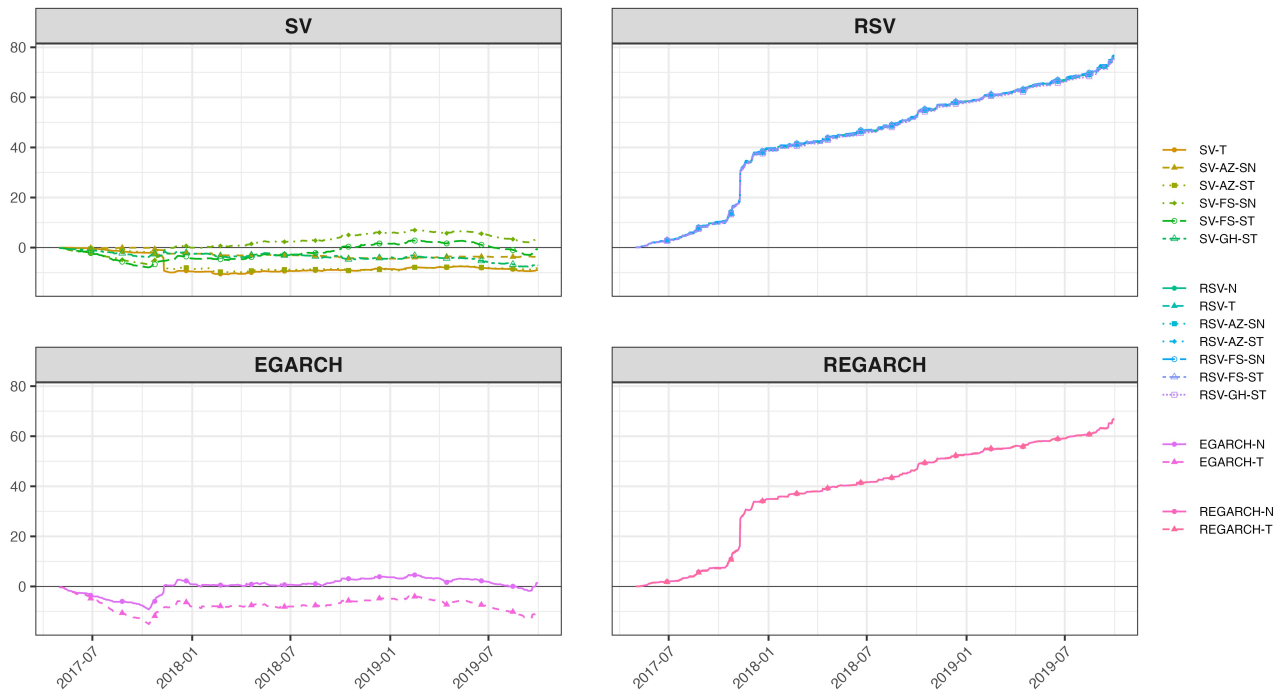


Figure 4: Cumulative QLIKE loss differences relative to the SV-N model, based on RK as the volatility proxy, for the N225.

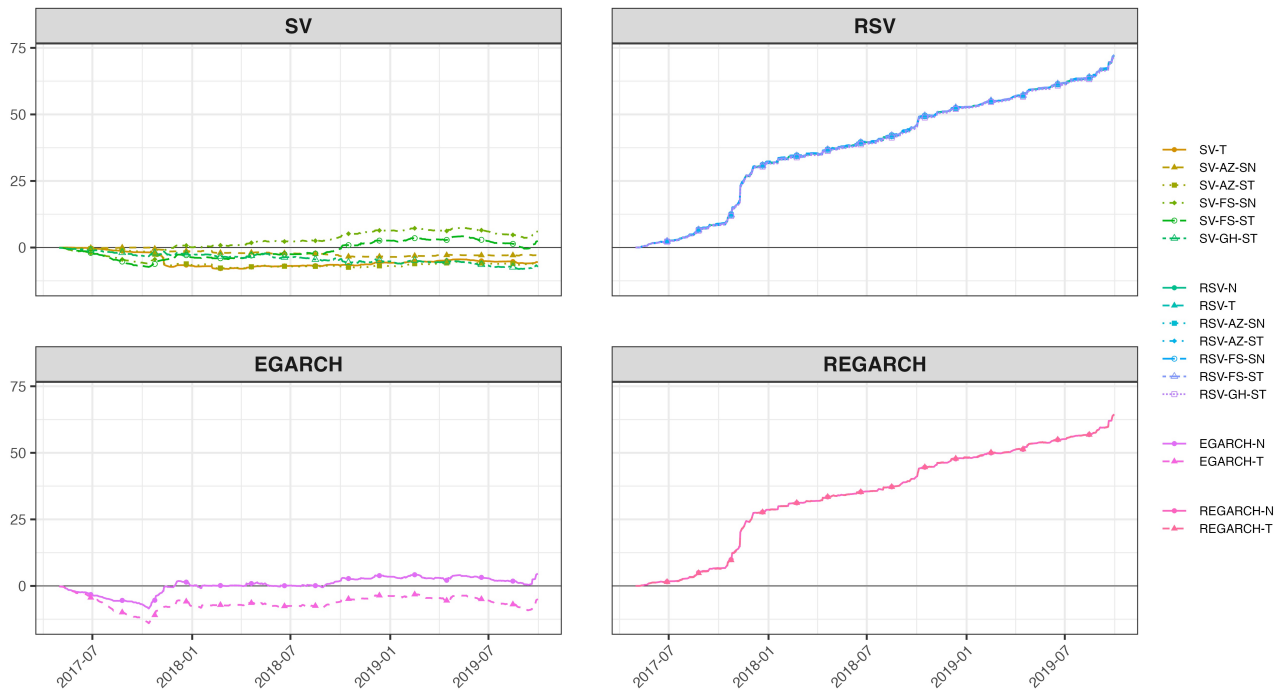


Figure 5: Cumulative QLIKE loss differences relative to the SV-N model, based on BV as the volatility proxy, for the N225.

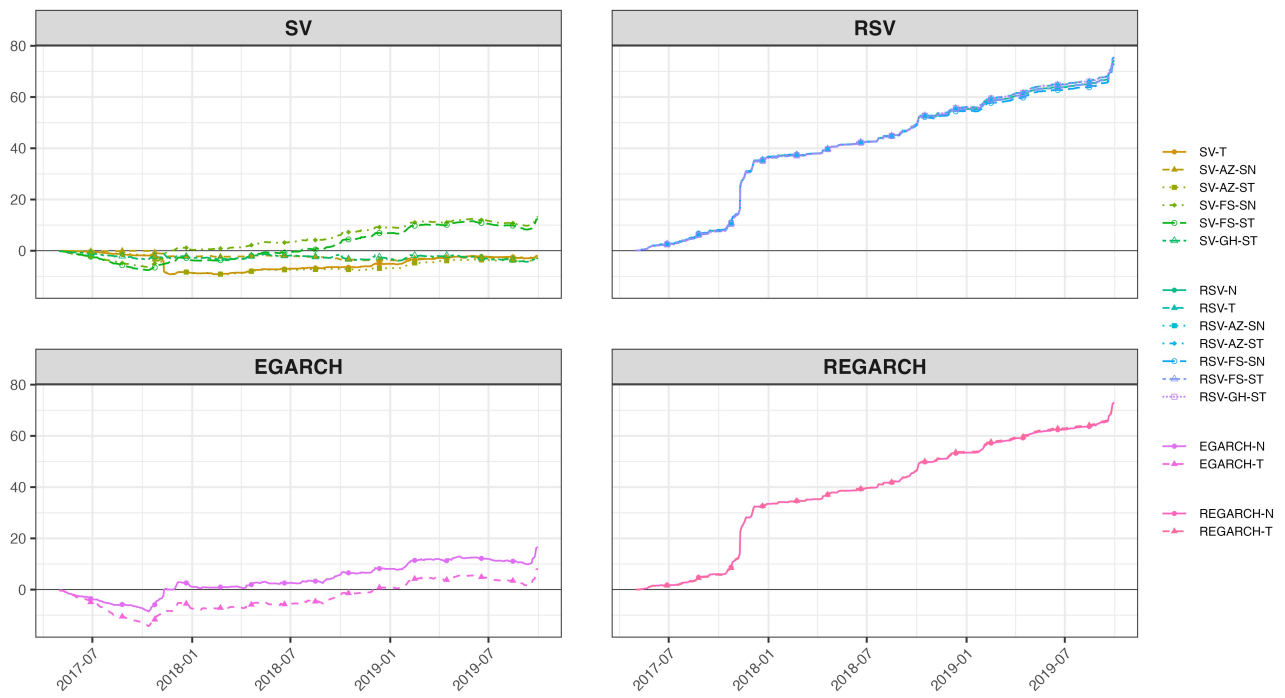


Figure 6: Cumulative QLIKE loss differences relative to the SV-N model, based on Med as the volatility proxy, for the N225.



Figure 7: Pairwise comparison of GW tests on QLIKE of volatility forecasts, based on RK as the volatility proxy, for the DJIA. The lower triangular part reports unconditional GW test statistics, while the upper triangular part shows win proportions. Lower values (green) indicate superior performance of the row model, whereas higher values (orange) favor the column model. Double and single asterisks (** and *) denote statistical significance at the 1% and 5% levels, respectively, based on unconditional GW test p-values for the lower triangular part and conditional GW test p-values for the upper triangular part.



Figure 8: Pairwise comparison of GW tests on QLIKE of volatility forecasts, based on BV as the volatility proxy, for the DJIA. See Figure 7 for additional details.



Figure 9: Pairwise comparison of GW tests on QLIKE of volatility forecasts, based on Med as the volatility proxy, for the DJIA. See Figure 7 for additional details.

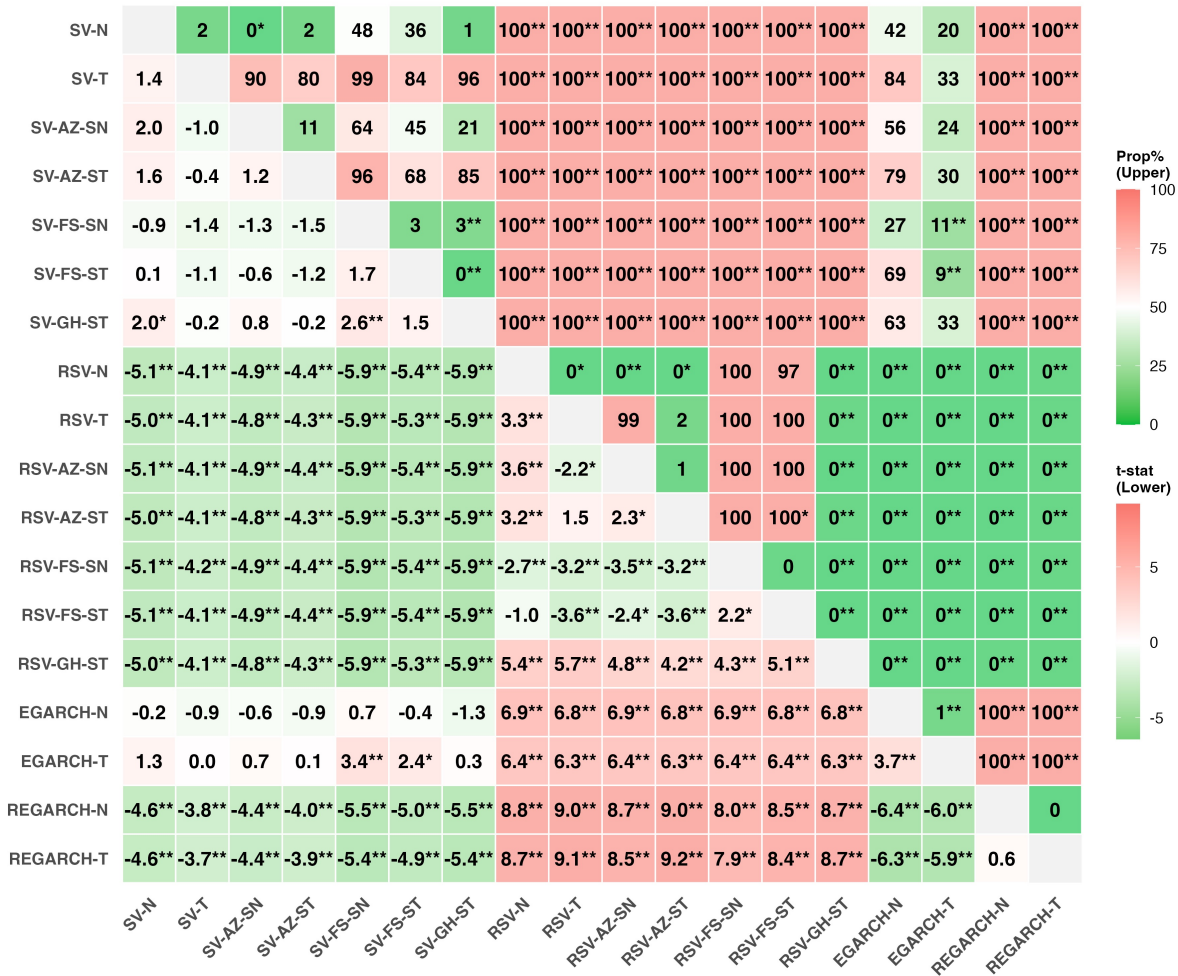


Figure 10: Pairwise comparison of GW tests on QLIKE of volatility forecasts, based on RK as the volatility proxy, for the N225. See Figure 7 for additional details.

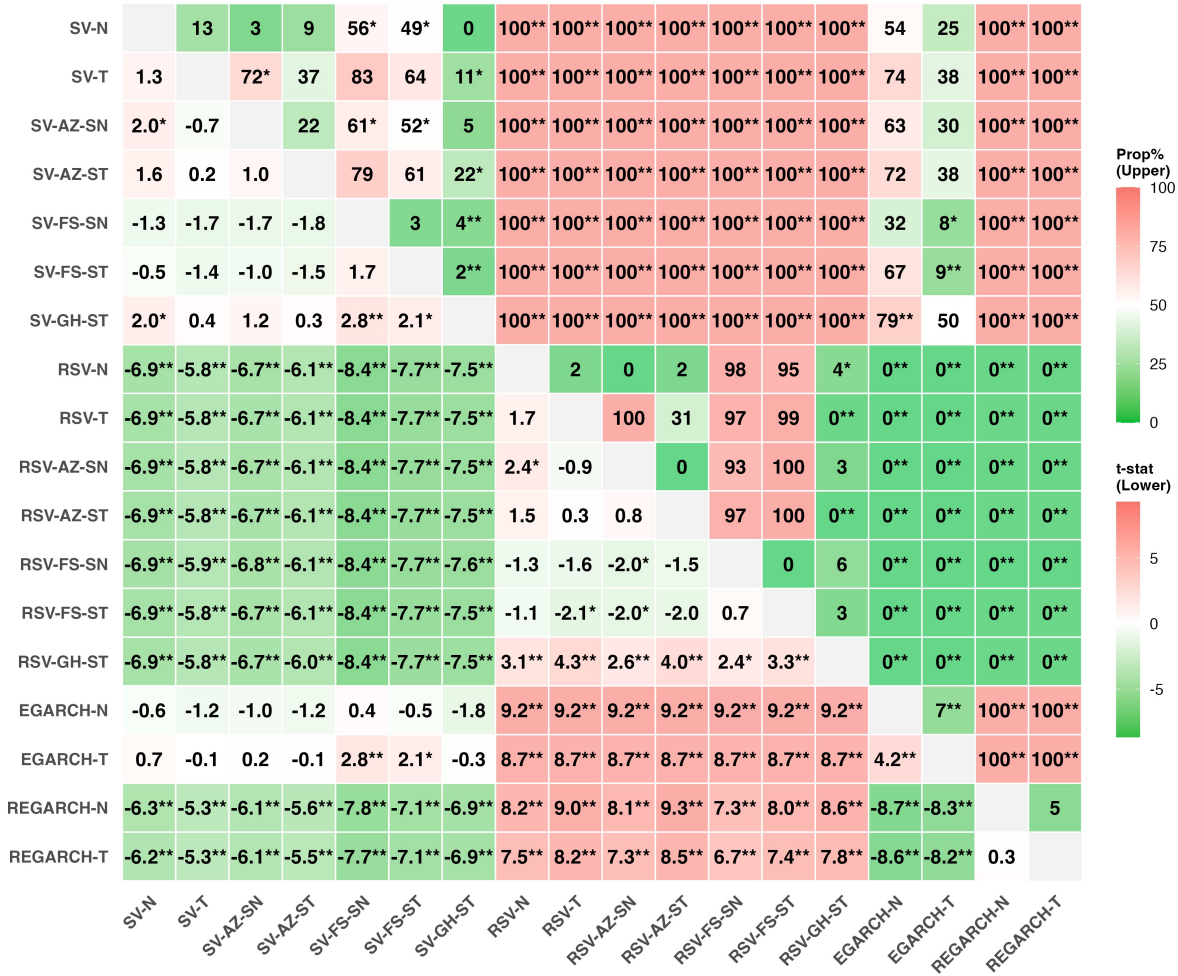


Figure 11: Pairwise comparison of GW tests on QLIKE of volatility forecasts, based on BV as the volatility proxy, for the N225. See Figure 7 for additional details.

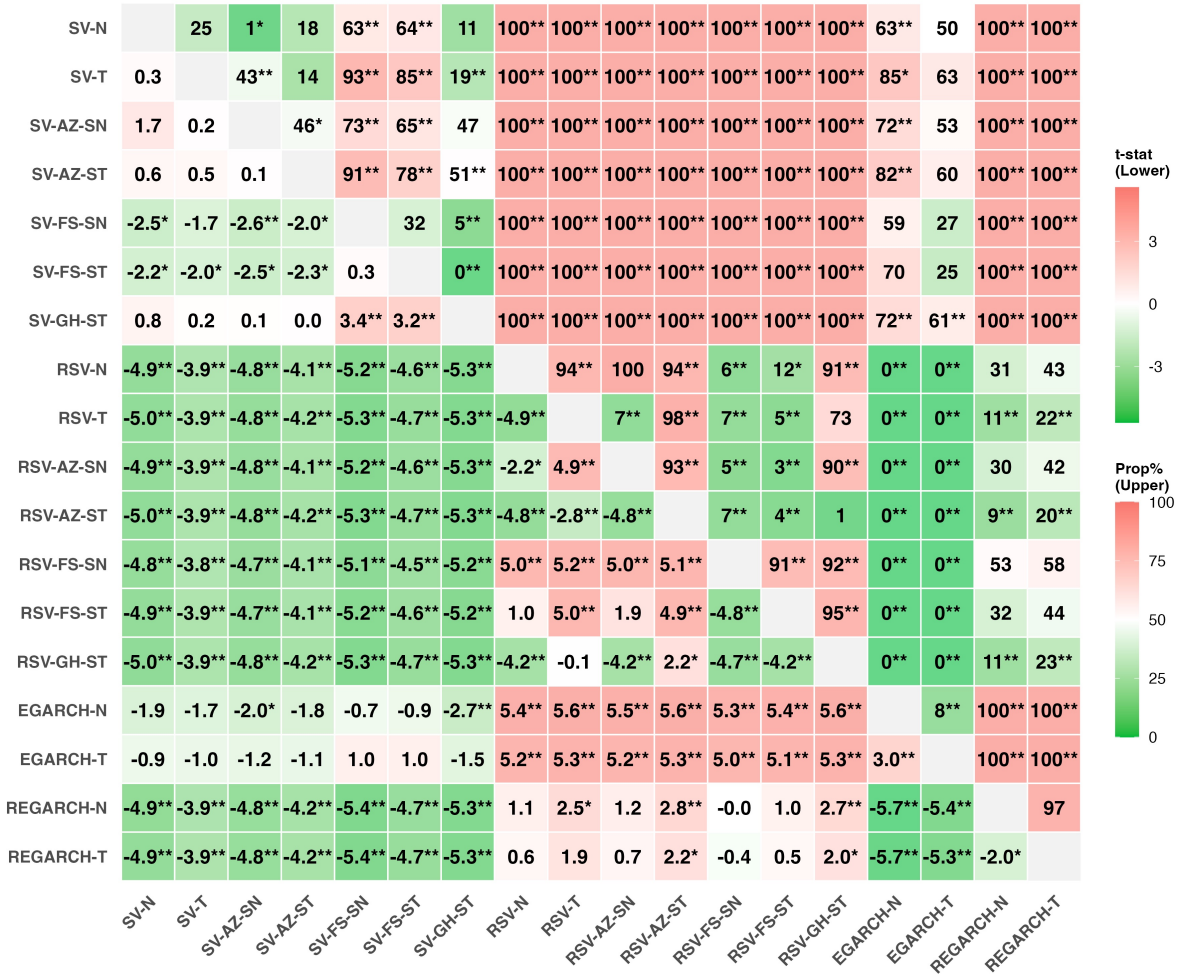


Figure 12: Pairwise comparison of GW tests on QLIKE of volatility forecasts, based on Med as the volatility proxy, for the N225. See Figure 7 for additional details.



Figure 13: Cumulative loss differences (FZ0) relative to the SV-N model ($\alpha = 1\%$) for the N225.

3 VaR and ES Forecasts

This section reports additional results for Value-at-Risk (VaR) and Expected Shortfall (ES) forecasts. These results complement the main text by providing robustness checks and extended evidence across alternative markets and forecast evaluation measures. Taken together, the results for the N225 reinforce the conclusions drawn from the DJIA, providing further evidence that RSV models—especially RSV-AZ-ST, RSV-FS-ST, and RSV-GH-ST—consistently deliver superior VaR and ES forecasts across varying levels of tail risk.

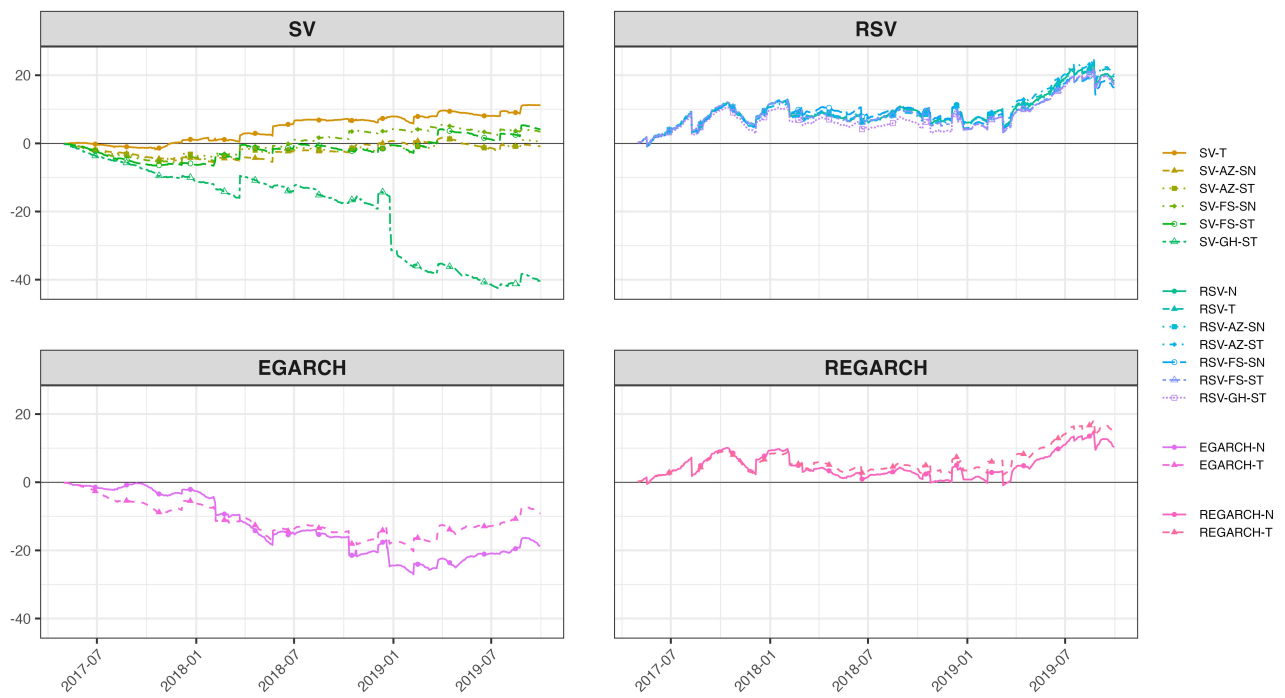


Figure 14: Cumulative loss differences (FZ0) relative to the SV-N model ($\alpha = 5\%$) for the N225.



Figure 15: Pairwise comparison of GW tests on FZ0 loss of VaR and ES forecasts ($\alpha = 1\%$) for the N225. See Figure 7 for additional details.

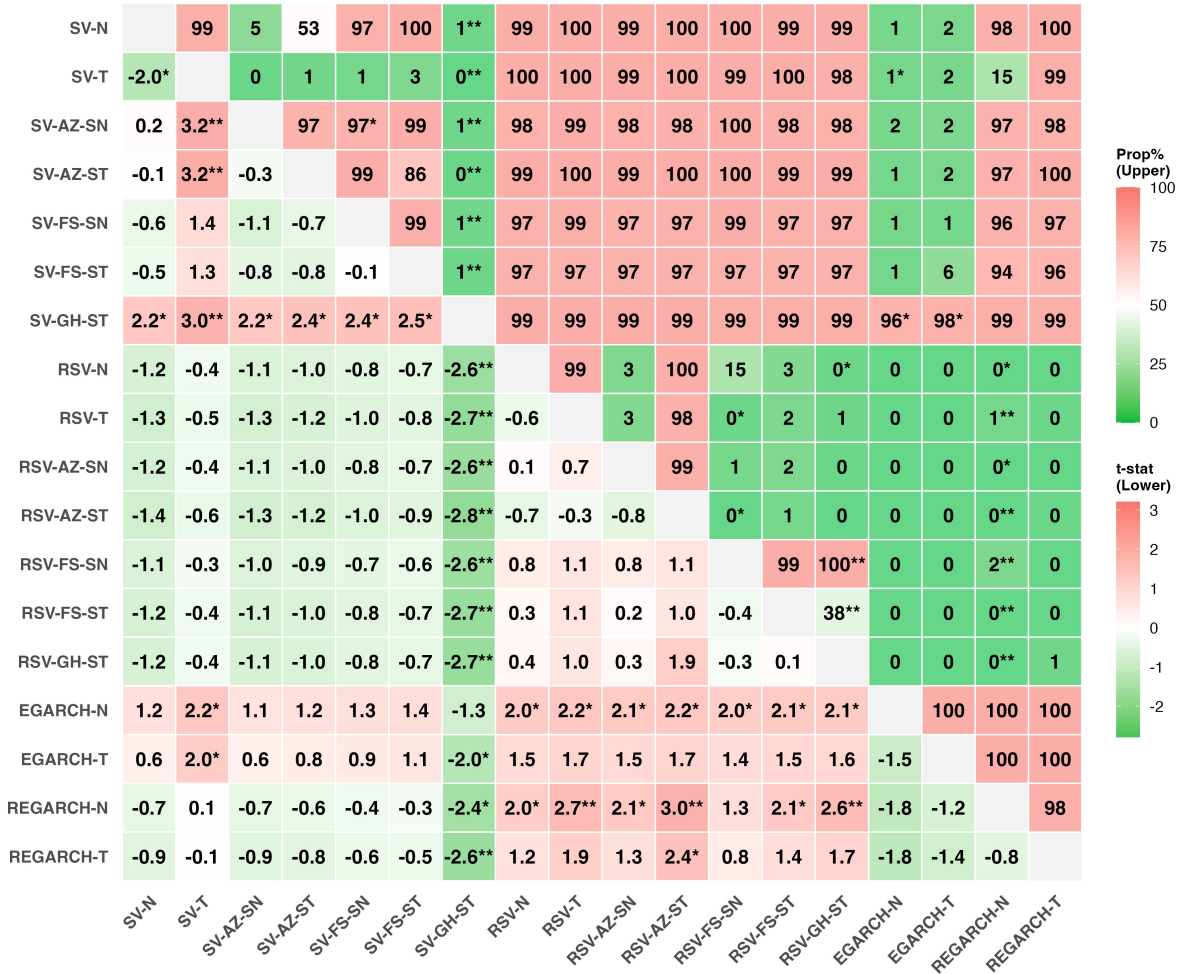


Figure 16: Pairwise comparison of GW tests on FZ0 loss of VaR and ES forecasts ($\alpha = 5\%$) for the N225. See Figure 7 for additional details.

4 MCMC Diagnostics

This section reports convergence diagnostics and prior–posterior comparisons for the Bayesian estimation of the RSV-AZ-ST model in the empirical analysis. To assess the stability of the Markov chain Monte Carlo (MCMC) procedure, Table 3 presents results for three representative rolling estimation windows applied to the DJIA.

For each window, the table reports posterior means, standard deviations, and 95% credible intervals, together with the p -values of the convergence diagnostic proposed by Geweke (1992) (CD) and inefficiency factors (IF). In all reported cases, the Geweke’s diagnostics do not reject convergence at conventional significance levels, indicating that the Markov chains are well mixed and stationary.

The table also facilitates a comparison between prior moments and posterior summaries. While relatively diffuse priors are imposed on the common parameters, the posterior distributions are substantially more concentrated and often shifted away from the prior means, suggesting that posterior inference is driven primarily by the information contained in the data rather than by prior assumptions. For variance-related parameters, priors are specified on σ^2 and σ_u^2 , and the reported prior moments for σ and σ_u are computed from the implied distributions.

Overall, these results confirm that the MCMC estimation of the RSV-AZ-ST model is numerically stable across different estimation windows and that prior dominance is not a concern in the empirical analysis. Similar convergence diagnostics and prior–posterior patterns were observed for other model specifications and estimation windows considered in the empirical analysis.

5 COVID-19 Period Analysis

To assess the robustness of our empirical findings during periods of extreme market stress, we conduct an independent analysis using data spanning from January 2012 to December 2020. This sample includes the COVID-19 crisis and is analyzed separately from the main sample to avoid overlap and contamination of inference across subsamples. In this COVID-19 period analysis, we exclude the SV-GH-ST model from the empirical evaluation, as its volatility forecasts become highly unstable and exhibit extreme spikes during this period.

The analysis focuses on daily close-to-close returns and the logarithms of 5-minute RVs for the N225. Table 4 reports the corresponding descriptive statistics. As in the full sample, daily returns exhibit pronounced non-normality, with negative skewness and excess kurtosis. The Jarque–Bera test strongly rejects normality, while the Ljung–Box statistic does not indicate significant linear autocorrelation in returns. The log-RV series displays strong serial dependence, as evidenced by the Ljung–Box test, together with positive skewness and leptokurtosis.

The time series plots in Figure 17 show a marked increase in RV from late February 2020 onward, coinciding with the global spread of COVID-19. This period is characterized by abrupt volatility spikes and heightened uncertainty, thereby providing a stringent environment for evaluating the performance of volatility and risk forecasting models.

5.1 Volatility forecasts

Figure 18 displays the log-scale volatility forecasts alongside the adjusted RV5 series. Forecast patterns are similar across models, while the RSV and REGARCH models appear to follow the volatility spikes more closely. These observations are consistent with the QLIKE results reported in Table 5, where the RSV and REGARCH models attain lower QLIKE scores than the SV and EGARCH models. In particular, the RSV-FS-SN model achieves the lowest scores under all volatility proxies and exhibits the best performance.

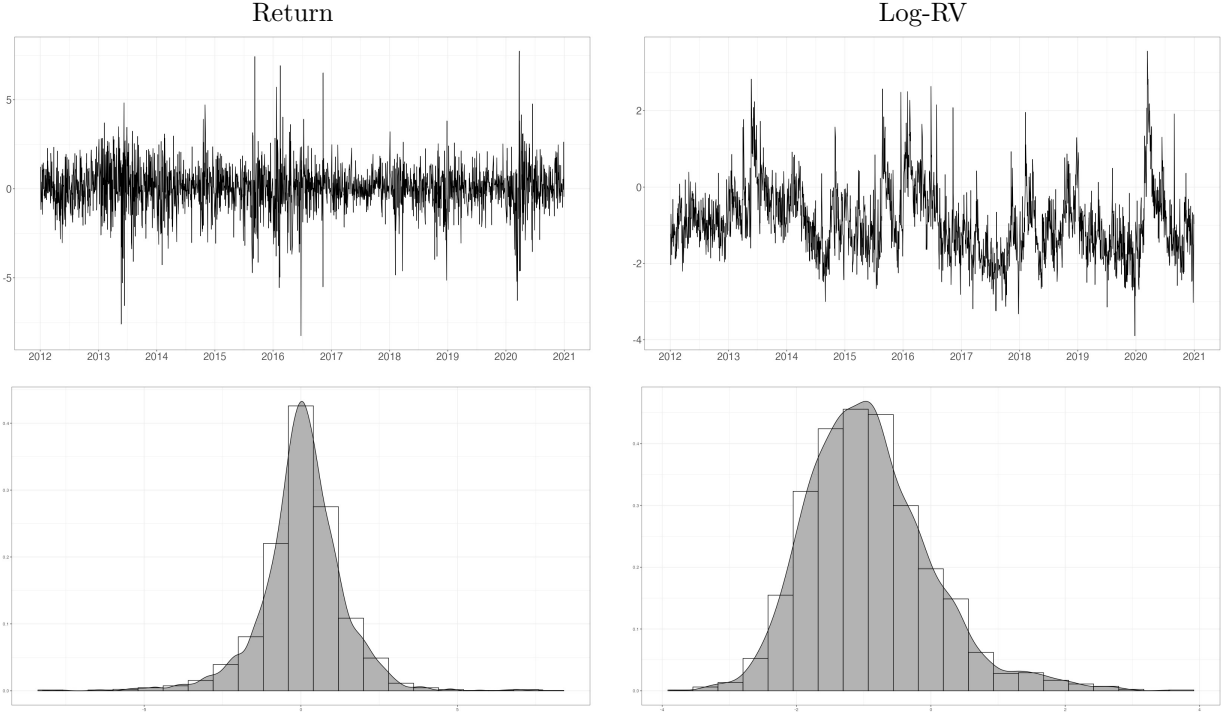


Figure 17: Time series plots (top) and histograms (bottom) of daily returns (in percentage points) and the logarithms of 5-minute RVs for the N225 (2012–2020).

The CLDs relative to the SV-N model, based on RV_5 as the volatility proxy, shown in Figure 19 reinforce the superior performance of the RSV and REGARCH models. Both the unconditional and conditional GW tests reported in Figure 20 further support the outperformance of the RSV and REGARCH models over their SV and EGARCH counterparts, with the RSV models outperforming the REGARCH models. Within the RSV framework, FS-type distributions further enhance forecast accuracy.

In summary, incorporating RV substantially improves forecast accuracy, with the RSV and REGARCH models consistently outperforming the SV and EGARCH models. These results are in line with the findings for the main sample.

5.2 VaR and ES forecasts

Figure 21 illustrates the VaR and ES forecasts generated by the RSV-AZ-ST and REGARCH-T models. VaR violations are observed around similar dates over the forecasting period. For clarity, the forecasts from other models are omitted.

Table 6 presents the empirical violation rates ($\hat{\alpha}$), the average FZ0 loss values, and the corresponding p -values from the DQ test and the MCS procedure. At the 1% level, the violation rates—especially for the SV models—are generally well aligned with the nominal level. In contrast, at $\alpha = 5\%$, all models except SV-AZ-ST tend to underestimate tail risk, as indicated by violation rates exceeding the target level.

Regarding predictive accuracy based on the FZ0 loss, the REGARCH-T and SV-AZ-SN models achieve the lowest losses at the 1% and 5% levels, respectively. All models are included in the 75% MCS, indicating broadly comparable performance in tail risk forecasting. The DQ test suggests that all models pass the independence test

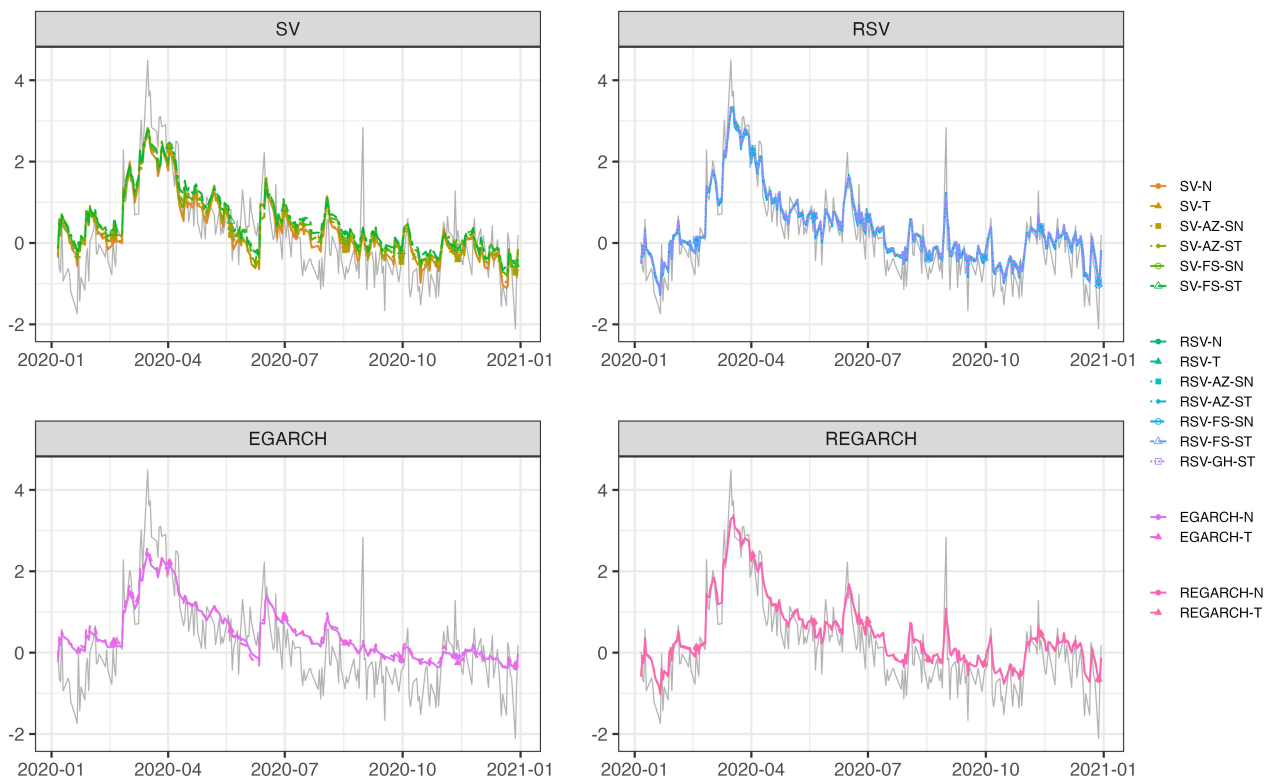


Figure 18: Log-scale volatility forecasts together with the adjusted RV5 for the N225 over the COVID-19 period (2020).

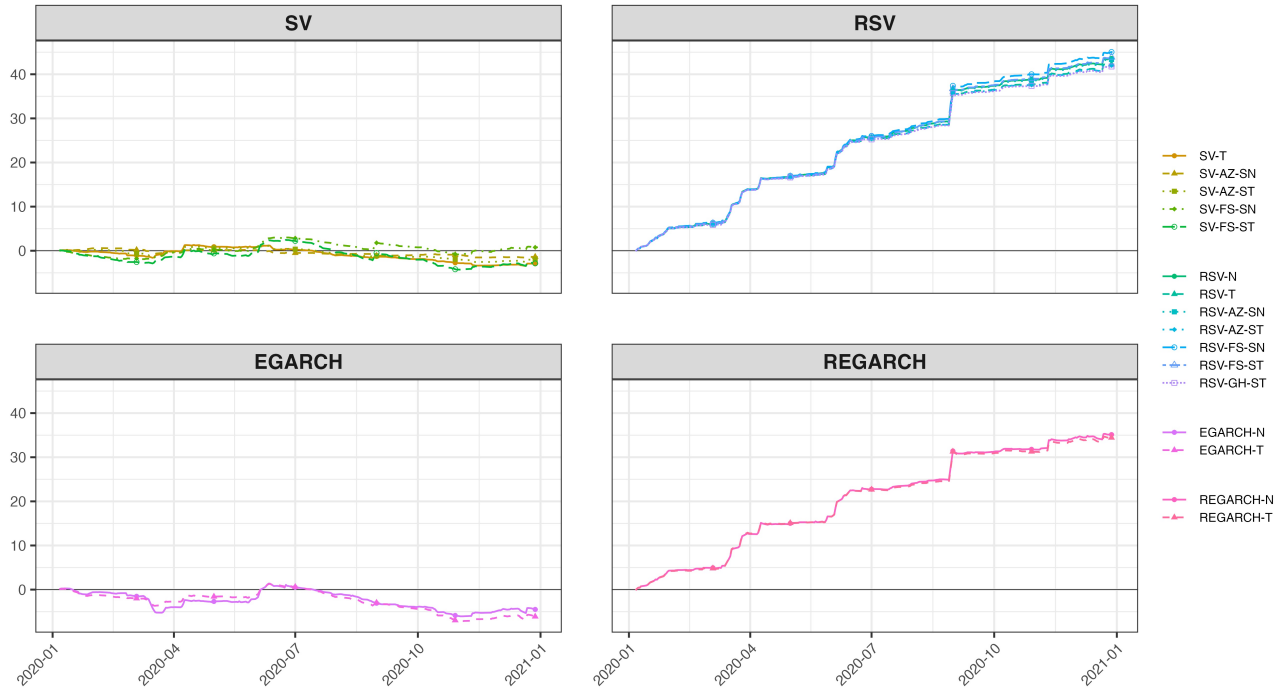


Figure 19: Cumulative QLIKE loss differences relative to the SV-N model, based on RV5 as the volatility proxy, for the N225 over the COVID-19 period (2020).

at the 1% level.

Figures 22 and 23 show the CLDs relative to the SV-N benchmark. At the 1% level, only the EGARCH-T and REGARCH-T models outperform the SV-N benchmark. At the 5% level, SV models with skew- t distributions exhibit relatively better performance. Contrary to the results for the main sample, incorporating RV does not necessarily improve VaR and ES forecasts in terms of the FZ0 loss during this period.

Figures 24 and 25 visualize the GW test results based on the FZ0 loss function. At the 1% level, the SV, EGARCH-T, and REGARCH-T models tend to show better performance, although the differences across models are not statistically significant in many cases. At the 5% level, the dominance of the SV models becomes more pronounced; however, the differences across models remain statistically insignificant in many cases.

References

- Diebold, F. X. (1988), *Empirical Modeling of Exchange Rate Dynamics*, Springer-Verlag, Berlin.
- Engle, R. F. & Manganelli, S. (2004), ‘CAViaR: Conditional autoregressive value at risk by regression quantiles’, *Journal of Business & Economic Statistics* **22**(4), 367–381.
- Geweke, J. (1992), Evaluating the accuracy of sampling-based approaches to the calculation of posterior moments, in J. M. Bernardo, J. O. Berger, A. Dawid & A. Smith, eds, ‘Bayesian Statistics 4’, Oxford, pp. 169–193.
- Ljung, G. M. & Box, G. E. P. (1978), ‘On a measure of lack of fit in time series analysis’, *Biometrika* **65**(2), 297–303.

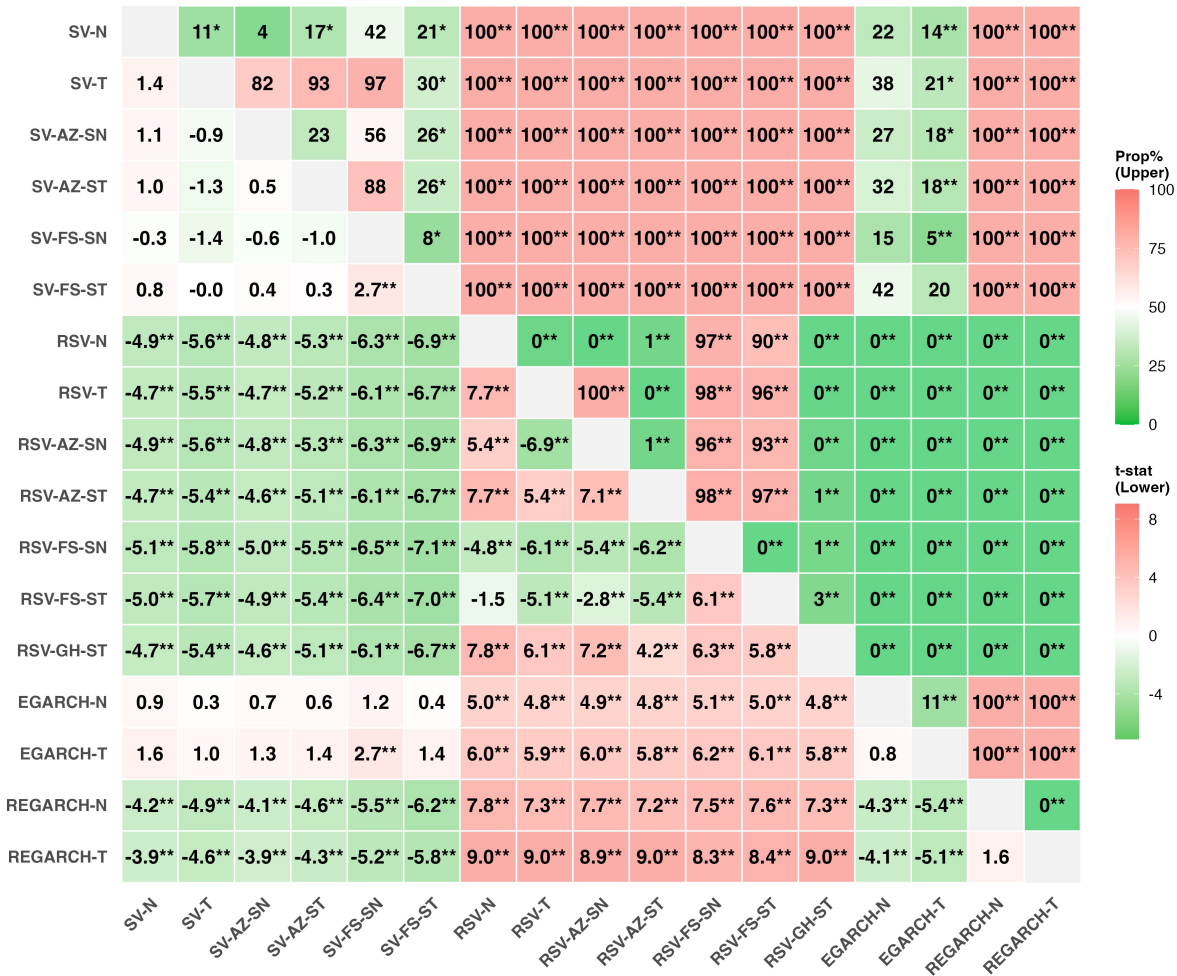


Figure 20: Pairwise comparison of GW tests on QLIKE of volatility forecasts, based on RV5 as the volatility proxy, for the N225 over the COVID-19 period (2020). See Figure 7 for additional details.

Table 3: MCMC diagnostics for the RSV-AZ-ST model applied to the DJIA over representative estimation windows.

Window	Parameter	Prior		Posterior					
		Mean	SD	Mean	SD	95%L	95%U	CD	IF
20090604–20170503	μ	0.00	10.00	-0.4775	0.0902	-0.6496	-0.2927	0.893	5.77
	ϕ	0.86	0.11	0.9326	0.0090	0.9143	0.9492	0.898	36.37
	σ	0.119	0.049	0.3035	0.0164	0.2717	0.3367	0.988	55.67
	ρ	-0.33	0.47	-0.7493	0.0524	-0.8451	-0.6421	0.435	153.70
	δ	-0.33	0.47	-0.8111	0.0355	-0.8663	-0.7232	0.734	132.17
	ν	10.00	4.47	20.9622	4.9318	13.1620	32.3571	0.071	260.55
	ξ	0.00	1.00	-0.2273	0.0400	-0.3029	-0.1469	0.862	33.33
	σ_u	0.238	0.104	0.5334	0.0121	0.5097	0.5570	0.834	21.43
20100409–20180314	μ	0.00	10.00	-0.5581	0.0970	-0.7421	-0.3633	0.292	6.25
	ϕ	0.86	0.11	0.9271	0.0089	0.9090	0.9440	0.967	20.09
	σ	0.119	0.049	0.3310	0.0169	0.2975	0.3644	0.682	40.05
	ρ	-0.33	0.47	-0.6620	0.0538	-0.7638	-0.5528	0.178	81.30
	δ	-0.33	0.47	-0.7897	0.0446	-0.8589	-0.6785	0.099	73.41
	ν	10.00	4.47	20.2447	4.5292	13.5480	30.4780	0.461	145.74
	ξ	0.00	1.00	-0.2835	0.0426	-0.3673	-0.2009	0.485	27.16
	σ_u	0.238	0.104	0.5255	0.0128	0.5013	0.5510	0.813	13.29
20110323–20190301	μ	0.00	10.00	-0.5694	0.0980	-0.7608	-0.3730	0.261	5.16
	ϕ	0.86	0.11	0.9279	0.0084	0.9107	0.9436	0.103	10.77
	σ	0.119	0.049	0.3251	0.0153	0.2959	0.3556	0.752	28.99
	ρ	-0.33	0.47	-0.6178	0.0530	-0.7152	-0.5105	0.062	76.07
	δ	-0.33	0.47	-0.7509	0.0724	-0.8439	-0.5576	0.256	140.99
	ν	10.00	4.47	20.5298	4.6395	12.9166	31.0128	0.204	133.55
	ξ	0.00	1.00	-0.3260	0.0439	-0.4126	-0.2398	0.313	22.84
	σ_u	0.238	0.104	0.5054	0.0122	0.4816	0.5299	0.561	11.91

Notes: The table reports prior moments, posterior summaries, and MCMC diagnostics for representative rolling estimation windows of the RSV-AZ-ST model. For variance parameters, priors are specified on σ^2 and σ_u^2 ; reported prior moments for σ and σ_u are computed from the implied distributions. CD denotes the p -value of the convergence diagnostic of Geweke (1992), and IF denotes the inefficiency factor.

Table 4: Descriptive statistics of daily returns and the logarithms of 5-minute RVs for the N225 (2012–2020).

	Mean	SD	Skew	Kurt	Min	Max	JB	LB
Return	0.053 (0.028)	1.323	-0.274 (0.052)	7.617 (0.104)	-8.253	7.731	0.00	0.64
Log-RV	-0.921 (0.020)	0.925	0.735 (0.052)	4.230 (0.104)	-3.894	3.562	0.00	0.00

Notes: Standard errors are shown in parentheses. JB refers to the p -value of the Jarque–Bera test. LB denotes the p -value of the Ljung & Box (1978) statistic, adjusted as in Diebold (1988).

Table 5: QLIKE scores of volatility forecasts for the N225 over the COVID-19 period (2020).

	Proxy				Average	
	RV5	RK	BV	Med	Score	Rank
SV-N	0.261	0.265	0.262	0.261	0.262	12.0
SV-T	0.274	0.281	0.273	0.254	0.270	14.2
SV-AZ-SN	0.266	0.271	0.266	0.262	0.267	13.2
SV-AZ-ST	0.269	0.277	0.269	0.254	0.267	13.0
SV-FS-SN	0.257	0.267	0.258	0.234	0.254	10.2
SV-FS-ST	0.273	0.285	0.273	0.238	0.267	13.8
RSV-N	0.081	0.092	0.084	0.063*	0.080	2.8
RSV-T	0.086	0.098	0.089	0.064*	0.084	4.8
RSV-AZ-SN	0.081	0.093	0.085	0.063*	0.081	3.2
RSV-AZ-ST	0.087	0.100	0.090	0.065*	0.085	6.0
RSV-FS-SN	0.074*	0.085*	0.079*	0.063*	0.076	1.5
RSV-FS-ST	0.079	0.091	0.084	0.065*	0.080	2.8
RSV-GH-ST	0.088	0.101	0.091	0.065*	0.086	7.0
EGARCH-N	0.279	0.293	0.278	0.253	0.276	15.0
EGARCH-T	0.286	0.299	0.286	0.258	0.282	16.5
REGARCH-N	0.115	0.129	0.116	0.081	0.110	8.2
REGARCH-T	0.118	0.132	0.119	0.081	0.113	8.8

Notes: An asterisk (*) indicates that the model belongs to the 90% MCS. The average columns report the mean QLIKE scores and ranks across the two indices.

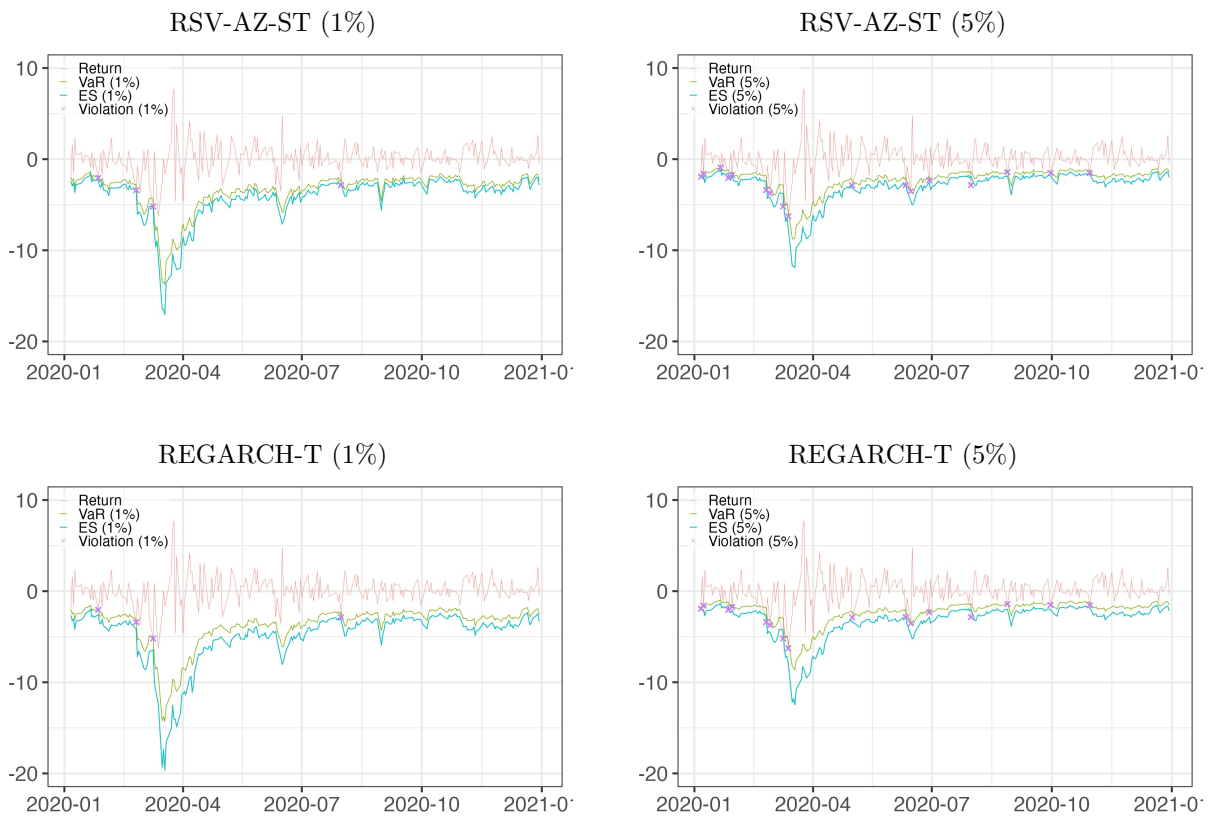


Figure 21: VaR and ES forecasts of RSV-FS-ST and REGARCH-T models for the N225 over the COVID-19 period (2020).

Table 6: Violation rates and FZ0 losses of VaR and ES forecasts for the N225 over the COVID-19 period (2020).

	$\alpha = 1\%$				$\alpha = 5\%$			
	$\hat{\alpha}$	p_{DQ}	FZ0	p_{MCS}	$\hat{\alpha}$	p_{DQ}	FZ0	p_{MCS}
SV-N	0.83	0.95	1.3999	1.00	6.20	0.57	1.0655	1.00
SV-T	0.83	0.96	1.4068	1.00	6.20	0.62	1.0660	1.00
SV-AZ-SN	0.83	0.96	1.3997	1.00	5.37	0.93	1.0465	1.00
SV-AZ-ST	0.83	0.95	1.4118	1.00	4.96	0.91	1.0594	1.00
SV-FS-SN	0.83	0.96	1.4024	1.00	5.79	0.78	1.0483	1.00
SV-FS-ST	0.83	0.96	1.4038	1.00	5.79	0.79	1.0509	1.00
RSV-N	2.48	0.88	1.5306	0.74	7.44	0.90	1.1085	0.78
RSV-T	2.07	0.95	1.4240	1.00	7.85	0.86	1.0990	0.92
RSV-AZ-SN	2.48	0.88	1.4983	0.90	7.85	0.86	1.1053	0.80
RSV-AZ-ST	1.65	0.95	1.4148	1.00	7.02	0.85	1.0960	0.96
RSV-FS-SN	1.65	0.94	1.4428	1.00	7.85	0.86	1.1097	0.77
RSV-FS-ST	1.65	0.95	1.4426	1.00	7.85	0.86	1.1011	0.86
RSV-GH-ST	1.65	0.95	1.4152	1.00	7.44	0.90	1.0892	1.00
EGARCH-N	2.07	0.92	1.4420	1.00	5.79	0.84	1.0922	1.00
EGARCH-T	0.83	0.95	1.3870	1.00	6.61	0.55	1.0821	1.00
REGARCH-N	2.07	0.95	1.4989	0.87	6.20	0.94	1.0997	0.92
REGARCH-T	1.65	0.95	1.3740	1.00	6.61	0.90	1.0932	0.98

Notes: $\hat{\alpha}$ represents the empirical violation rate (%). p_{DQ} indicates the p -value of the dynamic quantile test of Engle & Manganelli (2004). FZ0 denotes the average FZ0 loss. p_{MCS} indicates the MCS p -value.

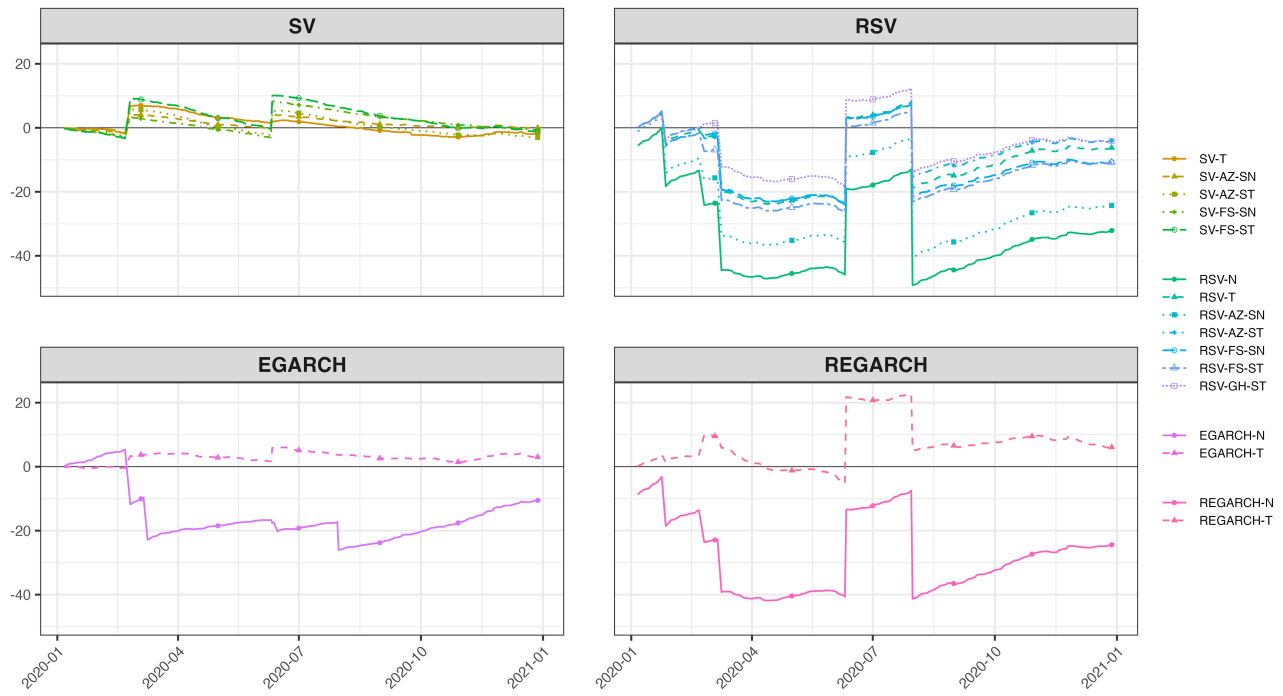


Figure 22: Cumulative loss differences (FZ0) relative to the SV-N model ($\alpha = 1\%$) for the N225 over the COVID-19 period (2020).



Figure 23: Cumulative loss differences (FZ0) relative to the SV-N model ($\alpha = 5\%$) for the N225 over the COVID-19 period (2020).

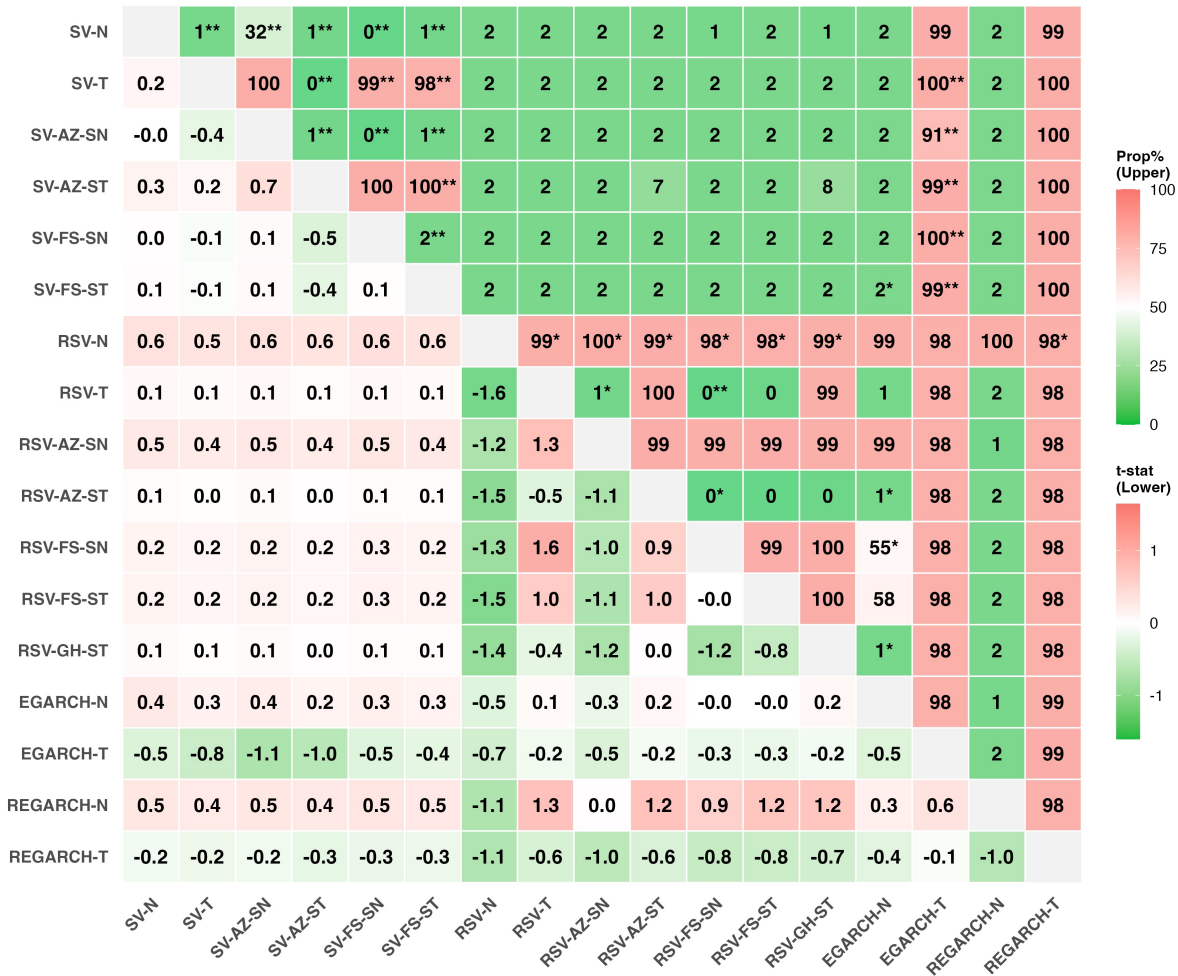


Figure 24: Pairwise comparison of GW tests on FZ0 loss of VaR and ES forecasts ($\alpha = 1\%$) for the N225 over the COVID-19 period (2020). See Figure 7 for additional details.

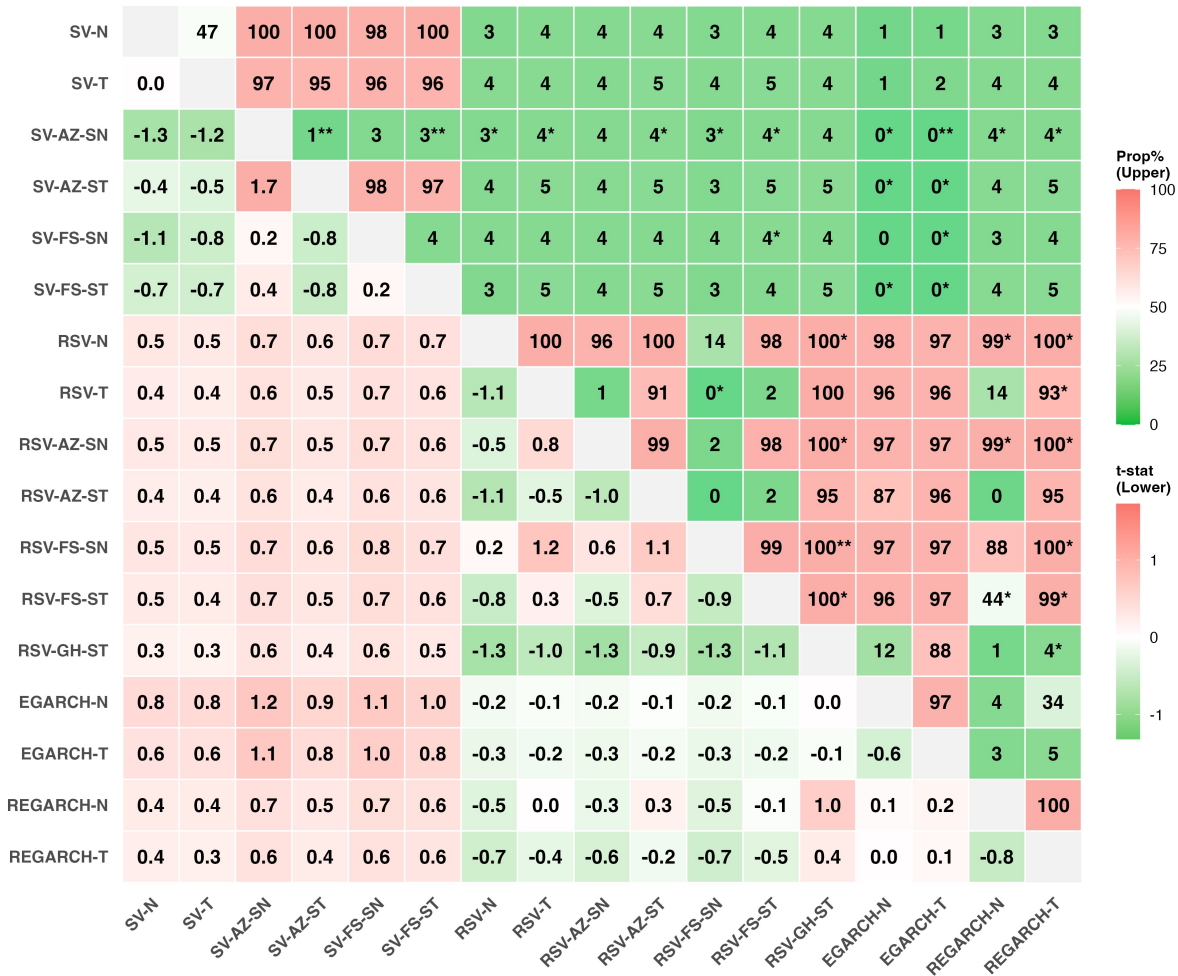


Figure 25: Pairwise comparison of GW tests on FZ0 loss of VaR and ES forecasts ($\alpha = 5\%$) for the N225 over the COVID-19 period (2020). See Figure 7 for additional details.